University of South Alabama

# JagWorks@USA

5-2022

# STAT3 Dysregulation of XRCC1 Results on Altered Base Excision Repair

Griffin Wright
*University of South Alabama*, gmw1821@jagmail.southalabama.edu

Follow this and additional works at: https://jagworks.southalabama.edu/theses_diss

Part of the Medical Genetics Commons

## Recommended Citation

THE UNIVERSITY OF SOUTH ALABAMA

COLLEGE OF MEDICINE

STAT3 DYSREGULATION OF XRCC1 RESULTS IN ALTERED BASE EXCISION
REPAIR

A Dissertation

Submitted to the Graduate Faculty of the
University of South Alabama
in partial fulfillment of the
requirements for the degree of

Doctor of Philosophy

In

Basic Medical Sciences

By
Griffin M. Wright
B.S., Auburn University, 2017
2022

## ACKNOWLEDGMENTS

Foremost, I would like to first thank my mentor, Dr. Natalie Gassman, for her support during the completion of this endeavor. Her constant encouragement, guidance and advice has not only exemplified what it means to be a successful scientist, but also what it means to a successful leader and mentor inside and outside of the laboratory. I also would like to thank my lab mates: Dr. Kevin Lee, Dr. Manoj Sonavane, Dr. Kelly Smith, and Arlet Hernandez for their companionship and support inside and outside of the laboratory.

Additionally, I give the sincerest thanks to Dr. Michele Schuler and Dr. Marie Migaud for their willingness to provide advice, support, and guidance. The guidance and contributions provided by my dissertation committee; Dr. Sarah Sayner, Dr. Robert Barrington, Dr. Christopher M. Francis, and Dr. Aishwarya Prakash is greatly appreciated.

I would like to thank my mother, Crissy Blackmon, my father, Dennis M. Wright, my stepmother, Melissa Wright, my brother, Grant Wright, my sister, Gracie-Ray Vining, and my stepsisters, Emily and Madelyn Burns, for the support, love, and care. I also want to thank my grandparents, Janice Wright (Nana), Reginald Wright (Papa) , Charles Griffin (Grandad), and Jane Griffin (Mono) as well as Catherine Robinson, James T. Tunick (Geekaw), and Rebecca Tunick for the love and support.

Sincerest thanks to my wife, Anna Robinson Wright, for her unwavering love and support during this endeavor, without which none of this work would be possible. Her steadfast motivation encouraged me to continue when I did not see a path forward, her

companionship made the trials and tribulations of graduate school and life possible, and

for this I am incredibly grateful, my heartfelt thanks.

**TABLE OF CONTENTS**

# LIST OF FIGURES

xi

# LIST OF ABBREVIATIONS

| Abbreviation | Explanation |
|---|---|
| AA | African American |
| APE | Apurinic/Apyrimidinic Endonuclease |
| AP2 | Activating Protein 2 |
| ATF-1 | Activating Transcription Factor 1 |
| ATM | Ataxia Telangiectasia Mutated |
| BC | Breast Cancer |
| BER | Base Excision Repair |
| BG | Basal Glucose (11mM or 25mM) |
| BRCTa | BRCA1 C-Terminus Domain |
| EA | European American |
| ChIP | Chromatin Immunoprecipitation |
| CREB1 | cAMP Response Element Binding Protein 1 |
| EGF | Epidermal Growth Factor |
| EGFR | Epidermal Growth Factor Receptor |
| ER | Estrogen Receptor |
| ETS | ETS Transcription Factor |
| E2F1 | E2 Transcription Factor 1 |
| HEK293T | Human Embryonic Kidney Cell Line |
| HER2 | Human Epidermal Growth Factor Receptor 2 |

| | |
|---|---|
| HG | High Glucose (30mM) |
| IFN$\gamma$ | Interferon gamma |
| IL-6 | Interleukin-6 |
| IL-6R$\alpha$ | Interleukin-6 Receptor Alpha |
| IL-12 | Interleukin-12 |
| JAK | Janus Kinase |
| LIGIII$\alpha$ | Ligase III alpha |
| LG | Low Glucose (5mM) |
| LMP1 | Latent Membrane Protein 1 |
| MDA-231 | Triple Negative Breast Cancer Cell Line |
| MDA-468 | Triple Negative Breast Cancer Cell Line |
| MMS | Methyl Methanesulfonate |
| MNNG | Methylnitronitrosoguanidine |
| NF$\kappa B$ | Nuclear Factor Kappa-light-chain-enhancer |
| NRF2 | Nuclear-Erythoid 2-Related Factor 2 |
| PARP1 | Poly (ADP-Ribose) Polymerase 1 |
| POL $\beta$ | DNA Polymerase Beta |
| PKA | Protein Kinase A |
| PR | Progesterone Receptor |
| ROS | Reactive Oxygen Species |
| RT | Room Temperature |
| SEM | Standard Error of the Mean |

Sp1       Sp1 Transcription Factor

STAT3     Signal Transducer and Activator of Transcription 3

TCGA      The Cancer Genome Atlas

TEIF      Telomerase Transcription Element-Interacting Factor

TNBC      Triple Negative Breast Cancer

U2OS      Human Bone Osteosarcoma Cell Line

XRCC1     X-ray Cross Complementing Group 1

YY1      Yin Yang 1

$\gamma$H2AX     Phosphorylated Histone H2AX S139

# ABSTRACT

Griffin M. Wright, Ph.D.,University of South Alabama, May 2022. STAT3 DYSREGULATION OF XRCC1 RESULTS IN ALTERED BASE EXCISION REPAIR. Chair of Committee: Michele Schuler, Ph.D.

Base Excision Repair (BER) is a critical DNA repair pathway, repairing base damage, the spontaneous decay of bases, abasic sites, and single-strand DNA breaks. BER requires the sequential action of multiple proteins, including poly(ADP ribose) polymerase 1 (PARP1), X-ray cross complementing group 1 (XRCC1), and DNA polymerase beta (POL $\beta$). Expression changes and polymorphisms in BER proteins alter the response of cancer cells to multiple DNA damaging chemotherapeutics, with overexpression of XRCC1 increasing chemoresistance in gastric, gallbladder, and ovarian cancer. However, the transcriptional regulation of XRCC1 remains largely understudied. Here, we identify the signal transducer and activator of transcription 3 (STAT3) as a novel regulator of *XRCC1* in TNBC cell line models, the osteosarcoma cell line U2OS, and the human embryonic kidney cell line HEK293T. Glucose, epidermal growth factor (EGF) and interleukin 6 (IL-6) are all known to activate STAT3 and promote transcription We have found that this constitutive activation results in persistent occupancy of STAT3 at the *XRCC1* promoter in TNBC cell lines, inducing overexpression of XRCC1 protein. However, the non-tumorigenic HEK293T cell line and osteosarcoma U2OS cell line do not have constitutively activated STAT3 but demonstrate an inducible response to the activation of STAT3 from exogenous stimuli.

Using acute exposures to EGF, IL-6, and glucose, we observed increased activated STAT3 and subsequent increases in XRCC1 expression in HEK293T and

U2OS cells. Critically, the increased XRCC1 expression induced by high glucose exposure resulted in increased DNA repair, measured through alkaline comet assay, and increased survival following methyl methanesulfonate (MMS) challenge in both HEK293T and U2OS cells. Furthermore, continued exposure to elevated glucose concentrations resulted in persistent STAT3 occupancy at the *XRCC1* promoter and elevated XRCC1 expression in both HEK293T and U2OS cells, similar to what is seen in constitutively active TNBC cell lines. Low glucose adaption reversed these effects by reducing STAT3 activation and occupancy at the *XRCC1* promoter in the HEK293T U2OS cells. However, low glucose adaptation in the MDA-MB-231, which have constitutively active STAT3, only slightly reduced STAT3 activation. Upstream regulators of STAT3 revealed a correlation between IL-6R$\alpha$ expression and the inducibility of STAT3 activation and subsequent XRCC1 expression. High EGFR expression and low IL-6R$\alpha$ expression resulted in minimal inducibility of MDA-231. In addition to these findings, we also identified *POLB* as a target for STAT3 regulation and mapped the STAT3 binding site within the *POLB* promoter.

These results demonstrate that activation of STAT3 regulates XRCC1 expression and altered BER functions across various cell line models. More importantly, it links constitutive activation of STAT3 with dysregulation of XRCC1 and BER in TNBC cells and undercovers a critical mechanism by which XRCC1 can become dysregulated in cancer and promote chemoresistance.

# CHAPTER I: BACKGROUND

## Base Excision Repair

It is estimated that each cell is subjected to 70,000 DNA damaging events daily, 75% of which are single-strand breaks [1].
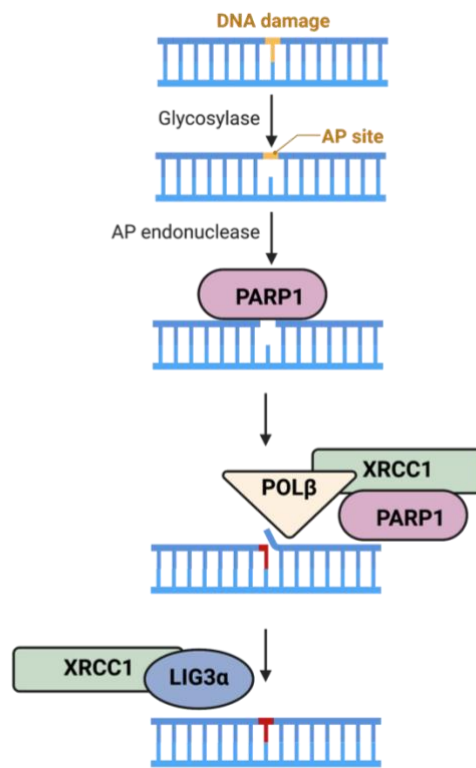


**Figure 1.1.** Base Excision Repair Pathway. Schematic representation of the BER pathway including multiple key enzymes PARP1, XRCC1, POL$\beta$, and LIG3$\alpha$. This Figure was generated using Biorender.com with citation provided in Appendix B.

If DNA damage persists within the genome, mutations can arise and drive transformation. Thus, DNA repair is critical in maintaining genomic stability [1,2]. Base excision repair (BER) is responsible for repairing DNA base lesions, the spontaneous decay of DNA bases, and single-strand breaks resulting from the endogenous and exogenous insults the cell faces [2-4]. In particular, BER is essential in repairing mutagenic DNA base modifications resulting from oxidation and alkylation of DNA bases, both of which can lead to non-Watson Crick base pairing and subsequent mutations [5]. The BER pathway is initiated by a DNA glycosylase, which recognizes and removes damaged DNA bases. DNA glycosylases belong to two families, mono-functional and bi-functional DNA glycosylase (Figure 1.1, Appendix B) [6]. Both mono-functional and bi-functional DNA glycosylases contain glycosylase activity, the ability to cleave glycosidic bonds; however, bi-functional glycosylases also have Apurinic/Aprimidine (AP) lyase activity catalyzing the cleavage of phosphodiester bonds [2,6]. Following base removal by a mono-functional glycosylase, an AP endonuclease (APE1) is needed to form the single-strand DNA breaks [2,3]. Single strand DNA breaks formed during the BER process are then recognized and bound by Poly(ADP Ribose) polymerase 1 (PARP1) [2,3,7]. Following binding to the DNA single-strand break, PARP1 undergoes an auto-modification by ADP-ribose, resulting in the formation of Poly ADP Ribose (PAR) chains [7,8]. PAR chains are responsible for recruitment of BER factors, including X-ray cross complementing protein 1 (XRCC1) [7,9,10]. The BRCTa domain of XRCC1 interacts with PARylated PARP1 bound to a single-strand break and serves as a scaffold protein responsible for the binding and facilitation of multiple BER factors, including DNA polymerase Beta (POL $\beta$) through the N-terminal domain and DNA Ligase III Alpha (LIGIIIα) through the C-terminal BRCT

domain [9]. POL $\beta$ removes the 5'-deoxyribose phosphate group following the action of

APE1 [2,3,9,11]. In addition, POL $\beta$ serves as the primary gap-filling polymerase during the

BER process [11]. LIGIIIα finalizes the repair process by catalyzing the formation of a

phosphodiester bond between the inserted DNA nucleotide and the adjacent DNA

nucleotide [2,3].

## Transcriptional Regulation of XRCC1

Although XRCC1 plays a critical role in maintaining genomic stability, little is

known regarding its transcriptional regulation (Figure 1.2, Appendix A) [1,12]. Two

transcription factors have been identified in the regulation of *XRCC1*, Sp1 and E2

transcription factor 1 (E2F1) [13,14]. Basal transcription of *XRCC1* occurs through the

binding of Sp1 to a GC rich target sequence upstream of the transcription start site [13].

However, following persistent DNA damage, activation of the DNA damage sensor,

ataxia telangiectasia mutated (ATM), results in the phosphorylation and degradation of

Sp1, resulting in reduced *XRCC1* expression promoting apoptosis [13]. The cell cycle

regulator E2F1 serves as a transcription factor with a consensus binding sequence

upstream of the Sp1 site [14]. E2F1 regulation of XRCC1 is responsible for inducing a

robust repair response following DNA damage induced by MMS [14]. Outside of E2F1 and

Sp1, no other transcription factors sites within the *XRCC1* promoter have been extensively studied.
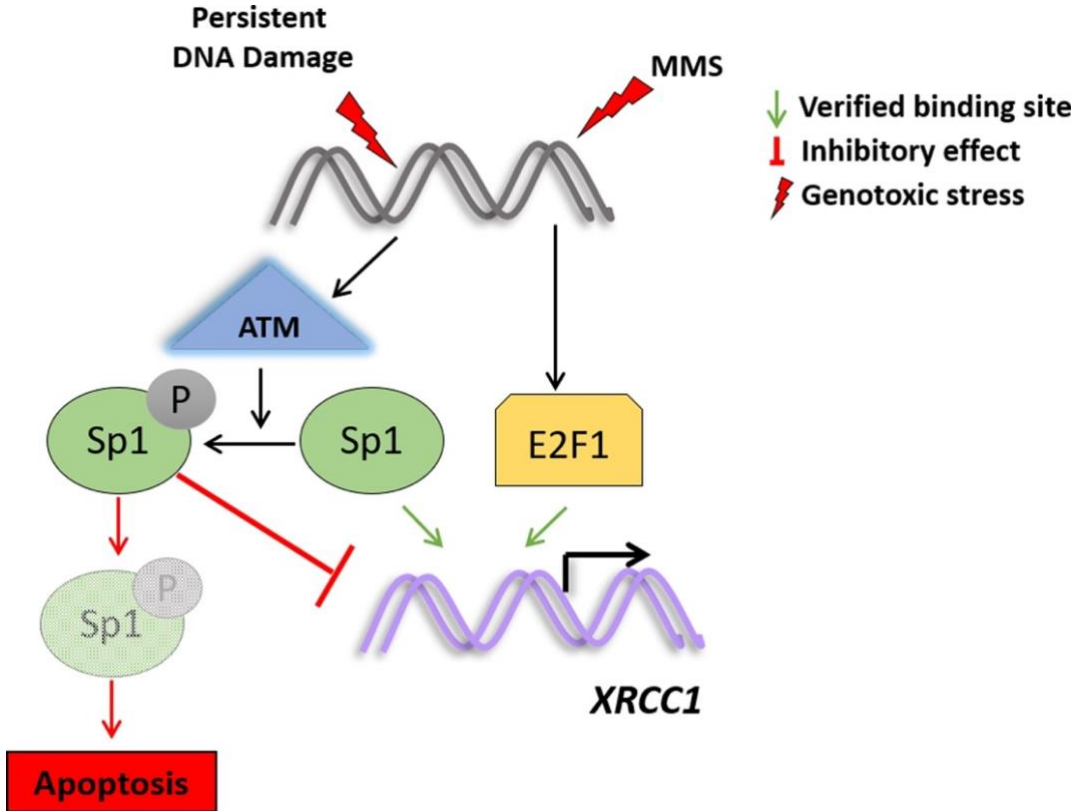


**Figure 1.2.** Transcriptional Regulation of *XRCC1*: Two Transcription Factors have been identified in the regulation of XRCC1; Sp1 serves as the basal transcription factor and is negatively regulated through an ATM dependent phosphorylation, E2F1 is responsible for producing a robust increase in XRCC1 following MMS-induced DNA damage. This figure was adapted from "Transcriptional dysregulation of base excision repair proteins in breast cancer" published in DNA Repair with the journal's permission provided in Appendix A.

## Transcriptional Regulation of *POLB*

Transcriptional regulation of *POLB* has been more extensively studied, with six transcription factors regulating *POLB* expression (Figure 1.3, Appendix A) [12]. Like

*XRCC1*, Sp1 is responsible for driving the basal expression of *POLB* by increasing the

rate of RNA polymerase promoter closed complex formation [15].
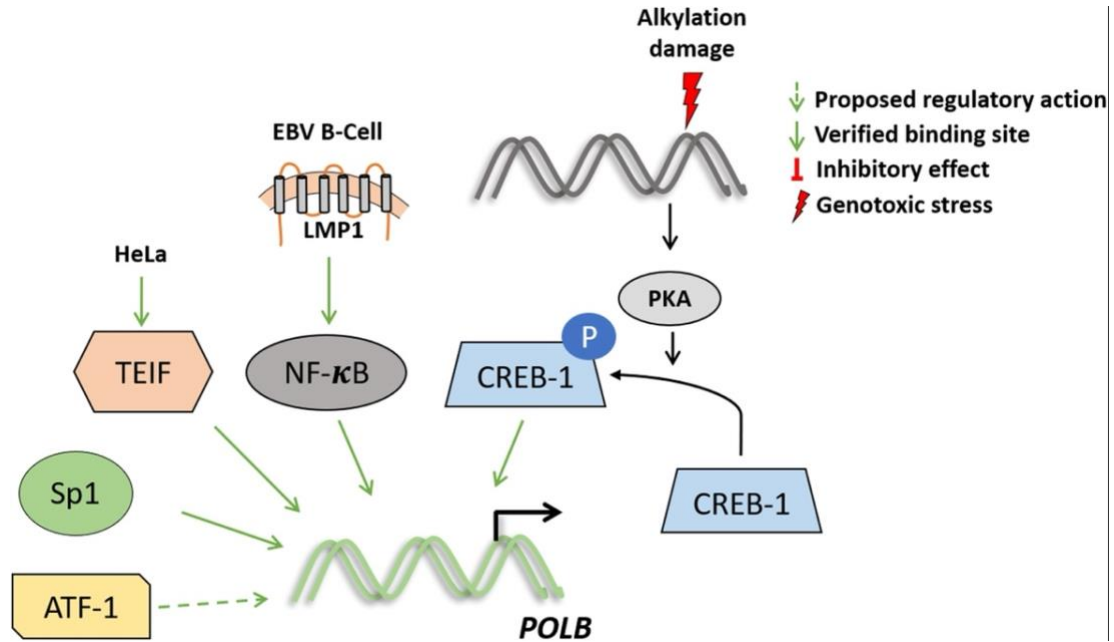


**Figure 1.3.** Transcriptional Regulation of *POLB*: Like XRCC1, Sp1 serves as a basal transcription factor of polymerase beta. Multiple cell line specific regulatory mechanisms have been identified including TEIF regulation in HeLa cells and NF-kB regulation in EBV B-cells. PKA activation following alkylating DNA damage induces CREB-1 phosphorylation and subsequent regulation of *POLB*. An ATF-1 site has been proposed but not validated. This figure was adapted from "Transcriptional dysregulation of base excision repair proteins in breast cancer" published in DNA Repair with the journal's permission provided in Appendix A.

An activating transcription factor 1 (ATF-1) site has been proposed but not

validated [16]. Increased expression of *POLB* following alkylating DNA damage has been

reported through cAMP-dependent protein kinase A (PKA) phosphorylation of cAMP

responsive element binding protein 1 (CREB-1), increasing the binding of the

transcription factor to the *POLB* promoter [17,18]. *POLB* regulation in specific cell lines has

also been reported, including Telomerase transcriptional element-interacting factor

(TEIF) regulation of *POLB* in HeLa cells as well as regulation of *POLB* through the

Epstein Barr virus-associated activation of Nuclear Factor Kappa-light-chain-enhancer of

activated B cells (NF-kB) by associated viral protein latent membrane protein 1 (LMP1)

[19,20].

## Transcriptional Regulation of PARP1

PARP1 has multiple roles outside of its DNA repair duties, including modulation

of transcription either as a transcription factor or by regulating the activity of other

transcription factors through post-translation modification, including Yin-yang 1 (YY-1),

Activating protein 2 (AP-2) and STAT3 [21-24]. Like *POLB*, transcriptional regulation of

*PARP1* has been more widely studied with five identified transcription factors (Figure

1.4, Appendix A) [12]. Sp1 binds a GC rich region within the *PARP1* promoter and

regulates the basal transcription of *PARP1* [12,23]. However, in rats, the regulation by Sp1 is

inhibited by the binding of nuclear factor 1 (NF1) to the GC rich Sp1 binding site,

blocking the binding of Sp1 to the *PARP1* promoter [25]. Additionally, PARP1 regulates its

own expression through the PARylation of Sp1, reducing the DNA binding ability of Sp1

to its target sequence in the *PARP1* promoter [23]. YY-1 has been shown to regulate the

transcription of *PARP1* through a putative binding site within the *PARP1* promoter [22].

However, this regulation is altered during DNA damage through YY-1 mediated

increases in enzymatic activity of PARP1, but during severe stress, YY-1 is PARlyated

reducing the binding activity of YY-1, subsequently reducing *PARP1* transcription [22].

AP-2 also has a putative binding site within the *PARP1* promoter. A dual regulatory role

has been proposed for AP-2 in which AP-2 is activated by PARP1 and inactivated by

PARylation [21].
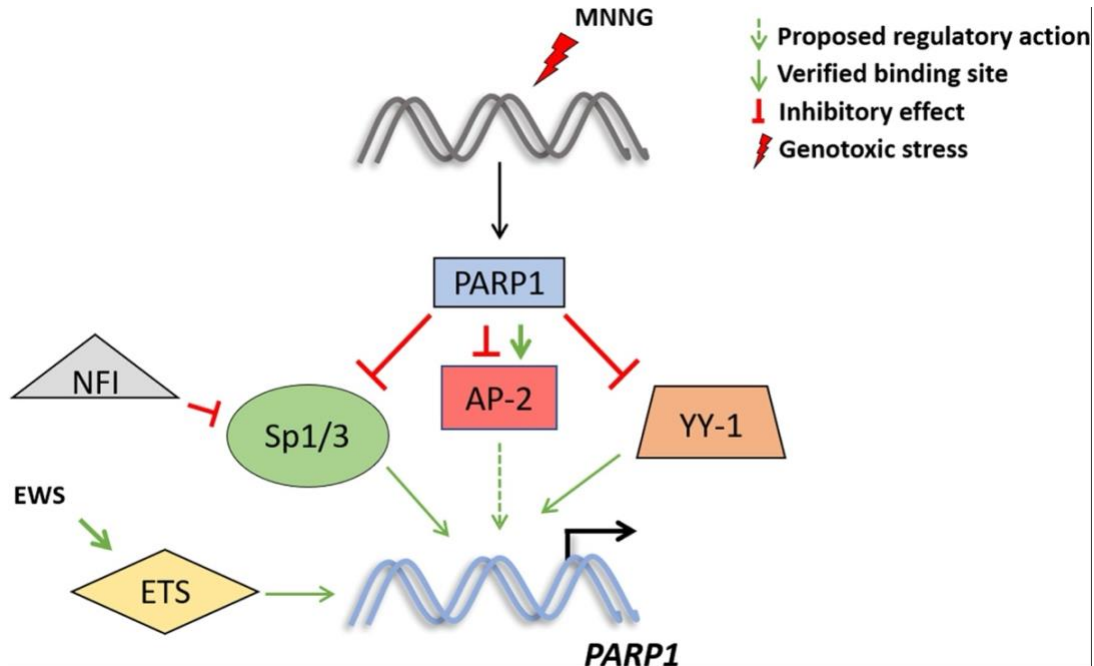


**Figure 1.4.** Poly(ADP Ribose) Polymerase 1 Transcriptional Regulation: Sp1 and Sp3 have been shown to drive the basal transcription of PARP1. A cell specific mechanism has been proposed in Ewing's Sarcoma through the action of ETS. YY-1 drives PARP1 expression but is also regulated itself by PARP1 following DNA damage. A dual regulatory mechanism has been proposed but not verified for AP-2 and NFI has been shown to bind the Sp1 site within the *PARP1* promoter blocking the action of Sp1. This figure was adapted from "Transcriptional dysregulation of base excision repair proteins in breast cancer" published in DNA Repair with the journal's permission provided in Appendix A.

## Base Excision Repair and Cancer

The BER pathway plays a major role in maintaining genomic stability;

thus, single nucleotide polymorphisms (SNPs) in BER proteins and alterations in BER

protein expression occur in multiple cancers [5]. SNPs have been observed in various BER

proteins, including XRCC1 and POL $\beta$. The XRCC1 variant Arg399Gln is associated

with increased risk of prostate cancer and postmenopausal breast cancer [26,27]. Mutations

in POL $\beta$ have been observed in 30% of human tumors. These mutations are not found in

the germline but have functional phenotypes associated with reduced polymerase or lyase

activity [5]. SNPs in APE1 and other DNA glycosylases have also been identified in many

cancers [5]. Beyond mutations, alterations in BER protein expression are also found in

numerous cancers [4,5,28,29]. Elevated XRCC1 expression occurs in gastric, ovarian,

gallbladder, and breast cancers [4,30-32]. Upregulation of XRCC1 alters cisplatin response in

gastric and ovarian cancer, while low expression increases sensitivity to PARP inhibitors

in breast cancer [30-34]. Increased POL $\beta$ expression occurs in breast, colon, and prostate

cancer tissue samples [35].

      Our lab has identified dysregulation of BER proteins in Triple Negative Breast

Cancer (TNBC) cells lines [4]. TNBC accounts for 15-20% of breast cancer cases and is the

deadliest of breast cancer subtypes with high metastasis and recurrence rates [4,36-38].

TNBC is characterized by the lack of estrogen receptor (ER) and progesterone receptor

(PR) expression as well as no human epidermal growth factor receptor 2 (HER2)

amplification [4,36-38]. Breast cancer treatment was revolutionized with the discovery of

hormone and targeted therapeutics such as monoclonal antibodies [39]. However, due to the

receptor status, TNBC is unresponsive to molecularly targeted therapies such as

tamoxifen and trastuzumab, which have become mainstay treatment options for hormone

receptor-positive breast cancers and HER2 amplifying breast cancers, respectively [36,39,40].

The lack of these targets results in a primary systemic treatment course for TNBC

consisting of chemotherapeutics used in both the neoadjuvant and adjuvant setting.

Dysregulation of BER in breast cancer requires further investigation due to the

critical role that estrogen metabolism plays in the promotion as well as maintenance of

breast cancer [41,42]. Outside of its role in driving breast cancer cell proliferation, estrogen

also presents a problem in maintaining genomic stability [43]. During estrogen metabolism,

reactive oxygen species (ROS) and depurinating adducts are generated [41]. ROS interacts

with DNA bases, resulting in oxidized DNA bases, most commonly guanine due to its

low redox potential, resulting in DNA mutation through non-Watson Crick base pairing

promoting transversion guanine to thymine mutations [44]. BER repairs oxidative DNA

damage by recognizing and removing the damaged base with specific DNA glycosylases

[6,44]. Metabolism of estrogen also results in the formation of depurinating estrogen-DNA

adducts, ultimately resulting in the formation of abasic sites on DNA. APE1 then

recognizes abasic sites, promoting the formation SSBs, which are then repaired by the

overlapping BER and single-strand break repair pathways [2,3].

Our lab has identified dysregulation of BER proteins including XRCC1, POL $\beta$,

and PARP1 in TNBC cell lines, the most aggressive form of breast cancer [4].

Additionally, dysregulation of these BER factors resulted in a varied response to MMS

and other DNA damaging agents [4,37].


**Signal Transducer and Activator of Transcription 3 (STAT3)**

The signal transducer and activator of transcription (STAT) family is a seven-

member group of transcription factors: STAT1, STAT2, STAT3, STAT4, STAT5a,

STAT5b, and STAT6. STAT1 is associated with increased tumor suppression signaling, including interleukin 12 (IL-12) and interferon gamma (IFN$\gamma$); thus, increased STAT1 activation in multiple cancer is associated with better clinical outcomes [45,46]. Like STAT1, STAT2 plays a tumor-suppressive role. This has been illustrated by increased tumor formation in STAT2-deficient mice [46,47]. STAT3 is the only STAT family transcription factor whose deletion is embryonically lethal [46]. STAT3 is highly associated with cancer growth, immune evasion, metastasis, and cancer development. It is widely regarded as an oncogene with aberrant activation of STAT3 occurring in 70% of human cancers, including breast cancer [46]. High STAT3 activation is associated with poor clinical outcomes [46]. Although its role in cancer is not widely studied, increased expression of STAT4 is a positive prognostic factor in breast, ovarian, and gastric cancer [46]. STAT5 consists of two proteins that share 94% homology, STAT5a and STAT5b. STAT5 has been described to have both tumor-suppressing and tumor-promoting roles. STAT5 serves as a poor prognostic marker in prostate cancer and is associated with migration and invasion [46]. However, in breast cancer, STAT5a and STAT5b have a tumor-suppressive role, and high expression serves as a positive prognostic marker [46]. Increased STAT6 expression is associated with poor clinical outcomes through its role in metastasis in breast, prostate, and gastric caners [46].

STAT3 signaling serves as a critical mediator of normal mammary development, in particular the process of involution, the process by which mammary glands undergo massive cell death and remodeling returing to the pre-preganant state [48]. STAT3 has been widely described as a cancer-promoting oncogene by regulating target genes associated with multiple cancer-associated processes, including anti-apoptosis, proliferation,

angiogenesis, and metastasis. These target genes include c-MYC, BCL-2, Cyclin D1,

Vimentin, VEGF-A, IL-6, and survivin, which are detailed further in [49].
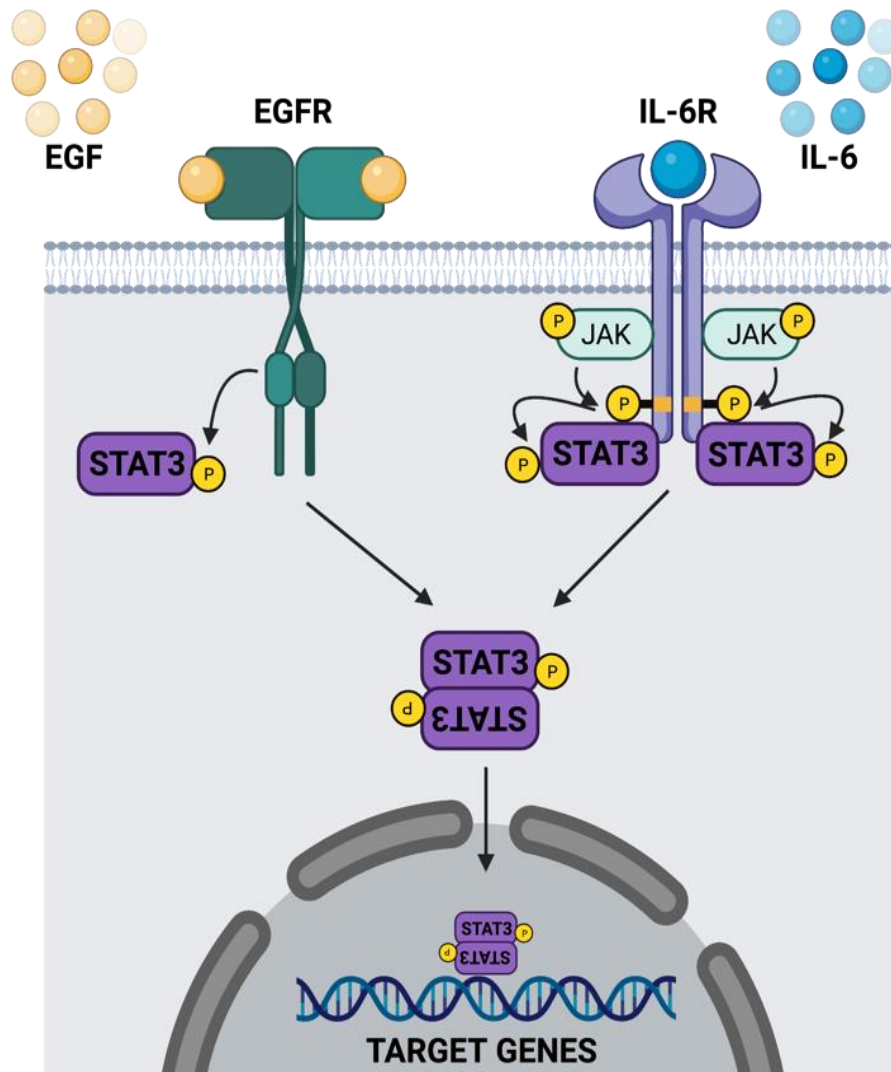


**Figure 1.5.** Canonical STAT3 Signaling STAT3 is activated by multiple cytokines, growth factors, and inflammatory associated signaling pathways. Canonically STAT3 is activated through the binding IL-6 to the IL-6R resulting in the activation and phosphorylation of JAK and STAT3. Additionally, STAT3 is activated through the binding of EGF to EGFR resulting in STAT3 phosphorylation. Following phosphorylation, STAT3 dimerizes and shuttles into the nucleus, binding the consensus sequences within its target genes. This Figure was generated using Biorender.com with citation provided in Appendix B.

Constitutive activation of STAT3 through sustained phosphorylation of the Y705 residue has been documented in numerous cancer types, including breast cancer [45,50]. Canonical signaling of STAT3 involves the binding of cytokines and growth factors, including IL-6 and epidermal growth factor (EGF) to their respective receptors (Figure 1.5, Appendix B) [50-53]. Following ligand binding, receptor-associated Janus kinases (JAKs) are activated and undergo transphosphorylation of the cytoplasmic tail of the receptor [51]. Tyrosine phosphorylation serves as a docking site for unphosphorylated STAT3 [51]. STAT3 is then phosphorylated at Y705 and subsequently homodimerizes. [51]. Homodimerized STAT3 then undergoes nuclear translocation where it can bind target sequences on genes through the action of the DNA binding domain [51,53].

STAT3 is constitutively activated in 40% of breast cancer cases [50-53]. Among the breast cancer subtypes or subclasses with constitutively activated STAT3 is TNBC. TNBC most commonly gains constitutive activation of STAT3 through sustained autocrine and paracrine signaling of IL-6 [50]. STAT3 phosphorylation is tightly regulated through a series of negative regulators, including suppressors of cytokine signaling (SOCS), protein inhibitor of activated STAT (PIAS), and various phosphatases [50,54]. During constitutive activation of STAT3, a breakdown in these negative regulators occurs, allowing for sustained signaling promoting STAT3 signaling [50,54].

The following work aimed to investigate transcriptional dysregulation of BER proteins XRCC1, POL $\beta$, and PARP1 in TNBC and determine whether the mechanism of transcription regulation translated to other tissues. I hypothesize that STAT3 regulates BER proteins XRCC1, POL $\beta$, and PARP1 promoting the dysregulation of BER. The

constitutive activation and transcriptional activities of STAT3 made it a unique potential

regulator for BER factors in TNBC and likely other cancers.

# CHAPTER II: STAT3 SERVES AS A NOVEL TRANSCRIPTIONAL REGULATOR OF XRCC1

## Introduction

There are significant gaps in our understanding of the transcriptional regulation of multiple BER proteins, XRCC1, POL $\beta$, and PARP1. As noted, two transcription factors have been identified to regulate XRCC1 expression- Sp1, the basal regulator of XRCC1, and E2F1, the cell cycle-associated transcription factor [13,14]. XRCC1 serves as a critical scaffold protein in the BER pathway coordinating and facilitating other BER factors, including POL $\beta$ and DNA LIGIII$\alpha$. Outside of BER, XRCC1 has also been implicated in other DNA repair pathways, including nucleotide excision repair and alternative non-homologous end joining [55-58]. XRCC1 is ubiquitously expressed in most tissues, and knockout of XRCC1 is embryonically lethal in mice [59-61]. Overexpression of the BER protein XRCC1 has been observed in breast cancers, including TNBC.

Breast cancer is the second most diagnosed cancer in women in the United States, accounting for 42,000 new cancer cases in 2017. Triple Negative Breast Cancer (TNBC) accounts for 15-20% of breast cancer cases and is the deadliest of breast cancer subtypes with high metastasis and recurrence rates [4,36-38]. TNBC is characterized by the lack of estrogen receptor (ER) and progesterone receptor (PR) expression as well as no human epidermal growth factor receptor 2 (HER2) amplification [4,36-38]. Targeted therapeutics for hormone receptors and related enzymes have revolutionized breast cancer treatment [39]. However, the receptor status of TNBC makes it unresponsive to molecularly-targeted therapies such as tamoxifen and trastuzumab, which have become mainstay treatment

options for hormone receptor-positive breast cancers and HER2 amplified breast cancers, respectively [36,39,40]. For TNBC, the primary treatment course consists of neo-adjuvant DNA damaging chemotherapeutics following surgical resection and radiation. The Cancer Genome Atlas (TCGA) expression portal UALCAN shows a significant increase in XRCC1 transcripts per million in TNBC samples compared to normal breast samples [62]. Overexpression of XRCC1 has been shown to increase resistance to the first-line chemotherapeutics, including cisplatin [30-33,63]. Conversely, low XRCC1 expression increases the efficacy of PARP inhibitors [33,34]. As a result, a greater understanding of the transcriptional regulation of *XRCC1* would provide a biomarker or a therapeutic target to increase cancer cell killing. However, our knowledge about transcription factors driving this overexpression is currently lacking.

STAT3, an oncogene, is a transcription factor that regulates a host of cancer-related genes, including those involved in inflammation [49]. STAT3 is constitutively activated in a host of cancers, including TNBC. In TNBC, autocrine and paracrine production of IL-6 results in sustained activation of STAT3 [50]. This is further exacerbated due to the critical role STAT3 as in the regulation of the IL-6 gene, meaning STAT3 activation results in a positive feedback loop further increasing STAT3 activation [49,50,64]. Additionally, autonomous production of IL-6 occurs in TNBC tumor cells [50,64]. Here, we identify STAT3 as a novel regulator of XRCC1 in TNBC, providing a potential mechanism driving resistance to DNA damaging chemotherapeutics. The results presented here were adapted from "Activated STAT3 Is a Novel Regulator of the *XRCC1* Promoter and Selectively Increases XRCC1 Protein Levels in Triple Negative Breast

Cancer" published in International Journal of Molecular Sciences with the journal's permission provided in Appendix A [65].


## Material and Methods

### Chemicals

Alantolactone was acquired from Selleckchem (Selleckchem #S8318) and resuspended in anhydrous DMSO to a concentration of 15mM. Carboplatin was acquired from Sigma (Sigma #C2538) and resuspended in molecular grade water. A solution of Doxorubicin in DMSO was obtained from Selleckchem (Selleckchem #S1208).

### Cell Culture

MDA-MB-231(MDA-231), MDA-MB-468 (MDA-468), and HEK293T were purchased from the American Type Culture Collection (ATCC HTB-26, HTB-132, and CRL-3216, respectively; Manassas, VA, USA) within the last 24 months and passaged < 15 times for all experiments. Cells were tested biweekly during experiments for mycoplasma contamination using the Lonza MycoAlert® (Lonza #LT07-318). MDA-231 and MDA-468 cells were grown in DMEM High Glucose + GlutaMAX™ (Life Technologies, Carlsbad, CA, USA, #10566016) and supplemented with 1% sodium pyruvate (Life Technologies, #11360070) and 10% FBS (Premium Select, R&D systems, Minneapolis, MN, USA). HEK293T cells were grown in DMEM High Glucose + L-Glutamine (HyClone, Logan, UT, USA, # SH30022.01) and supplemented with 1%

sodium pyruvate (Life Technologies #11360070) and 10% FBS. Cells were maintained in a humidified 37 °C incubator with 5% carbon dioxide.

## Promoter Luciferase Reporter Assay

Transcriptional activity at the *XRCC1* promoter was measured using a dual promoter-luciferase assay similar to those previously reported [14,65]. The pGL3 plasmid containing the full-length *XRCC1* promoter from Chen et al. was provided by Dr. Charles Lopez (Oregon Health Sciences University, Portland, OR, USA). XRCC1 promoter fragments XRCC1, Δ766, Δ612, Δ310, and Δ35 were cloned using *XRCC1* promoter-specific primers from genomic DNA harvested from MDA-231 cells. Promoter PCR fragments were digested with NheI Anza™ (Thermo Fisher Scientific, Waltham, MA, USA, #IVGN0066) and NcoI Anza™ (Thermo Fisher Scientific#IVGN0026) and then ligated into a pGL3 plasmid backbone with Anza™ T4 DNA Ligase (Thermo Fisher Scientific #IVGN2104). The final plasmid constructs with the correct promoter fragment insertion were confirmed by Sanger sequencing by Eurofins. MDA-231 cells were transfected with 0.4 μg of plasmid DNA and 0.1 μg of pRSV β galactosidase plasmid DNA using Jetprime (Polyplus transfection, New York, NY, USA, #114−15, 1:6). HEK293T cells were transfected with 0.4 μg of plasmid DNA and 0.1 μg of pRSV β galactosidase plasmid DNA (Promega, Madison, WI, USA) using Jetprime transfection reagent (1:2). pGL3 was used as a negative control to ensure the assay worked correctly. Using the β-Galactosidase Enzyme Assay System with Reporter Lysis Buffer (Promega #E2000) and the Luciferase Assay System (Promega #E1500), transfected cells were lysed 24 h after transfection, and luminescence and absorbance were collected using an Infinite® M1000 PRO, TECAN (Mannedorf, Switzerland). Luminescence values were

normalized to the respective β-galactosidase absorbance to control for transfection efficiency. The assay was performed in parallel plates in technical triplicate over three biological replicates. Results represent the average of the three biological replicates ± standard error of the mean (SEM).

## *In Silico* Transcription Factor Search

Potential transcription factor targets for the *XRCC1* promoter were identified using multiple *in silico* softwares. First, an Encode database search was performed to identify transcription factors binding the promoters of interest. CiiiDER (www.ciiider.org) was used to identify potential transcription factor binding sites. IgV browser was used to further identify potential transcription factor binding sites.

## Transcription Factor Binding Plate

Potential transcription factors binding the *XRCC1* promoter were identified using the transcription factor binding array (Signosis Santa Clara, CA, USA #FA-1001-NE). Following the manufacturers' instructions, nuclear extracts were isolated from MDA-231, and the binding of transcription factors was tested using the *XRCC1* full length and *XRCC1* Δ35 PCR products described in the promoter-luciferase sections. The promoter binding ELISA was performed with two biological replicates, using Sp1 as a positive binding control.

## Chromatin Immunoprecipitation

MDA-231, MDA-468, and HEK293T cells were grown to confluency in a 150 mm dish. The cells were crosslinked by adding 1% formaldehyde in DMEM with gentle rocking at room temperature (RT ~23 °C) for 8–10 min. Then, 0.1 M glycine was added for 5 min at RT to quench the formaldehyde. The cells were washed with cold 1×

phosphate-buffered saline (PBS) and subsequently lysed with 1 mL of farnham lysis buffer (5 mM HEPES pH 8.0, 85 mM KCl. 0.5% NP-40) for 20 min on ice, then pelleted by centrifugation at 2000 rpm and resuspended in RIPA buffer (50mM Tris-HCl pH 8, 150mM NaCl, 1% sodium deoxycholate, 1mM EDTA, 0.1% SDS, 1% Triton X-100) for 20 min. Isolated chromatin was then sonicated on ice at an amplitude of 12 on a Misonix S-4000 with 15 s on/50 s off for a total process time of 2.5 min for MDA-231 and MDA-468 and amplitude of 10 on a Misonix S-4000 with 15 s on/50 s off for a total process time of 3.5 min for HEK293T. Chromatin was incubated overnight at 4 °C on a rotator using an anti-STAT3 antibody diluted to manufacture's recommendations for chromatin immunoprecipitation (Cell Signaling Technology, Danvers, MA, USA #9131S), an anti-Sp1 antibody (Abcam Cambridge, MA, USA #ab13370) diluted 1:100 as a positive control, a mouse IgG isotype control (Cell Signaling Technology #5415S) and with Protein A/G magnetic beads (Thermo Fisher Scientific #88802). Magnetic beads were washed with cold LiCl wash buffer (100 mM Tris-HCl, 500 mM LiCl, 1% NP-40, 1% Triton X-100) and TE Buffer (10mM Tris-HCl pH 7.5, 0.1mM EDTA). Proteinase K (VWR Life Science Radnor, PA, USA # E195-5ML) was then added with ChIP Elution Buffer (1% SDS, 0.1 M $NaHCO_3$) and incubated at 65 °C 950 rpm for 2 h. Proteinase K was then inactivated at 90 °C for 10 min. DNA was purified using a PureLink PCR Purification Kit (Life Technologies #K310002 kit). An IgV browser was used to design primers examining the occupancy across the *XRCC1* promoter.

## Western Blotting

Briefly, the cells were grown in 150 mm dishes and cultured to 70–80% confluence. Cells were rinsed with PBS, scraped, stored overnight at −80 °C, then lysed.

Protein content was quantified using a Bradford assay. Then, 20 µg of lysate was separated on 7.5% or 4–15% SDS Page gel (Bio-Rad #s, 4561025 and 4561084) and transferred to a nitrocellulose membrane. Membranes were blocked in 5% non-fat dry milk in Tris-buffered saline (VWR #J640-4L) containing 0.1% Tween20 (Thermo Fisher Scientific #BP337, TBS-T) and raised against the following primary antibodies: XRCC1 (1:1000 #MS434P1) from Fisher Scientific (Pittsburgh, PA, USA); STAT3 (1:1000, #9139) and pSTAT3 Y705 (1:500, #9131) from Cell Signaling Technology, Inc.; and α-tubulin (1:5000, #T9026) from Millipore Sigma (St. Louis, MO, USA). The blots were incubated with either of the horseradish peroxidase (HRP)-labeled secondary antibodies: goat anti-rabbit-HRP or goat anti-mouse-HRP (#7074P2 and #7076S respectively) from Cell Signaling Technology, Inc. HRP antibody target proteins were detected by incubating with WesternBright Sirius (Advansta San Jose, CA, USA #K-12043-D20). All immunoblotting was conducted with three biological replicates. Where indicated, protein quantification was conducted with Image Lab Software (Bio-Rad, Hercules, CA, USA). Band intensity was normalized to loading controls and averaged over the three biological replicates with SEM presented.

## Gene Expression and qPCR

Relative gene expression was performed through mRNA isolation from MDA-231, MDA-468, and HEK293T cell lines using Invitrogen Cell to $C_t$ kit (Life Technologies #4399002). Following the manufacturers' recommendations, the cells were plated in a 96-well plate, and the untreated cells were grown to 75% confluency. For transfection, 0.1 µg of plasmid DNA was added with Fugene 6 transfection reagent in a 1:6 ratio (plasmid DNA to Fugene). Cells were then allowed 48h to recover before being

lysed for mRNA isolation using an Invitrogen Cell to $C_t$ kit (Life Technologies #4399002). The cells were then lysed, and RT-PCR was performed to produce cDNA using the reagents from the kit. After cDNA synthesis, qPCR was performed using TaqMan Gene expression primers XRCC1 (Hs00959834_m1 FAM), STAT3 (Hs00374280_m1 FAM), and Actin (Hs01060665_g1 VIC) and the TaqMan master mix provided with the kit (Applied Biosystems Foster City, CA, USA #4369016). The assay was performed in technical triplicate over three biological replicates. Results represent the average of the three biological replicates ± standard error of the mean (SEM).

**Modulation of STAT3**

Plasmid constructs for stable depletion of human STAT3 mRNA, pSIH-puro-STAT3 shRNA (referred two as shRNA #1), and its control were gifts from Frank Sinicrope (Addgene plasmid #26596 and #26597; Watertown, MA, USA). An additional shRNA construct specific for STAT3 (shRNA Clone ID:NM_003150.3-458s21c1 referred to as shRNA #2 hereafter) and the pLKO.1 control were purchased from Sigma-Aldrich (St. Louis, MO, USA). Both shRNA constructs and their controls were used to validate the STAT3 binding site and expression changes. MDA-231 cells were plated at 200,000 cells/well in a 6-well culture plate. After 48 h, cells were transfected with 5 µg plasmid DNA (shRNA# 1 or 2 or appropriate vector control) and FuGene 6 (Promega) at a 1:6 ratio (DNA to FuGene). Cells were allowed to recover for 48h following transfection. STAT3 was overexpressed using a pcDNA3.1+ STAT3 ORF clone from Genscript (Piscataway, NJ, USA) with a C-terminal Flag-tag. MDA-231 cells were plated at 200,000 cells/well in a 6-well culture plate, and HEK293T were plated in 10 cm plates at 500,000 cells/plate. After 48 h, MDA-231 cells were transfected with 5 µg of plasmid

DNA (STAT3-FLAG and proper vector control) and Fugene 6 (Promega) in a 1:6 ratio (DNA to Fugene). HEK239T cells were transfected with 10 μg of plasmid DNA (STAT3-FLAG and proper vector control) and Jetprime transfection agent at a 1:2 ratio (DNA to Jetprime). 48 h post-transfection, cells were rinsed with 1X PBS, plates were scraped, and the pelleted cells were stored overnight at −80 °C. Immunoblot was then performed as described below.

## Cytokine and Growth Factor Exposure

Cytokine exposure was performed using recombinant Human IL-6 protein (R&D Systems, Minneapolis, MN, USA, #206-IL-010/CF). IL-6 was aliquoted in PBS at 100 μg/mL concentration and stored at −80 °C for no longer than three months before use, as recommended by the manufacturers. Aliquoted IL-6 and EGF were added to the cell culture medium to a final concentration of 50ng/mL and 30ng/mL, respectively. MDA-231 and HEK293T cells were plated in 15 mm dishes and cultured to 70–80% confluency. Cells were then exposed to IL-6 at a final concentration of 50ng/mL for 30 min, 1 and 4 h, and EGF at a final concentration of 30ng/mL for 1, 4, and 24 h. Cells rinsed with 1X PBS plates were scraped, and pelleted cells were stored overnight at −80 °C. Immunoblot was performed as described above.

## XRCC1-RFP Cloning

Stable transfection of XRCC1-RFP overexpressing clones was accomplished using Fugene 6 transfection agent as described above. Briefly, cells were plated in a 6 well dish allowing 24 h to adhere. Cells were then transfected with XRCC1-RFP vectors, allowing 48 h to recover. Following recovery, puromycin selection medium was then added to cells. Following selection, cells were transferred to a 96-well culture dish at a

density of 1 cell-per-well and maintained in puromycin selection medium. Single-cell colonies were then expanded and frozen in liquid nitrogen. XRCC1-RFP transfection into MDA-231 clones was confirmed using immunoblot.

## Growth Inhibition Assay

Cell counts were aquired for XRCC1-RFP using cell counting and STAT3-FLAG using Cell-titer Glo® (Promega #G7570). For growth inhibition using cell counting, cells were plated at a density of $2X10^4$ (MDA-231) in 12 well-dishes and allowed 48 h to adhere. Stably transfected MDA-231 XRCC1-RFP and parental MDA-231 cells were then treated with 5,10, 20, and 40 $\mu$M carboplatin and 10,25,50, 75, and 100nM doxorubicin. Cells were allowed to recover for 5 days before being trypsinized and resuspend in 1mL of PBS. Resuspended cells were counted using BioRad TC10 Automated Cell Counter. Cell counts were performed in triplicate normalized to control wells for a total of three biological replicates. Values were plotted as mean $\pm$ standard error of mean (SEM). Cell Titer Glo was performed per the manufacture's instruction. Briefly, cells were plated $(2X10^3)$ in a 96 well cell culture dishes, allowing 24 h to adhere. Cells were then transiently transfected as described above with STAT3-FLAG expression vectors. 50ng/mL IL-6 was predosed 30 min prior to challenge with carboplatin followed by continuous 50ng/mL IL-6 dosing in MDA-231. Cells were then dosed with 0, 50, 100, 250, 500, and 1000$\mu$M carboplatin. Luminescence was then collected using an Infinite® M1000 PRO, TECAN (Mannedorf, Switzerland).

## Statistical Analysis

Assays were performed as three biological replications. One-way ANOVA and means were compared with Dunnett's post hoc analysis. Comparison groups are indicated

in graphs. All means are reported $\pm$ SEM. $* p < 0.05$, $** p < 0.01$, $*** p < 0.001$, $**** p < 0.0001$.

## Results

### A novel regulatory site exists in the *XRCC1* promoter

A promoter-luciferase assay was performed first to assess the potential for a novel regulator of XRCC1. PCR fragments from sequential segments of the *XRCC1* promoter were cloned and inserted into a pGL3 plasmid. Luminescence collected from MDA-231 and HEK293T revealed a potential novel regulatory site not associated with either previously identified transcription factor, E2F1 and Sp1 (Figure 2.1). These findings showed sustained luminescence through the -310 site, differing from those previously

reported in the SAOS2 osteosarcoma cell line [14]. With these findings, we next wanted to

investigate the potential for a novel transcription factor binding the *XRCC1* promoter.
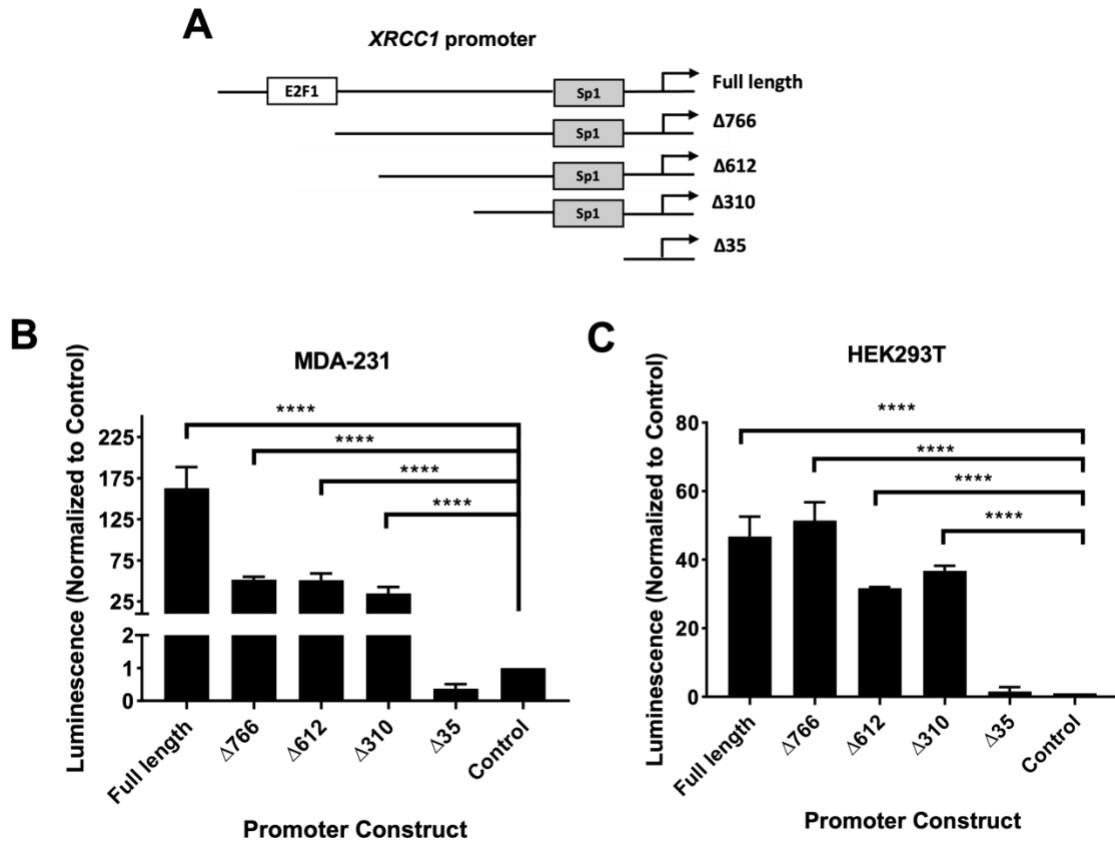


**Figure 2.1**. Reporter assay indicates a novel regulatory region in *XRCC1*. A) *XRCC1* promoter fragments with known transcription factor sites inserted into the pGL3 luciferase reporter. B) Reporter plasmids were transfected into MDA-231 and luminescence read after 24 h. C) Reporter plasmids were transfected into HEK293T and luminescence read after 24 h ****$p<0.0001$. This figure was adapted from "Activated STAT3 is a Novel Regulator of the *XRCC1* Promoter and Selectively Increases XRCC1 Protein Levels in Triple Negative Breast Cancer" published in IJMS with the journal's permission provided in Appendix A.

## The *XRCC1* promoter contains a STAT3 binding site

Using a transcription factor binding ELISA, potential transcription factor candidates were identified.
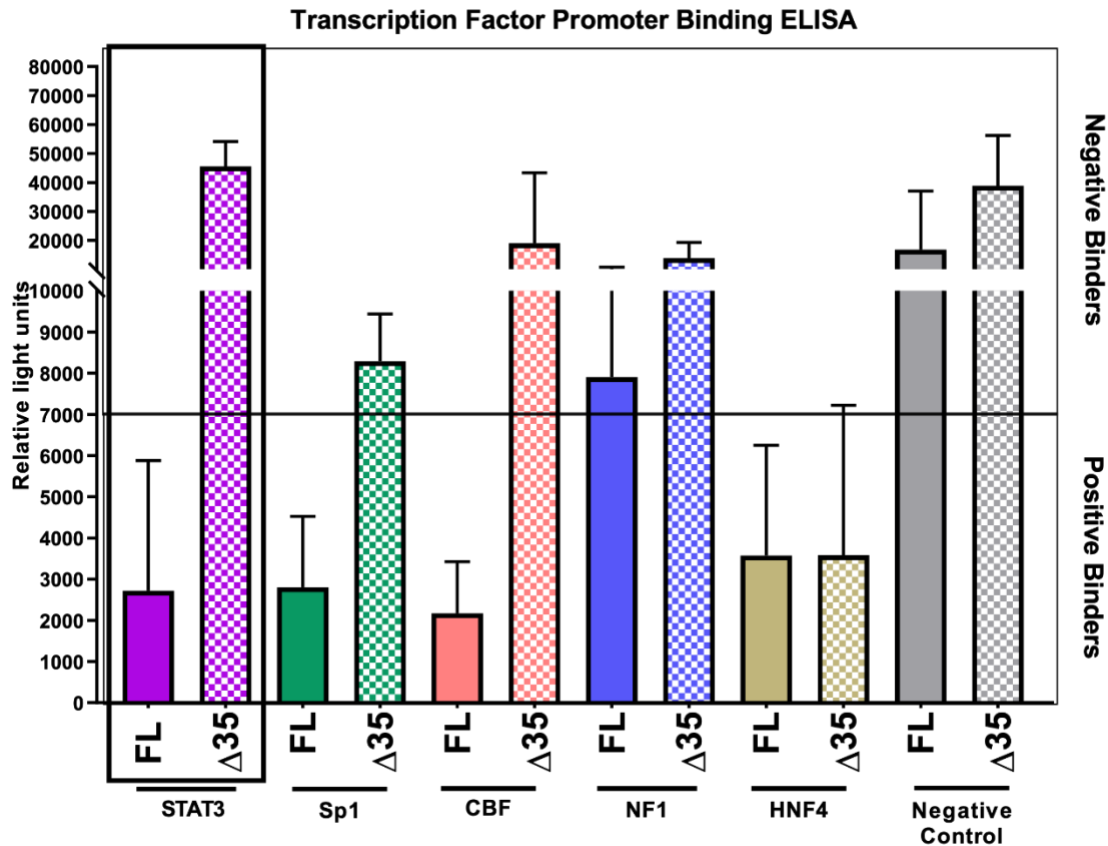


**Figure 2.2**. Promoter Binding ELISA Identifies STAT3. A) Full Length (FL) and Δ35 luminescence in specific transcription factor coated wells; STAT3, Sp1, CBF, NF1, HNF4, and a Negative control.

Binding to the *XRCC1* full length promoter (FL) occurred in several transcription factors, including Sp1 (positive control), CBF, NF1, HNF4, and STAT3 (Figure 2.2). To further explore the potential transcription factors acquired from the ELISA, *in silico* searches were performed using IgV Browser and CiiiDER. IgV browser uses publicly

26

available ChIP seq data from the Encode database to show potential DNA binders and histone modification to the genome at genes of interest. CiiiDER is a predictive tool to identify transcription factor binding sites within a DNA region of interest. IgV browser searches revealed a potential STAT3 binding site within the *XRCC1* promoter corresponding to the region identified from the promoter-luciferase assay. This potential STAT3 binding site was further affirmed through the input of the *XRCC1* promoter into the CiiiDER program.

Now armed with a potential transcription factor and a region of interest, we sought to confirm the binding site within the *XRCC1* promoter. Using ChIP, the binding of STAT3 to the *XRCC1* promoter was mapped in the MDA-231 (Figure 2.3). A significant enrichment above the IgG control was seen at a region corresponding to the sequence identified by the promoter-luciferase assay and *in silico* searches. The highest enrichment occurred at a 96 base pair region -452 to -358 ($2.426 \pm 0.11$), downstream of the E2F1 binding site but upstream of the Sp1 binding. Sp1 was used as a positive control, and a non-binding region in the genome was selected as a negative control to ensure the experiment was performed with high fidelity. MDA-468 also showed a significant enrichment at the same 96 base pair region ($1.826 \pm 0.066$). The binding of STAT3 to the *XRCC1* promoter was attenuated following shRNA-mediated knockdown of STAT3 in MDA-231 ($0.868 \pm 0.11$) compared to the respective vector control ($1.67 \pm 0.14$). Analysis of the 96 base pair region revealed a potential consensus binding

sequence for STAT3. Together these data show that STAT3 binds to the *XRCC1* promoter. We next wanted to explore the role that STAT3 has in regulating XRCC1.
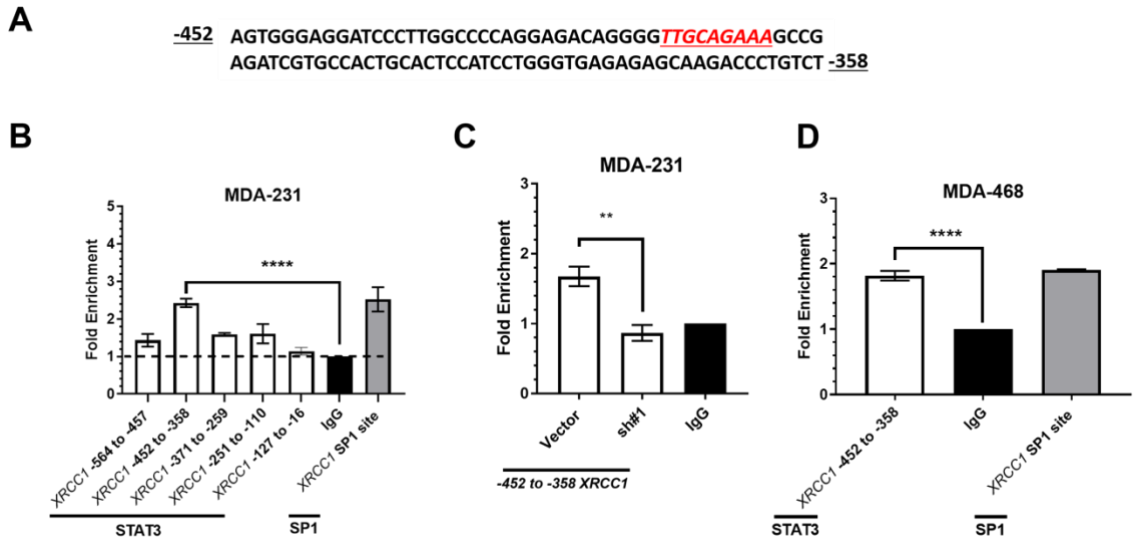


**Figure 2.3**. The *XRCC1* promoter contains a STAT3 binding site. A) The CiiDER identified STAT3 binding sequence within the *XRCC1* promoter (red font). B) CHiP analysis of XRCC1 promoter in MDA-231 cells show a significant enrichment of STAT3 between -452 and -358. C) Knockdown of STAT3 with shRNA #1 eliminates the STAT3 binding within the -452 to -358 fragment. D) STAT3 binding also occurs within the -452 to -358 fragment of the *XRCC1* promoter in MDA-468 cells. **p< 0.01, ****p<0.0001. This figure was adapted from "Activated STAT3 is a Novel Regulator of the *XRCC1* Promoter and Selectively Increases XRCC1 Protein Levels in Triple Negative Breast Cancer" published in IJMS with the journal's permission provided in Appendix A.

## Modulation of STAT3 results in attenuated XRCC1 expression

To test the role that STAT3 plays in the regulation of XRCC1, we first performed an shRNA-mediated knockdown of STAT3 using two different shRNA constructs to control for potential off-target effects.

**Figure 2.4**. shRNA knockdown of STAT3 reduces the expression of XRCC1 in MDA-231 cells. A) Representative immunoblots of phospho-STAT3 (Y705), STAT3 and XRCC1 protein expression following shRNA mediated knockdown of STAT3. α-tubulin is used as a loading control. B) Quantification of protein expression changes in XRCC1 resulting from shRNA-mediated knockdown of STAT3. C) Quantification of *XRCC1* mRNA expression following shRNA-mediated knockdown of STAT3. *p< 0.05, **p< 0.01, ***p<0.001, ****p<0.0001. This figure was adapted from "Activated STAT3 is a Novel Regulator of the *XRCC1* Promoter and Selectively Increases XRCC1 Protein Levels in Triple Negative Breast Cancer" published in IJMS with the journal's permission provided in Appendix A.

**Figure 2.5**. shRNA knockdown of STAT3 reduces the expression of XRCC1 in MDA-468 cells. A) Representative immunoblots of phospho-STAT3 (Y705), STAT3 and XRCC1 protein expression following shRNA mediated knockdown of STAT3. α-tubulin is used as a loading control. B) Quantification of protein expression changes in XRCC1 resulting from shRNA-mediated knockdown of STAT3. C) Quantification of *XRCC1* mRNA expression following shRNA-mediated knockdown of STAT3. $*p < 0.05$, $**p < 0.01$, $***p<0.001$, $****p<0.0001$ * . This figure was adapted from "Activated STAT3 is a Novel Regulator of the *XRCC1* Promoter and Selectively Increases XRCC1 Protein Levels in Triple Negative Breast Cancer" published in IJMS with the journal's permission provided in Appendix A.

Knockdowns were performed in the MDA-231 and MDA-468. 48 h following shRNA knockdown of STAT3 gene expression analysis and immunoblots were performed to see changes in XRCC1 gene and protein expression, respectively. STAT3 attenuation by shRNA resulted in a significant reduction of *XRCC1* gene expression in MDA-231 (sh#1 $0.506 \pm 0.089$ and sh #2 $0.693 \pm 0.015$) (Figure 2.4) and in MDA-468 (sh#1 $0.626 \pm 0.11$ and sh #2 $0.554 \pm 0.10$) (Figure 2.5), indicating a decrease of XRCC1 associated mRNA. Knockdown of STAT3 resulted in a significant reduction of pSTAT3, the active STAT3 species, total STAT3, and XRCC1 protein expression in MDA-231 (sh#1 0.435

30

± 0.019 and sh #2 0.313 ± 0.063) and MDA-468 (sh#1 0.511 ± 0.066 and sh #2 0.445 ±

0.079). These data indicate a potential role for STAT3 in the regulation of XRCC1.

**Pharmacological inhibition of STAT3 attenuates XRCC1 expression**

Pharmacological inhibition of STAT3 was used to confirm the role that STAT3 plays in

the regulation of XRCC1. The STAT3 inhibitor alantolactone was used at a 15 $\mu$M for 4

and 24 h, which resulted in a significant reduction of pSTAT3. Attenuation of active

STAT3 resulted in a significant reduction of XRCC1 gene expression and protein

expression at 4 h (0.675 ± 0.038 and 0.649 ± 0.051) (Figure 2.6). Inhibition of active

STAT3 in MDA-468 with 15 $\mu$M for 4 h also resulted in a significant reduction of

XRCC1 gene and protein expression (0.758 ± 0.20 and 0.760 ± 0.026).

**STAT3 ectopic expression and exogenous exposures stimulate XRCC1 expression**

Knowing that attenuation of STAT3 through shRNA-mediated knockdown and

pharmacological inhibition resulted in an attenuation of XRCC1 expression, we next set

out to see if stimulation of STAT3 increased XRCC1 expression. STAT3 expression was

increased in MDA-231 cells through the transfection of a STAT3-FLAG ectopic

expression vector. Following transfection, STAT3 and active STAT3 were significantly

increased, resulting in a significant increase in XRCC1 protein expression (2.07 ± 0.19)

(Figure 2.7). STAT3-FLAG transfection also resulted in a significant increase in XRCC1

gene expression compared to the vector control (3.52 ± 0.086). Next, we wanted to test if

increased STAT3 activation resulted in increased XRCC1 protein and gene expression.

We exposed MDA-231 cells to IL-6 and EGF, both of which are known to stimulate

STAT3 activation. Following exposure to IL-6 (50 ng/mL) for 30 min, 1 and 4 h, a non-

significant increase in XRCC1 protein occurred at all time points, but a significant

increase in *XRCC1* gene expression occurred at all three time points (1.81 $\pm$ 0.25, 1.68 $\pm$ 0.14, and 1.66 $\pm$ 0.14 30 min, 1, and 4 h, respectively) (Figure 2.8).
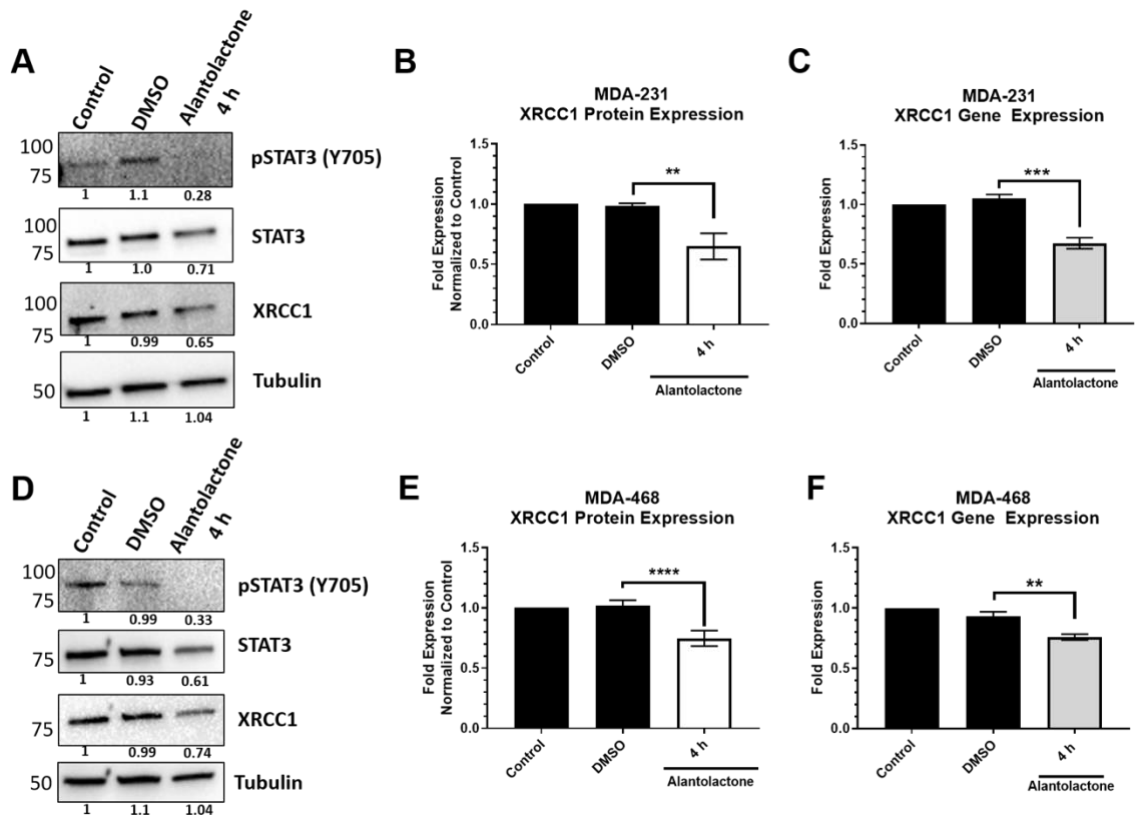


**Figure 2.6.** Chemical inhibition of the phosphorylation of STAT3 at Y705 by alantolactone decreases the expression of XRCC1 in MDA-231 and MDA-468 cells. A) Representative immunoblots of phospho-STAT3 (Y705), STAT3 and XRCC1 protein expression after 4 h exposure to 15 µM alantolactone in MDA-231 cells. α-tubulin is used as a loading control. B) Quantification of protein expression changes in XRCC1 resulting from 4 h alantolactone exposure in MDA-231 cells. C) Quantification of *XRCC1* mRNA expression following 4 h alantolactone exposure in MDA-231 cells. C) Representative immunoblots of phospho-STAT3 (Y705), STAT3 and XRCC1 protein expression after 4 h exposure to 15 µM alantolactone in MDA-468 cells. B) Quantification of protein expression changes in XRCC1 resulting from 4 h alantolactone exposure in MDA-468 cells. C) Quantification of *XRCC1* mRNA expression following 4 h alantolactone exposure in MDA-468 cells. **$p < 0.01$, ***$p < 0.001$, ****$p < 0.0001$. This figure was adapted from "Activated STAT3 is a Novel Regulator of the *XRCC1* Promoter and Selectively Increases XRCC1 Protein Levels in Triple Negative Breast Cancer" published in IJMS with the journal's permission provided in Appendix A.

MDA-231 were exposed to EGF (30 ng/mL) for 1, 4, and 24 h. Subsequent

protein expression revealed an increase in STAT3 activation and an increase active
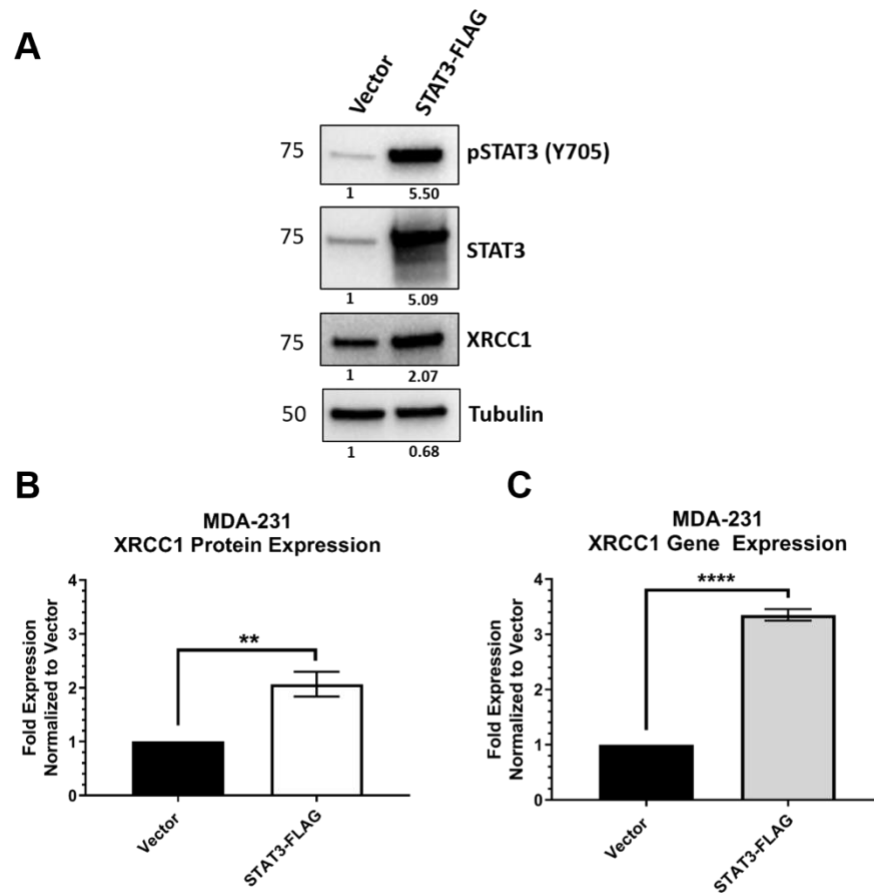


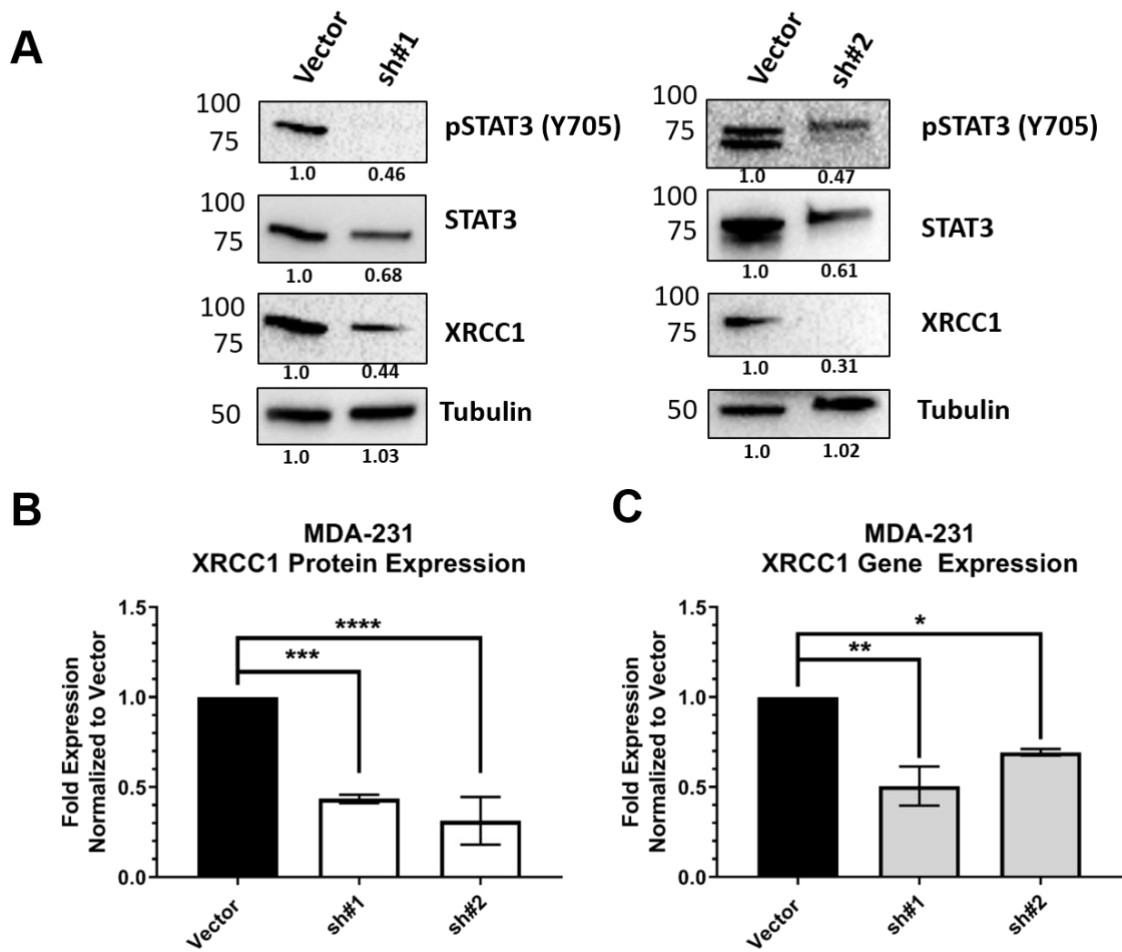**Figure 2.7**. Ectopic overexpression of STAT3 increases the expression of XRCC1 in MDA-231 cells. A) Representative immunoblot of phospho-STAT3 (Y705), STAT3 and XRCC1 protein expression following ectopic expression of STAT3-FLAG. α-tubulin is used as a loading control. B) Quantification of protein expression changes in XRCC1 resulting from ectopic expression of STAT3-FLAG. C) Quantification of *XRCC1* mRNA expression following ectopic expression of STAT3-FLAG. **p< 0.01, ****p<0.0001. This figure was adapted from "Activated STAT3 is a Novel Regulator of the *XRCC1* Promoter and Selectively Increases XRCC1 Protein Levels in Triple Negative Breast Cancer" published in IJMS with the journal's permission provided in Appendix A.
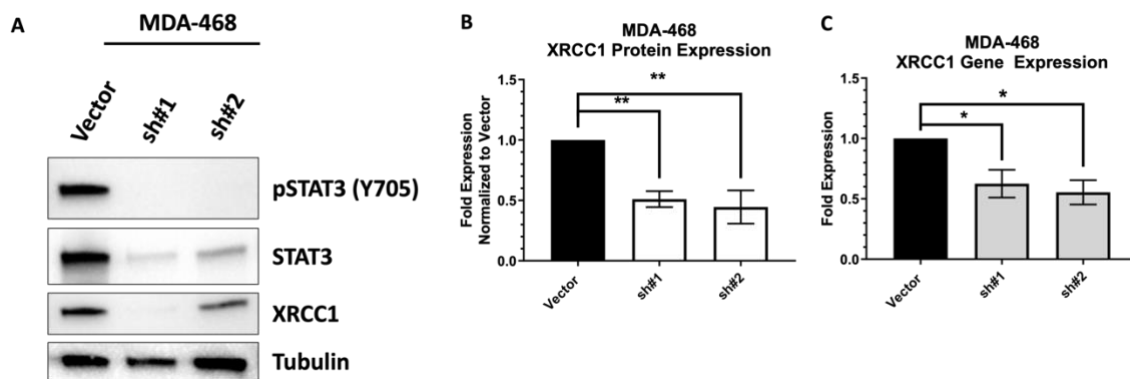
STAT3 expression at 24 h post-EGF exposure, resulting in a significant increase in

XRCC1 expression (1.73 $\pm$ 0.061) (Figure 2.9).
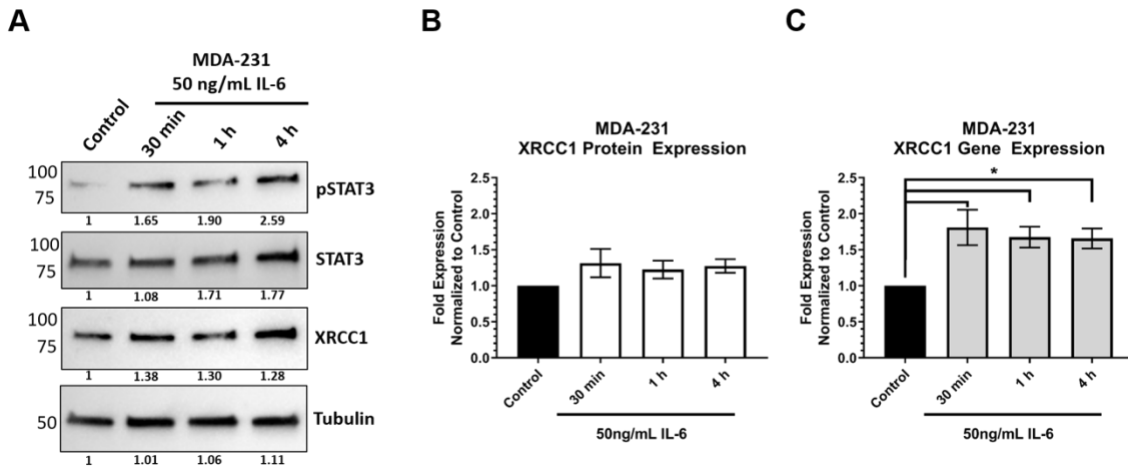


**Figure 2.8**. IL-6 increases phospho-STAT3 and increases the expression of XRCC1 in MDA-231. A) Representative immunoblot of phospho-STAT3 (Y705), STAT3 and XRCC1 protein expression after 1 and 4 h exposure to 50 ng/mL IL-6. $\alpha$-tubulin is used as a loading control. B) Quantification of protein expression changes in XRCC1 resulting from 50 ng/mL IL-6 exposure. C) Quantification of *XRCC1* mRNA expression following 50 ng/mL IL-6 exposure. *p< 0.05. This figure was adapted from "Activated STAT3 is a Novel Regulator of the *XRCC1* Promoter and Selectively Increases XRCC1 Protein Levels in Triple Negative Breast Cancer" published in IJMS with the journal's permission provided in Appendix A.

This also translated to a non-significant increase in *XRCC1* gene expression at all

three time points. Taken together, these data indicate STAT3 regulates XRCC1

expression in TNBC cell lines.
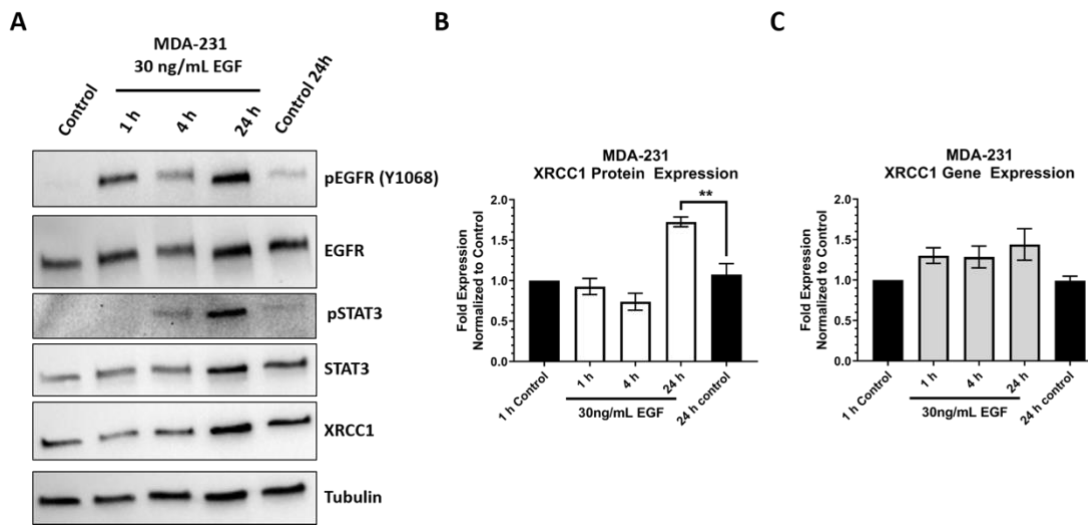
**Figure 2.9**. EGF increases phospho-STAT3 and increases the expression of XRCC1 in MDA-231. A) Representative immunoblot of phospho-EGFR(Y1068), EGFR, phospho-STAT3 (Y705), STAT3 and XRCC1 protein expression after 1, 4, and 24 h exposure to 30 ng/mL EGF. α-tubulin is used as a loading control. B) Quantification of protein expression changes in XRCC1 resulting from 30 ng/mL EGF. C) Quantification of *XRCC1* mRNA expression following 30 ng/mL EGF. **$p < 0.01$. This figure was adapted from "Activated STAT3 is a Novel Regulator of the *XRCC1* Promoter and Selectively Increases XRCC1 Protein Levels in Triple Negative Breast Cancer" published in IJMS with the journal's permission provided in Appendix A.

**STAT3 occupancy of the *XRCC1* promoter occurs only following STAT3 activation**

Because TNBC has constitutively active STAT3, we next wanted to see if the STAT3 regulation of XRCC1 occurred in a TNBC specific mechanism. HEK293T has a lower expression of STAT3 and pSTAT3 and a lower STAT3 occupancy of the *XRCC1* promoter ($1.49 \pm 0.28$) compared to TNBC cell lines MDA-231 ($2.43 \pm 0.19$) and MDA-468 ($1.82 \pm 0.073$) (Figure 2.10). To test if the STAT3 regulatory mechanism of XRCC1 in the HEK293T was inducible, we wanted to stimulate STAT3 activation and STAT3 expression using the STAT3-FLAG ectopic expression vector in the HEK293T. We

found that the STAT3 occupancy of the *XRCC1* promoter significantly increased to the

level seen in the TNBC cell lines MDA-231 ($2.43 \pm 0.19$) and MDA-468 ($1.82 \pm 0.073$)

only following ectopic expression of STAT3 in HEK293T ($3.93 \pm 1.00$) (Figure 2.11).
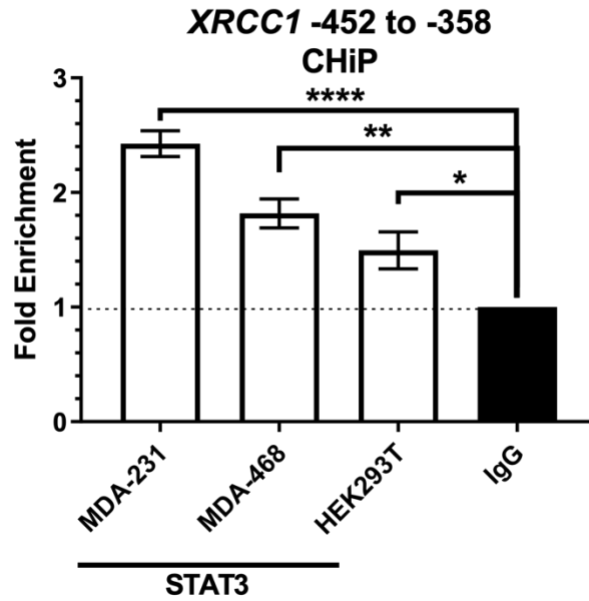


**Figure 2.10**. STAT3 occupancy of the *XRCC1* promoter across cell lines. ChIP analysis
of the *XRCC1* promoter (-452 to -358) in MDA-231, MDA-468, and HEK293T,
normalized to the respective IgG controls *$p<0.05$, **$p< 0.01$, ***$p<0.001$,
****$p<0.0001$. This figure was adapted from "Activated STAT3 is a Novel Regulator
of the *XRCC1* Promoter and Selectively Increases XRCC1 Protein Levels in Triple
Negative Breast Cancer" published in IJMS with the journal's permission provided in
Appendix A.

However, this ectopic expression of STAT3 did not significantly increase the

protein expression of XRCC1 in the HEK293T ($1.03 \pm 0.035$).

**STAT3 regulation of XRCC1 requires stimulation in the HEK293T**
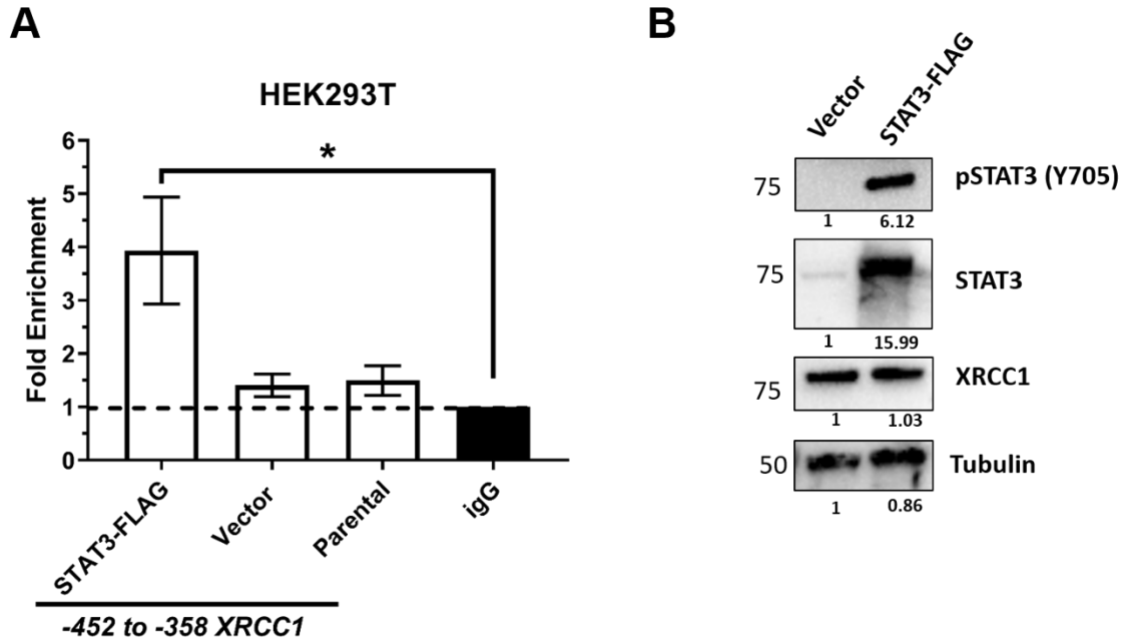


**Figure 2.11**. Ectopic overexpression of STAT3 increases the STAT3 occupancy within the *XRCC1* promoter. A) CHiP analysis of STAT3 binding to the -452 to -358 *XRCC1* promoter fragment. *p< 0.05. B) Representative immunoblots of phospho-STAT3 (Y705), STAT3 and XRCC1 protein expression following ectopic expression of STAT3-FLAG. α-tubulin is used as a loading control *p<0.05. This figure was adapted from "Activated STAT3 is a Novel Regulator of the *XRCC1* Promoter and Selectively Increases XRCC1 Protein Levels in Triple Negative Breast Cancer" published in IJMS with the journal's permission provided in Appendix A.

To further probe the regulatory mechanism occurring in the HEK293T, we next stimulated the cell line using the inflammatory cytokine IL-6. IL-6 stimulates the phosphorylation of STAT3 at the Y705 residue, resulting in homodimerization,

subsequent nuclear translocation, and binding of STAT3 homodimers to target sequences on genes as introduced in Figure 1.5 [53,54].
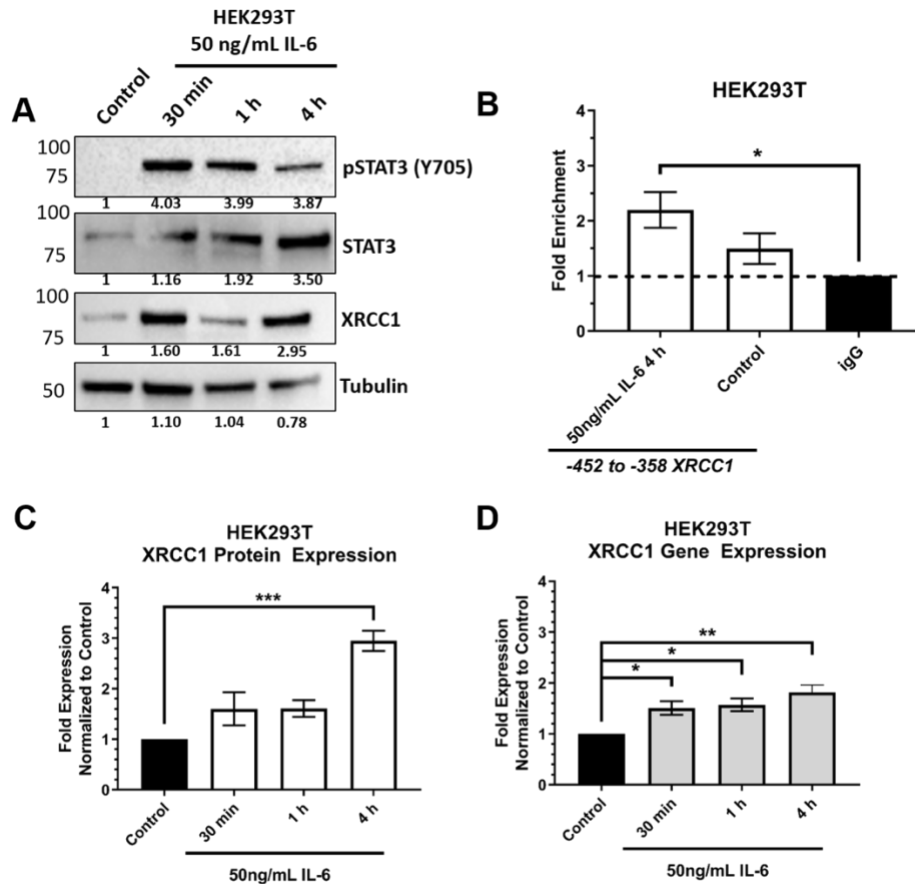


**Figure 2.12**. IL-6 increases phospho-STAT3, increases the occupancy of STAT3 at the *XRCC1* promoter, and increases the expression of XRCC1 in HEK293T. A) Representative immunoblot of phospho-STAT3 (Y705), STAT3 and XRCC1 protein expression after 1 and 4 h exposure to 50 ng/mL IL-6. α-tubulin is used as a loading control. B) CHiP analysis shows IL-6 increases the STAT3 occupancy on the *XRCC1* promoter. C) Quantification of protein expression changes in XRCC1 resulting from 50 ng/mL IL-6. D) Quantification of *XRCC1* mRNA expression following 50 ng/mL IL-6. $*p < 0.05$, $**p < 0.01$, $***p < 0.001$. This figure was adapted from "Activated STAT3 is a Novel Regulator of the *XRCC1* Promoter and Selectively Increases XRCC1 Protein Levels in Triple Negative Breast Cancer" published in IJMS with the journal's permission provided in Appendix A.

HEK293T were dosed with IL-6 (50ng/mL) for 30 min, 1, and 4 h

immunoblotting revealed an increase of pSTAT3 and XRCC1 with a significant peak of

XRCC1 protein occurring at 4 h (mean $\pm$ SEM) and a significant increase in XRCC1

gene expression at all three time points ($1.51 \pm 0.13$, $1.57 \pm 0.13$, and $1.82 \pm 0.15$,

respectively) (Figure 2.12). Because the largest increase in XRCC1 gene and protein

expression occurred at 4 h, HEK293T were exposed to IL-6 (50ng/mL) for 4 h to test for

changes in occupancy of the *XRCC1* promoter. ChIP revealed a significant increase in the

STAT3 occupancy of the *XRCC1* promoter ($2.20 \pm 0.32$) to a level comparable to that

seen in the MDA-231 ($2.43 \pm 0.19$). These data suggest that the constitutive activation of

STAT3 occurring through IL-6 autocrine and paracrine signaling in the TNBC cell lines

promotes dysregulation of XRCC1.

**Overexpression of XRCC1 increases resistance to carboplatin and doxorubicin**

Due to the widely reported role of XRCC1 expression on the modulation of

chemotherapeutic response, we next wanted to test if increased XRCC1 expression

independent of STAT3 could alter carboplatin and doxorubicin response. Using the

ectopic expression vector for XRCC1, XRCC1-RFP, we found a significant increase in

XRCC1 independent of STAT3. Stably transfected XRCC1-RFP MDA-231 cells were

isolated and subjected to increasing concentrations of carboplatin. Two MDA-231

XRCC1-RFP clones, XRCC1-RFP clone 2 and XRCC1-RFP clone 7, showed increased

resistance to carboplatin as indicated by increased $IC_{50}$ values compared to in MDA-231

parental cells (Figure 2.13). Increased resistance was also seen for doxorubicin for

XRCC1-RFP clone 2 compared to MDA-231 parental cells (Figure 2.14).

**Alteration in response to carboplatin following STAT3 modulation**
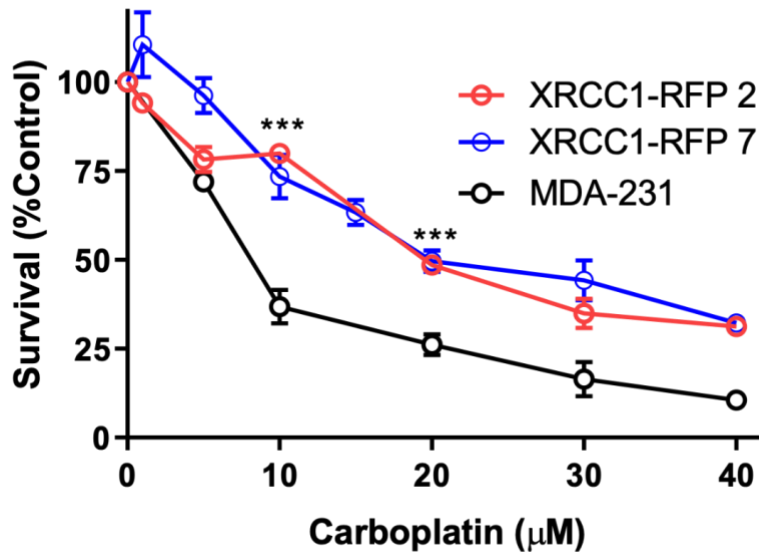


**Figure 2.13**.  Increased expression of XRCC1 results in increased carboplatin resistance independent of STAT3. MDA-231 XRCC1-RFP clones (Clone 2 and Clone 7) were generated and exposed to carboplatin; values are percentage of cell survival compared to untreated controls.

Having found increased resistance to carboplatin with XRCC1 overexpression independent of STAT3, we wanted to test if increased STAT3 and STAT3 activation also resulted in increased resistance to carboplatin. Using the STAT3 ectopic expression vector STAT3-FLAG, STAT3 was overexpressed in MDA-231 cells through the transient transfection. A slight increase in resistance, an increase in $IC_{50}$, to carboplatin,

was seen for STAT3-FLAG transfected cell lines compared to vector controls (Figure

2.15). To test if increased STAT3 activation resulted in increased resistance to

carboplatin, MDA-231 cells were pretreated with 50ng/mL of IL-6 for 30 min then

continuously dosed with IL-6 and carboplatin. IL-6 treatment resulted in a slight increase

in the $IC_{50}$ following carboplatin treatment compared to parental MDA-231.
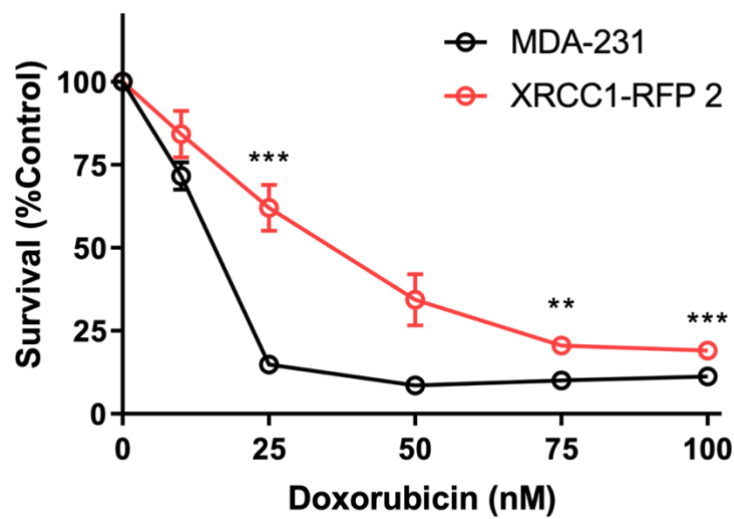


**Figure 2.14**. Increased expression of XRCC1 results in increased doxorubicin
resistance independent of STAT3. MDA-231 XRCC1-RFP clone were generated and
exposed to doxorubicin; values are percentage of cells compared to unexposed
controls.
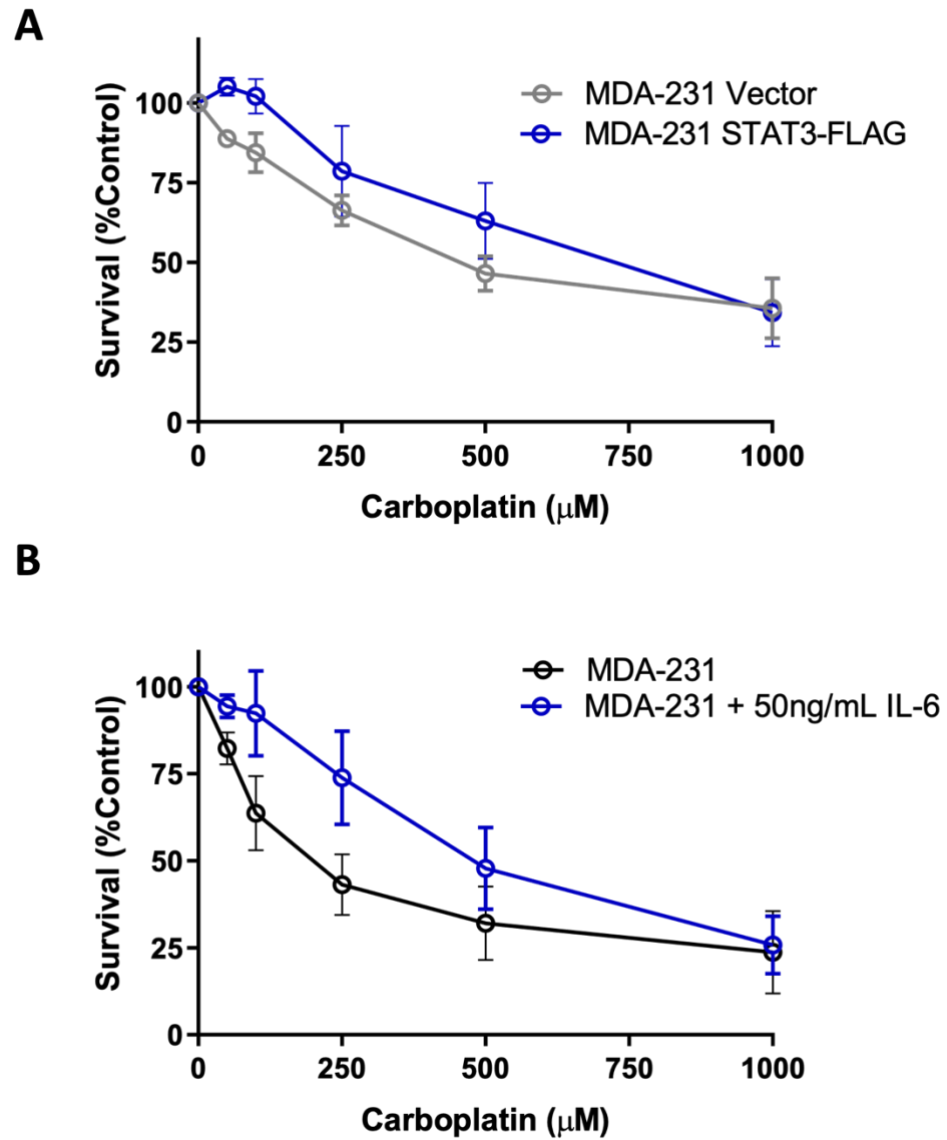
**Figure 2.15**. Increased STAT3 expression and activation increases resistance to carboplatin in MDA-231. A) STAT3-FLAG transiently transfected MDA-231 (48 h) were exposed to increasing concentrations of carboplatin. B) MDA-231 cells were pre-treated with 50ng/mL of IL-6 for 30 min, then co-exposed to carboplatin and IL-6.

## Discussion

Dysregulation of DNA repair proteins is a hallmark of cancer. Changes in the expression of DNA repair proteins can increase susceptibility to DNA damaging therapies or increase chemoresistance [4,37]. While various factors can regulate gene expression, transcription factors play a critical role in basal transcription and response to stress and stimuli. Despite BER's crucial role in addressing exogenous and endogenous threats, our knowledge of the transcription factors that regulate BER factors is lacking [12,17]. Surprisingly, only two transcription factors, E2F1 and Sp1, have been identified in the transcriptional regulation of *XRCC1* [13,14].

This study has identified a novel regulator of *XRCC1*, STAT3, which selectively upregulates XRCC1 in TNBC. Previously, we showed that XRCC1 gene and protein expression alterations occur across a panel of TNBC cell lines [4]. Here, we determined that STAT3 binds within the *XRCC1* promoter in MDA-231, MDA-468, and HEK293T cells (Figures 2.3, 2.10, and 2.11). Yet, the site only has significant occupancy when STAT3 is activated. Constitutive activation of STAT3 occurs in the TNBC cells and is reflected by increased occupancy at the binding site (Figure 2.3). However, pSTAT3 is low in the HEK293T cells, and occupancy at the STAT3 binding site in the *XRCC1* promoter is similarly low (Figure 2.10). This conditional regulation may explain why the promoter assay shows stable output between -612 and -310, despite the STAT3 site being deleted in the -310 construct (Figure 2.1).

shRNA-mediated knockdown of STAT3 significantly reduced both the gene and protein expression of XRCC1 (Figure 2.4). Importantly, it also reduced the occupancy at the STAT3 binding site within the *XRCC1* promoter in MDA-231 cells (Figure 2.3). We

further confirmed the dependence on activated, phosphorylated STAT3 (Y705) by chemical inhibition with alantolactone. Alantolactone targets the SH2 domain of STAT3 and prevents phosphorylation at Y705 [66]. In the presence of 15 μM alantolactone, we again showed a significant reduction in both gene and protein expression of XRCC1 (Figure 2.6).

Given that TNBC cell lines showed higher levels of pSTAT3, we examined physiologically relevant stimuli that could lead to activated STAT3 and increased XRCC1 expression. Several reports have demonstrated that inflammatory signaling through IL-6R promotes constitutive activation in TNBC [67-69]. These signaling events are proposed to play a role in breast cancer development and progression through aberrant signaling [68]. Using IL-6, we demonstrated that STAT3 is activated in HEK293T and MDA-231 and subsequently increases the gene and protein expression of XRCC1 (Figures 2.8). More importantly, we showed that IL-6 increased the occupancy of STAT3 at the STAT3 binding site within the HEK293T *XRCC1* promoter, which showed low occupancy under normal growth conditions (Figure 2.12).

These data provide evidence that STAT3 is a conditional regulator of *XRCC1* in response to stress and inflammatory signals. Under normal physiological conditions, activation of STAT3 is tightly controlled by several intrinsic inhibitors, including protein tyrosine phosphatases, the suppressors of cytokine signaling, and the protein inhibitor of activated STAT [51]. These regulatory mechanisms allow STAT3 to exert its physiological functions and limit the aberrant signaling seen in cancer. The low level of STAT3 and pSTAT3 in the HEK293T cells confirmed the tightly checked role of STAT3 in these non-tumorigenic cells and demonstrated that STAT3 does not drive *XRCC1* expression in

this cell line. Interestingly, the ectopic overexpression of STAT3 increased the levels of pSTAT3 and the occupancy of STAT3 at the *XRCC1* promoter in HEK293T but did not increase the expression of XRCC1 (Figure 2.11). However, after stimulation with IL-6, we see a dramatic increase in the presence of activated pSTAT3 and increased XRCC1 protein and gene expression (Figure 2.12). Therefore, the expression and activation of STAT3 alone is not enough to stimulate the transcription of *XRCC1* in this non-tumorigenic cell line.

Transformation involves numerous cellular and genomic changes that reduce inhibition on growth and proliferation signals. These changes also reduce apoptotic signaling and cell cycle control mechanisms as well as alter DNA damage response. As a result, we the see overexpression of STAT3 being sufficient to drive *XRCC1* expression in the MDA-231 cells (Figure 2.7). Stimulation by exogenous exposures IL-6 and EGF also resulted in increased XRCC1 expression (Figure 2.8 and 2.9). These results are consistent with two recent studies which examined the role STAT3 plays in regulating growth and invasion in TNBC cell lines [70,71]. Both studies used ChIP-seq to examine the transcriptional regulation of genes by STAT3. While their focus was on proliferation, migration, and invasion genes, examination of the ChIP-seq results (GSE85579 and GSE152203) at the *XRCC1* promoter showed STAT3 binding sites within the MDA-MB-231, MDA-MB-468, and HCC70 cells [70,71]. These ChIP-seq results in basal-like TNBC cell lines support our findings of higher expression and activation of STAT3, resulting in increased XRCC1 expression [4,70,71]. Further validation of pSTAT3 dependence of these

45

sites is needed to better understand the impact of conditional regulation of XRCC1 by pSTAT3 in TNBC.

The more blunted response in HEK293T cells and reports of under-expression of XRCC1 in hormone-positive breast cancers suggest that activated STAT3 regulation of XRCC1 may be highly tissue-specific and dependent on exogenous signals like IL-6 or EGF [34]. Tissue specificity is supported by the finding that stimulation by IL-6 is more robust than the ectopic expression alone (~ 3-fold vs. 2-fold) in HEK293T. The difference in expression from IL-6 vs. ectopic STAT3 may be related to the downregulation of inhibiting factors, such as SOCS3, or could reflect the additional changes in redox balance and reactive species induced by IL-6 [68,72-74]. Additional studies are needed to differentiate these contributors in the STAT3-related transcriptional control of *XRCC1*, though, in all likelihood, these mechanisms are probably interrelated.

In TNBC, IL-6 plays a critical role in breast cancer growth and maintenance [64,68,74]. TNBC tumor cells can autonomously produce IL-6, resulting in the constitutive activation of STAT3 [64,74]. Activated STAT3 acts as a transcription factor controlling the expression of genes involved in regulating cell proliferation, anti-apoptosis, migration, invasion, angiogenesis, chemoresistance, immune escape, and autophagy [75]. Here, for the first time, we have linked STAT3 activation by cytokines and stress factors to regulating a DNA repair protein, XRCC1. In our previous work with TNBC cell lines, we noted over-expression of XRCC1 in pre-clinical TNBC cell lines, which contrasted with previous reports in hormone-positive breast cancers noting a deficiency in XRCC1 expression [4,33,34,37]. In examining the effects of XRCC1 over-expression, we noted resistance to the alkylating agent MMS in highly over-expressed XRCC1 cell lines. Other

46

reports have associated the up-regulation of XRCC1 with increased risk of breast cancer, poor survival across low and high-risk breast cancer subtypes, increased tumor aggressiveness, and resistance to cisplatin, PARP inhibitors, and ionizing radiation [28,34,61,76]. However, the mechanism driving the overexpression of XRCC1 in TNBC and other cell lines has not been identified. Here, we show that XRCC1 overexpression, independent of STAT3, increases carboplatin and doxorubicin resistance. Likewise, increasing STAT3 expression and STAT3 activation through STAT3 ectopic expression and IL-6 exposure resulted in increased resistance to carboplatin. These data indicate a role for STAT3 regulation of XRCC1 expression in the development of chemoresistance in TNBC.

We reversed MMS resistance through shRNA-mediated knockdown of XRCC1 expression [4]. Additionally, the under-expression of XRCC1, seen in some hormone-positive breast cancers, is correlated with increased sensitivity to chemotherapeutics, including ionizing radiation, cisplatin, and PARP inhibitors [28,33,34,77]. Together, these results suggest that attenuation of XRCC1 expression influences breast cancer etiology and response to therapy. While we have identified pSTAT3 as a novel regulator of XRCC1 in TNBC, it is also likely that activated STAT3 regulates *XRCC1* under stress and growth conditions in non-tumorigenic cells. However, it is not until pSTAT3 levels become dysregulated that sustained increases in XRCC1 expression and subsequent changes in BER and SSBR would be observed, contributing to chemoresistance and

tumor aggressiveness. The constitutive activation of STAT3 in TNBC allowed this regulation to be identified more readily.

This work illuminates the complex regulatory mechanisms for BER proteins like XRCC1. Dysregulation of DNA repair proteins is a hallmark of cancer, yet basal and stress-induced regulatory mechanisms for these proteins are poorly delineated [12,17]. Here, we have identified a stress-specific regulatory mechanism for increasing protein levels of XRCC1, which becomes dysregulated in TNBC, and potentially other cancers.

# CHAPTER III: HIGH GLUCOSE INDUCES XRCC1 EXPRESSION RESULTING IN INCREASED DNA REPAIR FOLLOWING DAMAGE

## Introduction

Changes in the balance of DNA repair proteins contribute to cancer initiation, progression, and treatment. Somatic and germline mutations, altered epigenetic regulation, and overexpression of DNA repair proteins are observed in various cancers, but the underlying mechanisms are just beginning to be unraveled. While dysfunction of DNA repair proteins through their loss or mutations has garnered significant research focus, factors driving the overexpression of DNA repair proteins and improving DNA repair capacity in cancer cells are not well understood.

We have identified dysregulation of DNA repair proteins in TNBC cells that alter the DNA repair capacity of these cells [4,37]. We also recently linked overexpression of XRCC1, BER protein, to the transcriptional activities of STAT3 [65]. BER is essential to repairing the myriad of DNA base lesions accumulated from endogenous and exogenous exposures daily. XRCC1 has no enzymatic function but serves as a scaffold protein facilitating the actions of other DNA repair proteins [2,9]. Although it lacks enzymatic activity, XRCC1 plays a critical role in efficient BER repair, and deletion of *XRCC1* is embryonically lethal. In addition to its role in BER, XRCC1 has been shown to function in multiple other DNA repair pathways, including nucleotide excision repair (NER), through its interaction with DNA ligase III$\alpha$ and double-strand break repair through its interactions with PARP1 in alternative non-homologous end-joining [55,58]. XRCC1 is dysregulated in multiple cancers beyond breast cancer [4]. XRCC1 overexpression has been

shown to increase resistance to DNA damaging chemotherapeutics in gastric and ovarian cancers, while low XRCC1 is correlated with hypersensitivity to DNA damaging agents [30-32,34,78,79]. However, little is known about the transcriptional regulation of XRCC1 and the exposures that drive dysregulation [13,14].

Since the discovery of the Warburg effect over a century ago, the role of glucose in cancer formation and progression has seen increased attention. Chronic inflammation and hyperglycemia result in increased prevalence and mortality associated with many cancers, including breast and colorectal [80-83]. Normal circulating blood fasting glucose concentrations range from 3.9 mmol/L to 5.6 mmol/L, and acute hyperglycemia is defined by a circulating glucose concentration of 6.1 mmol/L to 11.0 mmol/L [84]. Inflammation and hyperglycemia also induce oxidative stress and DNA damage that are significant factors contributing to disease development and progression [85,86]. While there has been considerable focus on changes in antioxidant systems and regulatory responses driven by nuclear-erythoid 2-related factor 2 (NRF2) and NFκB, several studies have noted DNA damage and repair changes [85].

Hyperglycemia causes DNA lesions and strand breaks and alters the DNA damage response in renal and prostate cancers [87,88]. Notably, a reduction in the expression of DNA repair proteins involved in nucleotide excision repair, homologous recombination, and mismatch repair were observed [87-89]. Chemo- and radiation resistance was also noted in normal renal epithelial cells and renal cell carcinoma after high glucose exposure and is attributed to altered DNA damage response and reduced repair, though DNA repair protein expression changes were not examined [87]. Alterations in XRCC1 gene and protein expression were reported following glucose concentration changes in

breast cancer cell lines and hepatocytes, suggesting differences in the response between tissue and cell types [79,90].

Our previous work demonstrated that STAT3 was a novel regulator of XRCC1 in TNBC cell lines, which have constitutive activation of STAT3 [50,65]. STAT3 transcriptional activities are induced by phosphorylation at tyrosine 705 (Y705), leading to dimerization and translocation into the nucleus [91]. STAT3 activation following high glucose exposure has been documented in numerous cell lines [92,93]. We also found that STAT3 serves as an inducible regulator of XRCC1 in the non-tumorigenic human embryonic kidney cell lines HEK293T [65]. However, no links between increased glucose concentrations, activation of STAT3, and increased XRCC1 and DNA repair have been made.

This study identified high glucose concentrations as a driver of XRCC1 expression through increased STAT3 activation. We show increased STAT3 activation across cell line models following acute high glucose exposure, resulting in increased resistance to DNA damaging agents. Continuous exposure to high glucose concentrations promoted sustained STAT3 activation and XRCC1 expression, demonstrating that dysregulation of XRCC1 and DNA repair is achieved through STAT3 activation across different cell types.

## Materials and Methods

### Chemicals

Methyl Methanesulfonate (MMS) was acquired from Sigma Aldrich (Sigma #129925) and diluted in media to the desired concentrations. Alantolactone was acquired

from Selleckchem (Selleckchem #S8318) and resuspended in anhydrous DMSO to a concentration of 15mM.

## Cell Culture

HEK293T, U2OS, and MDA-MB-231 were purchased from the American Type Culture Collection (ATCC CRL-3216, HTB-26, and HTB-96, respectively) within the last 24 months and passaged < 10 times for all experiments (passage numbers from 6-15). Biweekly test mycoplasma contamination was performed using the Lonza MycoAlert (Lonza #LT07-318). HEK293T cells were grown in DMEM High Glucose + L-Glutamine (Hyclone #SH30022.01) supplemented with 1% sodium pyruvate and 10% Fetal Bovine Serum (FBS). U2OS cells were grown in RPMI 1640 with L-glutamine (Corning 10-040-CV) supplemented with 10% FBS. MDA-231 cells were grown in DMEM High Glucose + Glutamax (Life Technologies, #10566016) supplemented with 1% sodium pyruvate and 10% FBS.

Low glucose adapted HEK293T and MDA-231 were grown in DMEM low glucose, pyruvate (Thermo Fisher Scientific #11885084) supplemented with L-glutamine, 1% sodium pyruvate, and 10% FBS. Low glucose adapted U2OS were grown in RPMI 1640 with L-glutamine without Glucose (Life Technologies #11879020) supplemented with 5mM glucose (D-(+)-Glucose Solution Sigma #G8644) and 10% FBS.

## Immunoblot

Immunoblot was performed as previously described. Briefly, cells were grown in 150mm dishes and grown to 80% confluency. 1XPBS was used to rinse cells before cells were scraped and pelleted at 1000rpm and stored overnight at -80℃. Pellets were then lysed, and a Bradford assay quantified protein content before 20$\mu$g of lysate was

separated on 4-15% SDS Page gel (Bio-Rad #4561084) and transferred to nitrocellulose membrane (Bio-Rad #1704156EDU). Nitrocellulose membranes were blocked for 1 h at RT in 5% non-fat dry milk in Tris-buffered saline (VWR #J640-4L) containing 0.1% Tween20 (Thermo Fisher Scientific #BP337, TBS-T). Primary antibodies were incubated overnight: XRCC1 (1:1000 #MS434P1, Fisher Scientific), pSTAT3 Y705 (1:500 Cell Signaling Technology, #9131), STAT3 (1:1000 Cell Signaling Technology, #9139), pEGFR (1:500 Cell Signaling Technology, #3777) EGFR (1:1000 Cell Signaling Technology #4267), IL-6R$\alpha$ (1:1000 Cell Signaling Technology #39837). Blots were incubated with the proper horseradish peroxidase (HRP)-labeled secondary antibodies (goat anti-rabbit-HRP #7074P2 or goat anti-mouse-HRP #7076S from Cell Signaling Technology). WesternBright Sirius (Advansta #K-12043-D20) was used to detect target proteins. Immunoblotting was performed with three biological replicates; protein quantification was conducted using Image Lab Software (Bio-Rad).

**Gene Expression Analysis**

Isolation of mRNA using Invitrogen Cell to $C_t$ kit (Life Technologies #4399002) was used for the relative gene expression in HEK293T and U2OS following the manufactures recommendations as previously described [65]. Cells were plated in 96-well plates and grown to 70% confluency before treatment with high glucose media. Cells were then lysed and RT-PCR was performed to produce cDNA. Following cDNA synthesis, qPCR was performed using the appropriate TaqMan gene expression primers (XRCC1 Hs00959834_m1 FAM and IL-6 Hs00174131_m1 FAM) and TaqMan master mix. Gene expression following IL-6 exposure was performed as previously described . Briefly, cells were exposed to 50ng/mL IL-6 diluted in basal glucose media for 30 min, 1

h, and 4 h. Each gene expression experiment was performed in technical triplicates with three biological replicates. Quantifications are represented as the mean of the three biological replicates $\pm$ the standard error of the mean (SEM).

## Chromatin Immunoprecipitation

Chromatin immunoprecipitation was performed as previously described [65]. Briefly, cells were plated in 150mm dishes and grown to 80% confluency. Cells were crosslinked in 1% formaldehyde in 1X phosphate-buffered saline (PBS) at RT for 8-10min. Cells were then lysed in 1mL of Farnham lysis buffer (5mM HEPES pH 8.0, 85mM KCl, 0.5% NP-40) for 20min on ice, followed by centrifugation at 2000rpm to pellet the lysed sample. The pellet was then re-suspended in RIPA buffer (50mM Tris-HCl pH8, 150mM NaCl, 1% sodium deoxycholate, 1mM EDTA, 0.1% SDS, 1% Triton X-100) for 20 min followed by sonication on ice at an amplitude of 10 on a Misonix S-4000 with 15s on/50s off for a total time of 3.5 min for HEK293T and U2OS. Immunoprecipitation was performed by incubating chromatin with anti-STAT3 diluted to the manufactures' recommendation (Cell Signaling Technology #9131S) and Protein A/G magnetic beads (Thermo Fisher Scientific #88802) overnight at 4℃ with agitation on a rotator. Magnetic bead conjugated chromatin was then washed with ice-cold LiCl wash buffer (100mM Tris-HCl, 500mM LiCl, 1% NP-40, 1% Triton X-100) and TE buffer (10mM Tris-HCl pH 7.5, 0.1mM EDTA). Proteinase K was added in ChIP elution buffer (1% SDS, 0.1M $NaHCO_3$) and incubated at 65℃ with agitation (950rpm) for 2h, followed by proteinase K inactivation at 90℃ for 10 min. Isolated DNA was purified

using a PureLink PCR purification Kit (Life Technologies #K310002). *XRCC1* Primers were used as previously described [65].

## Cell Growth Inhibition

Cells were plated at a density of $1X10^4$ (HEK293T and U2OS) and $2X10^4$ (MDA-231) in 12 well-dishes and allowed 48 h to adhere. Cells were pretreated with high glucose media prior to challenge with MMS. Cells were exposed to MMS for 1 h to 0, 0.5mM, 1mM, and 2mM concentrations, MMS was washed using 1XPBS, and fresh high glucose media was added. Cells were allowed to recover for 5 days before being trypsinized and resuspend in 1mL of PBS. Resuspended cells were counted using BioRad TC-10 Automated Cell Counter. Cell counts were performed in triplicate normalized to control wells for a total of three biological replicates. Values were plotted as mean $\pm$ standard error of the mean (SEM)

## Immunofluorescence

Immunofluorescence was performed as previously described [4]. Briefly, cells were plated on 60mm fluorodishes pretreated with 1 mL EmbryoMax 0.1% Gelatin Solution (Millipore #ES-006-B) for 15-30 min at room tempreture. Cells were then plated at 2.5 X $10^4$ per plate, allowing 24 h for cells to adhere. For HEK293T dishes were pretreated with poly-L-lysine solution (Sigma #P4707-50mL) for 5 min and allowed to dry for 1 h before cell plating. Cells were pretreated with high glucose-containing media for 4 h before MMS exposure. Cells were exposed to MMS containing media for 1 h; cells were then washed with 1X PBS and allowed to recover in fresh high glucose-containing media for 4 h and 24 h. Dishes were fixed using 3.7% formaldehyde in 1X PBS. Nuclear permeabilization was accomplished by Permeabilization Buffer (Biotum #22016) 10min

incubation at RT. Dishes were then blocked using 2% BSA in PBS for 30 min at RT.

Anti-Phospho-Histone H2AX (Ser139) (EMD Millipore #05-636) primary antibody

diluted in 2% BSA in PBS (1:400) was then incubated for 1 h at RT. Dishes were washed

with 1X PBS and Alexa Fluor™ 546 goat anti-mouse IgG (H+L) (Thermo Fisher

Scientific #A11003) secondary antibody was applied (1:2000) for 1 h. Nuclei were

stained with Hoechst 33342 (Thermo Scientific #62249) for 15 min at RT. Dishes were

mounted in Prolong™ Gold Antifade Reagent (Life Technologies #P36930).

Fluorescence images were acquired using a Nikon A1 scanning confocal microscope with

a Plan-Apochromat 20x/0.75 objective. To quantify the nuclear mean intensity, a region

of interest (ROI) generator was used to detect nuclei automatically in the DAPI channel.

The nuclear mean intensity of $\gamma$H2AX was exported for analysis.

## Single Cell Gel Electrophoresis (Comet Assay)

Cells were plated in 96-well plates at a density of 2.5 X $10^4$ per well, allowing

24h for the cells to adhere. Cells were pre-treated with high glucose media 4h before

MMS exposure. $IC_{25}$ concentrations were used to determine MMS dosing. Cells were

exposed to MMS containing media for 1h, then media was removed, and wells were

washed and replaced with fresh media. Following the indicated repair time, media was

removed and cells were trypsinized and resuspended in media. 100 $\mu$L of resuspended

cells were then transferred to a CometChip® (Trevigen #4260-096-01). Following

overlay with 0.75% low melting temperature agarose, CometChip® were lysed overnight

at 4℃ in CometAssay lysis solution (Trevigen #4250-010-01). CometChip were then

incubated in alkaline solution (200mM NaOH, 1mM EDTA, 0.1% Triton 100X) for a

total of 40min at 4℃ . Electrophoresis was then performed for 50min at 22V. The

alkaline solution was neutralized using 400mM Tris for a total of 30min at 4℃ followed by 20mM Tris for a total of 30min at 4℃. CometChips® were then stained in SYBR™ Gold Nucleic Acid Gel Stain (Thermo Fisher Scientific #S11492) in 20mM Tris for 1h at 4℃ followed by a 30 min de-stain in 20mM Tris at 4℃. CometChips were imaged using Celigo S Imaging Cytometer (Nexcelom Bioscience). Acquired images were analyzed using Trevigen CometChip® analysis software.

## Cell Adaptation

Basal glucose HEK293T and MDA-231 were grown in 25mM glucose-containing DMEM, and U2OS were grown in 11mM containing RPMI. Adaptation to low glucose (5mM) medium was accomplished in HEK239T and MDA-231 by briefly growing cells in 17mM glucose-containing DMEM for 3 days, and the media was then changed to 10mM glucose-containing media for 1 week. Finally, cells were grown in low glucose (5mM) DMEM for 1.5 weeks before being frozen and stored in liquid nitrogen. Similarly, U2OS were adapted to low glucose containing RPMI by growing cells in 7mM containing RPMI for 6 days before changing media to low glucose RPMI (5mM) for 1.5 weeks before being frozen and stored in liquid nitrogen. High glucose adaptation was accomplished similarly. First, HEK293T and MDA-231 were grown in 27.5mM containing DMEM for 1 week before being grown in high glucose (30mM) DMEM for 1.5 weeks. Following adaptation, cells were frozen and stored in liquid nitrogen. Finally, U2OS cells were adapted to high glucose-containing RPMI (30mM) by briefly growing cells in 20mM RPMI for 3 days followed by 1 week growth in 25mM RPMI. Finally, cells were grown in high glucose RPMI (30mM) for 1.5 before being frozen and stored in liquid nitrogen. HEK293T were adapted from passage 8 HEK293T, low glucose and high

glucose HEK293T adapted cells were frozen at passage 12 and passage 11 respectively. U2OS cells were adapted from passage 8 U2OS, low glucose and high glucose U2OS were frozen at passage 10. MDA-231cells were adapted from passage 6 MDA-231, low glucose MDA-231 were frozen at passage 11.

## IL-6 ELISA Quantification

IL-6 media concentrations were measured using the Quantikine®ELISA Human IL-6 kit (R&D systems #S6050) following the manufacturer's instructions. Briefly, cells were plated in 150mm dishes and allowed to grow to 70—80% confluency before media was collected. The ELISA was performed in technical triplicates with the mean ± standard error of the mean (SEM) of three biological replicates presented.

## Statistical Analysis

Assays were performed as three biological replications. One-way ANOVA and means were compared with Dunnett's post hoc analysis. Comparison groups are indicated in graphs. All means are reported ± SEM. * $p < 0.05$, ** $p < 0.01$, *** $p < 0.001$, **** $p < 0.0001$.

## Results

### Acute high glucose stimulates activation of STAT3 and XRCC1 expression

To examine the high glucose regulation of XRCC1, we exposed cells to 30mM glucose for up to 24 h. We selected the osteosarcoma cell line U2OS, which has high STAT3 activation, and HEK293T, which we showed previously has an inducible STAT3

response [65]. HEK293T cells were grown in 25mM glucose (BG) and had low XRCC1

expression (Figure 3.1A).
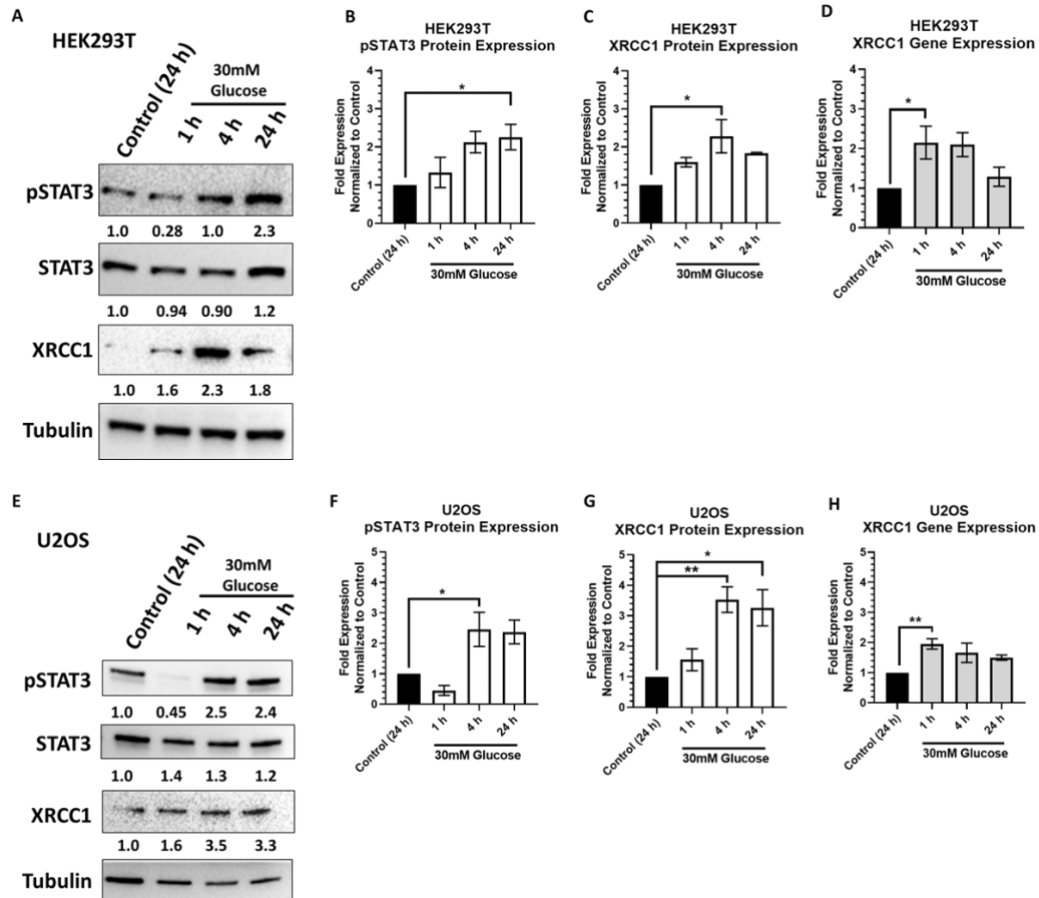


**Figure 3.1.** High glucose activates STAT3, subsequently increasing XRCC1 protein and gene expression : A) Representative western blot showing increased XRCC1 following acute high glucose (30mM) for 1 h, 4 h, and 24 h in HEK293T, including mean values for three repeats B) Quantification of pSTAT3 protein expression in HEK293T normalized to control C) Quantification of XRCC1 protein expression in HEK293T normalized to control D) Quantification of XRCC1 gene expression in HEK293Tnormalized to control E) Representative western blot showing increased XRCC1 following acute high glucose (30mM) for 1 h, 4 h, and 24 h in U2OS, including mean values for three repeats F) Quantification of pSTAT3 protein expression in U2OS normalized to control G) Quantification of XRCC1 protein expression in U2OS normalized to control H) Quantification of XRCC1 gene expression in U2OS normalized to control * $p < 0.05$ ** $p < 0.01$,*** $p < 0.001$, **** $p < 0.0001$.

The U2OS cells were grown in 11mM (BG) and had high initial XRCC1 expression (Figure 3.1E). Cells were then exposed to 30mM high glucose (HG) through glucose addition to the basal medium for 1, 4, and 24 h. We observed an increase in STAT3 activation as indicated by an increase in STAT3 phosphorylation at Y705 in the HEK293T and U2OS cells (Figure 3.1A, B, E and F). A significant increase in XRCC1 protein and gene expression occurred in the HEK293T and U2OS cells (Figure 3.1C and G). In HEK293T, *XRCC1* gene expression increased at 1 and 4 h (2.2 ± 0.41 and 2.1 ±
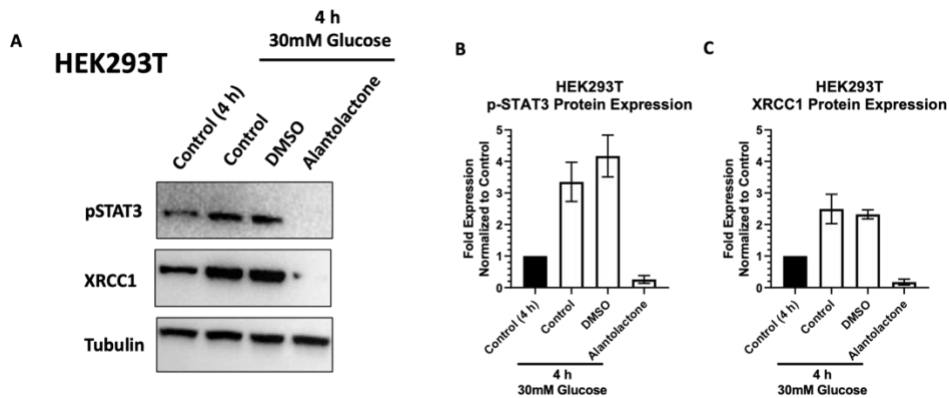


**Figure 3.2.** 15$\mu$M Alantolactone treatment reverses acute high glucose increases in pSTAT3 and XRCC1 protein expression in HEK293T: A) Representative western blot of Control (4 h), Control 4 h 30mM glucose, DMSO 4 h 30mM, and 4 h 30mM glucose 4 h 15$\mu$M alantolactone in HEK293T  B) Quantification of two western blots  of pSTAT3 expression normalized to control (4 h) HEK293T C) Quantification of two western blots  of  XRCC1 expression normalized to control (4 h) HEK293T.

0.30, respectively) following high glucose exposure, and the XRCC1 protein showed a sustained increase at 4 h (2.3 ± 0.44) (Figure 3.1C and D).

For U2OS, XRCC1 protein expression peaked at 4 h and continued 24 h (3.5 ± 0.42 and 3.3 ± 0.59, respectively), and *XRCC1* gene expression increased only at 1 h after high glucose exposure (2.0 ± 0.20, Figure 3.1G and H).
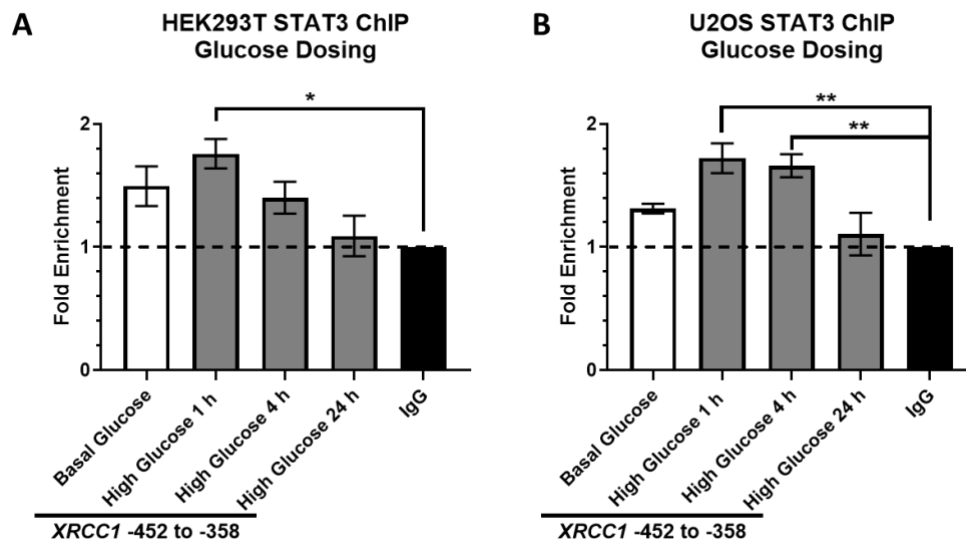


**Figure 3.3.** Increased STAT3 occupancy of the *XRCC1* promoter following acute high glucose: A) ChIP analysis of STAT3 occupancy at the *XRCC1* promoter following acute high glucose (30mM) for 1 h, 4 h, and 24 h in HEK293T normalized to respective IgG controls B) ChIP analysis of STAT3 occupancy at the *XRCC1* promoter following acute high glucose (30mM) for 1 h, 4 h, and 24 h in U2OS normalized to respective IgG control * $p < 0.05$, ** $p < 0.01$.

The role of STAT3 in this regulatory mechanism was further confirmed using the STAT3 inhibitor alantolactone, which was shown to reduce XRCC1 expression following 4 h 15$\mu$M alantolactone exposure (Figure 2.6). Alantolactone exposure in HEK293T

resulted in attenuation of acute high glucose induced pSTAT3 and XRCC1 protein

expression (Figure 3.2A, B, and C)

**STAT3 occupancy of the XRCC1 promoter increases following acute high glucose**

**exposure.**

To confirm acute high glucose increases XRCC1 expression through a STAT3

transcription mechanism, we performed chromatin immunoprecipitation (ChIP) to follow

occupancy changes of STAT3 at the XRCC1 promoter with a 96 bp region (-452 to -358)

previously identified as a STAT3 binding site within the XRCC1 promoter [65]. The

occupancy of STAT3 at the XRCC1 promoter was assessed in HEK293T and U2OS cells

following the 30mM glucose exposure for 1, 4, and 24 h (Figure 3.3A). In the HEK293T,

STAT3 occupancy of the XRCC1 promoter increased significantly 1 h following high

glucose ($1.8 \pm 0.12$, enrichment compared to IgG control) before lowering at 4 and 24 h.

The U2OS cells showed a more sustained peak of STAT3 occupancy at the XRCC1

promoter 1 and 4 h following high glucose exposure ($1.7 \pm 0.12$ and $1.7 \pm 0.093$,

enrichment compared to IgG control), returning to a level slightly below control at 24 h

(Figure 3.3B). These data indicated STAT3 activation following acute high glucose

exposure resulted in increased XRCC1 gene and protein expression through increased

STAT3 occupancy at the *XRCC1* promoter.
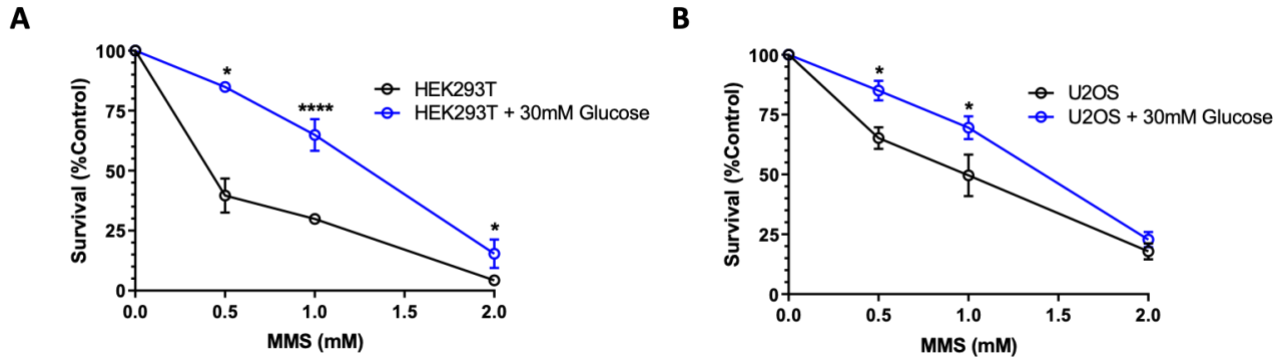


**Figure 3.4**. Increased MMS survival following acute high glucose: A) Cell
counting survival curve following dosing of MMS in HEK293T, HEK293T
30mM high glucose for 4 h followed by continuous high glucose exposure,
mean survival (%) and SEM (%) normalized to 0mM control HEK293T B)
Cell counting survival curve following dosing of MMS in U2OS, U2OS
30mM high glucose for 4 h followed by continuous high glucose exposure,
mean survival (%) and SEM (%) normalized to 0mM control U2OS* $p < 0.05$,
** $p < 0.01$, **** $p < 0.0001$.

**High glucose induced XRCC1 promotes cell survival through increased DNA repair**

Increased XRCC1 expression is associated with increased survival against

genotoxic stress [78]. We next examined the extent that high glucose induced XRCC1

expression altered cell survival after exposure to the classic BER alkylating agent MMS.

Cytotoxicity of MMS was assessed by cell growth inhibition. Cells were treated with

high glucose for 4 h before MMS exposure to ensure XRCC1 expression was increased (Figure 3.1).
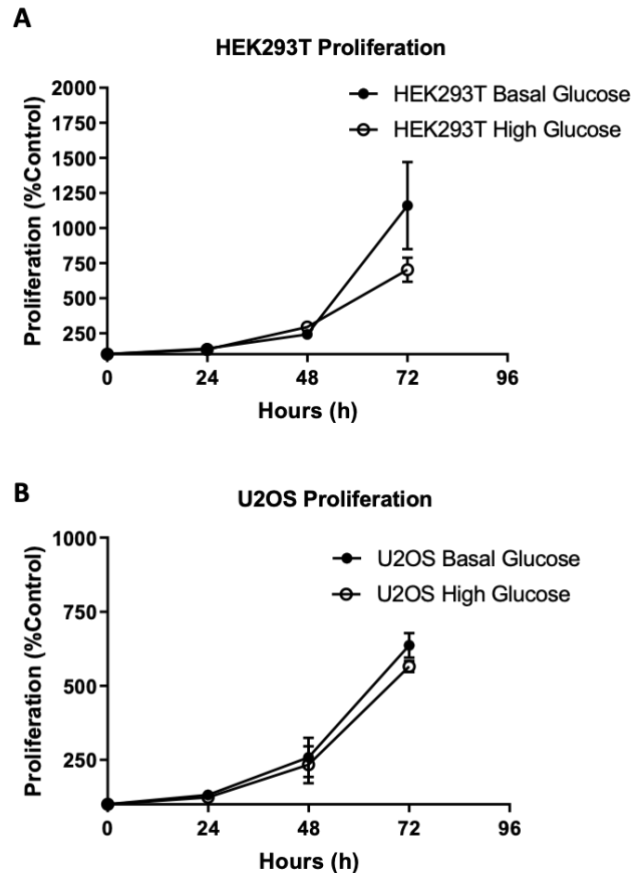


**Figure 3.5**. Doubling time for BG HEK293T and BG U2OS continuous exposure to HG A) Proliferation of HEK293T BG and continuous HG exposure HEK293T values presented as cell count % of control B) Proliferation of BG U2OS and continuous HG exposure U2OS values presented as cell count % control.

Cells were then exposed to increasing concentrations of MMS for 1 h in high glucose and sustained in high glucose after exposure (Figure 3.4). To confirm the changes in survival were not due to increased proliferation, the doubling time for acute

high glucose exposure was assessed out to 72 h, with only a slight, non-significant, increase in basal glucose HEK293T proliferation occurring compared to acute HG HEK293T (Figure 3.5).
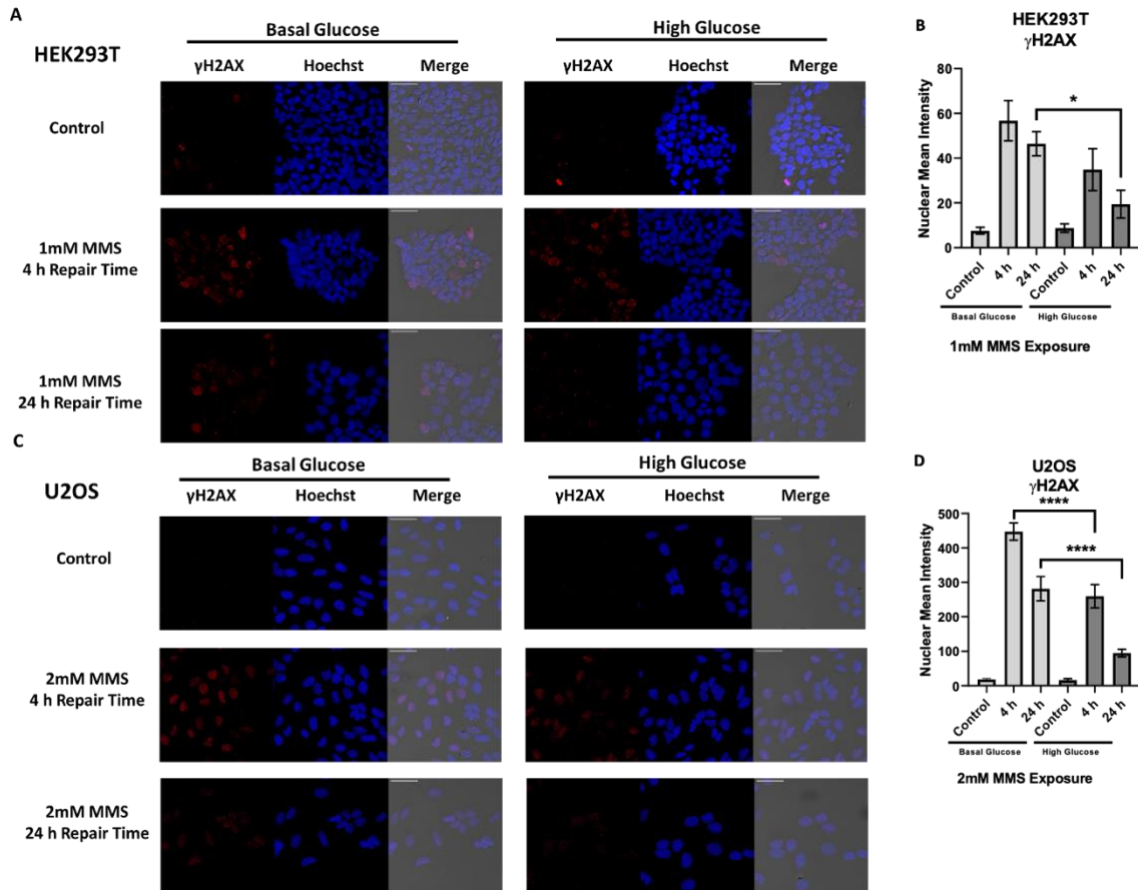


**Figure 3.6.** Reduced gamma-H2AX indicates increased repair of MMS induced damage following acute high glucose : A) Representative immunofluorescence images of HEK293T and acute HG HEK93T 4 h and 24 h post 1mM MMS B) Quantification of nuclear mean intensity of immunofluorescence images of HEK293T and acute HG HEK293T C) Representative immunofluorescence images of U2OS and acute HG U2OS 4 h and 24 h post 2mM MMS D) Quantification of nuclear mean intensity of immunofluorescence images of U2OS and acute HG U2OS * $p < 0.05$ ** $p < 0.01$,*** $p < 0.001$, **** $p < 0.0001$.
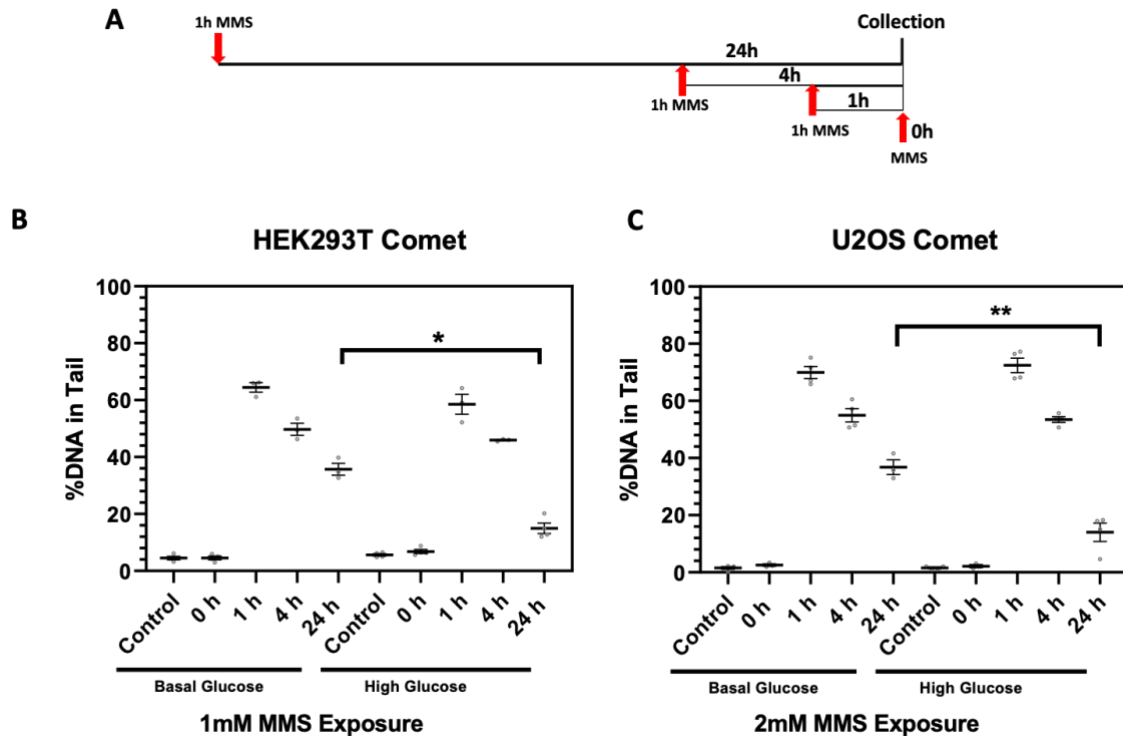
**Figure 3.7**. Comet assay indicates increased DNA repair following acute high glucose: A) Timeline of MMS dosing for the comet assay B) Comet assay, the % DNA in the comet tail in HEK293T and acute HG HEK293T 0h, 1, 4, and 24 h post 1mM MMS exposure C) Comet assay, the % DNA in the comet tail in U2OS and acute HG U2OS 0, 1, 4, and 24 h post 2mM MMS exposure * $p < 0.05$ ** $p < 0.01$,*** $p < 0.001$, **** $p < 0.0001$.

To confirm the increased survival is due to a change in DNA repair, we examined changes in DNA damage after MMS challenge in the basal and acute high glucose. HEK293T and U2OS cells were dosed with $IC_{25}$ doses of MMS 1 and 2mM, respectively (Figure 3.4). Phosphorylation of H2AX at the serine 139 residue (γ-H2AX) was used to assess the formation of single and double strand breaks following exposure to MMS. In

the HEK293T, a significant reduction in γ-H2AX nuclear signal was seen 24 h post-MMS exposure in the high glucose cells compared to their BG controls (Figure 3.6A and B). The U2OS cells saw a more significant reduction in γ-H2AX nuclear signal at 4 and 24 h post-MMS exposure than the BG controls (Figure 3.6C and D).

Finally, we examined repair dynamics using alkaline single cell gel electrophoresis (comet assay) under basal and acute high glucose conditions. DNA repair was assessed by monitoring the percentage of DNA in the comet tail in untreated cells and after 1 h exposure to 1 or 2mM MMS ($IC_{25}$) for 0, 1, 4, and 24 h of repair time in the HEK293T and U2OS, respectively (Figure 3.7A). Increased DNA in the comet tail indicates increased DNA strand breaks and alkaline labile sites. Following MMS exposure, the acute high glucose pretreated HEK293T showed an increase in DNA repair as indicated by the reduction of the percentage of DNA in the comet tail at 24 h repair time (17% $\pm$ 2.2%) following MMS exposure compared to HEK293T BG control (36% $\pm$ 6.3% ) with similar increases in repair occurring in acture high glucose exposed U2OS at 24 h repair time following MMS exposure (37% $\pm$ 2.5) compared to U2OS BG control (17% $\pm$ 5.7%) (Figure 3.7B and C).

## Adaptive changes in glucose concentration alter STAT3 activation, XRCC1 expression, and STAT3 occupancy of the XRCC1 promoter

Next, we wanted to determine if adaptive changes due to long-term glucose concentration changes would drive dysregulation of XRCC1 in HEK293T and U2OS cells, similar to what we have previously reported in TNBC cells [65]. HEK293T and U2OS were adapted to low, physiologically relevant glucose (LG, 5mM), basal medium glucose (BG, 25mM for HEK293T and 11mM for U2OS), and high glucose (HG, 30mM)

medium by passaging the cells for 1.5 weeks in increasing mixtures of glucose followed

by growth in final desired glucose concentrations for at least 2 weeks before analysis [84].
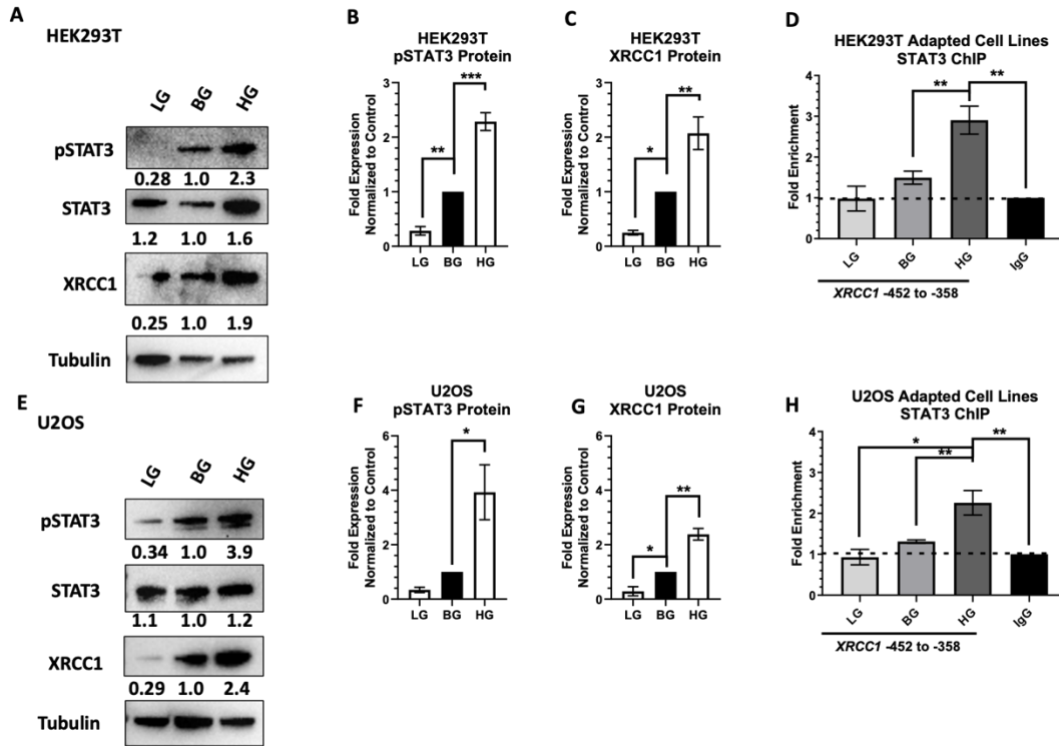


**Figure 3.8**. Adaptive alterations in XRCC1 expression following adaptation to glucose concentrations A) Representative western blot of pSTAT3 and XRCC1 in HEK293T adapted cell lines Low Glucose 5mM (LG), Basal Glucose 25mM (BG), and High Glucose 30mM (HG) including mean values for three repeats B) Quantification of pSTAT3 protein expression in HEK293T adapted cell lines LG, BG, and HG normalized to BG C) Quantification of XRCC1 protein expression in HEK293T adapted cell lines LG, BG, and HG normalized to BG D) ChIP analysis of STAT3 occupancy of the *XRCC1* promoter in adapted HEK293T cell lines LG, NG, and HG normalized to respective IgG controls E) Representative western blot of pSTAT3 and XRCC1 in U2OS adapted cell lines Low Glucose 5mM (LG), Basal Glucose 11mM (BG), and High Glucose 30mM (HG) including mean values for three repeats F) Quantification of pSTAT3 protein expression in U2OS adapted cell lines LG, BG, and HG normalized to BG G) Quantification of XRCC1 protein expression in U2OS adapted cell lines LG, BG, and HG normalized to BG H) ChIP analysis of STAT3 occupancy of the *XRCC1* promoter in adapted U2OS cell lines LG, BG, and HG normalized to respective IgG controls * $p < 0.05$ ** $p < 0.01$,*** $p < 0.001$, **** $p < 0.0001$.
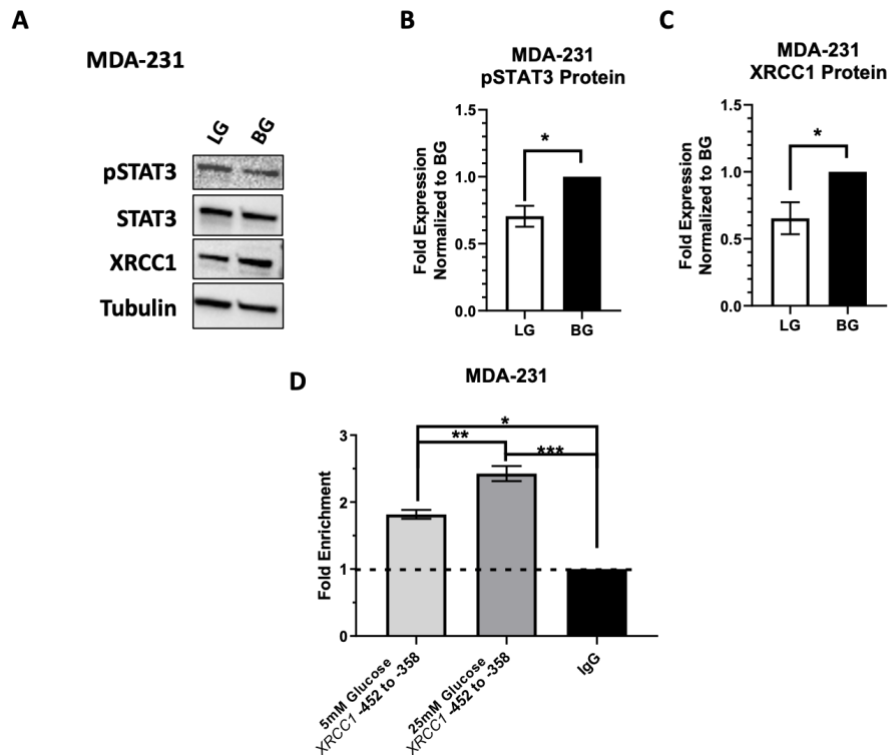
**Figure 3.9**. MDA-231 have reduced responsiveness to alterations in glucose concentrations: A) Representative western blot of pSTAT3 and XRCC1 in MDA-231 adapted cell lines Low Glucose 5mM (LG) and Basal Glucose 25mM (BG) B) Quantification of XRCC1 protein expression in MDA-231 adapted cell lines LG and BG C) Quantification of pSTAT3 protein expression in MDA-231 adapted cell lines LG and BG D) ChIP analysis of STAT3 occupancy of the *XRCC1* promoter in adapted MDA-231 cell lines LG and BG normalized to respective IgG controls * $p < 0.05$ ** $p < 0.01$,*** $p< 0.001$, **** $p < 0.0001$.

Reduced STAT3 activation (lower pSTAT3) was seen for LG HEK293T (0.28 $\pm$ 0.79) and U2OS (0.34$\pm$ 0.098) compared to their respective BG controls (Figure 3.8B

69

and F). Sustained STAT3 activation occurred in HG HEK293T (2.4 $\pm$ 0.16) and U2OS (3.9 $\pm$ 0.10) compared to BG controls (Figure 3.8B and F). Sustained alterations in STAT3 activation resulted in dysregulation of XRCC1 protein expression changes with reduced XRCC1 (0.25 $\pm$ 0.04) in LG HEK293T and increased XRCC1 (1.9 $\pm$ 0.34) in HG HEK293T compared to BG HEK293T controls (Figure 3.8C and G). Similar alterations occurred in U2OS with lower XRCC1 protein expression (0.29 $\pm$ 0.17) in LG U2OS and increased XRCC1 expression (2.4 $\pm$ 0.21) in HG U2OS than BG U2OS controls (Figure 3.7C and G). We also confirmed STAT3 occupancy at the XRCC1 promoter using ChIP. Decreases in STAT3 activation in LG HEK293T and U2OS correlated with a reduction below BG control of STAT3 enrichment at the XRCC1 promoter (0.98 $\pm$ 0.30 and 0.93 $\pm$ 0.19, compared to IgG controls, respectively) (Figure 3.8D and H). Sustained activation of STAT3 in HG HEK293T and HG U2OS correlated with an increase of enrichment of STAT3 at the XRCC1 promoter (2.9 $\pm$ 0.34 and 2.3 $\pm$ 0.30, compared to IgG control respectively) compared to BG HEK293T and U2OS (1.5 $\pm$ 0.16 and 1.3 $\pm$ 0.40, respectively) (Figure 3.8D and H).

## Low glucose adaptation of the TNBC cell line MDA-231 only partially reduces STAT3 occupancy of the XRCC1 promoter

We previously reported that STAT3 plays a major role in regulating XRCC1 in TNBC cell lines, including the MDA-231 [65]. Given the constitutive activation of STAT3 in MDA-231, we next wanted to see if glucose restriction altered the activation of STAT3 and regulation of XRCC1 in the MDA-231. MDA-231 cells were adapted to low glucose-containing media (5mM) as described above. Previous experiments were conducted in 25mM glucose (BG). Following the adaptation to LG, MDA-231 showed only a slight

70

reduction in the activation of STAT3 ($0.71 \pm 0.08$), which resulted in a slight decrease of XRCC1 protein expression ($0.65 \pm 0.12$) compared to the BG MDA-231 control (Figure 3.9A and B). Similarly, LG only slightly reduced the occupancy of STAT3 at the *XRCC1* promoter ($1.8 \pm 0.066$) compared to BG control MDA-231 ($2.4 \pm 0.11$), and both the LG and BG MDA-231 have a higher STAT3 occupancy at the promoter than that seen for BG HEK293T and U2OS (Figure 3.9D).

## IL-6 expression and stimulation increases pSTAT3 and XRCC1 in HEK293T and U2OS

In humans, hyperglycemia increases inflammatory cytokines, like IL-6, a known activator of STAT3 [94]. Increasing glucose concentrations in cell culture medium has also been shown to increase IL-6 production and secretion across various cell types [92,93,95,96]. We previously demonstrated that exogenous addition of IL-6 activated STAT3, increased the expression of XRCC1, and increased the occupancy of STAT3 within the *XRCC1* promoter in HEK293T and MDA-231 cells [65]. With the variations in responses between the HEK293T, MDA-231, and U2OS cells, we examined the exogenous IL-6 and IL-6R$\alpha$ levels and the effects of glucose stimulation and restriction. We first measured IL-6 concentrations in the HEK293T, MDA-231, and U2OS glucose-adapted cell lines (Figure 3.10A, B, and C). In the BG medium, HEK293T showed low IL-6 levels in the spent medium, while U2OS and MDA-231 showed high IL-6 concentrations in the spent medium. Changing the glucose concentrations induced IL-6 release into the spent medium for U2OS cells, but only slight increases were observed in HEK293T and MDA-231. Reducing the glucose in HEK293T and U2OS also reduced

the IL-6 released into the medium (Figure 3.10A and C). We also examine the expression

of IL-6R$\alpha$ under different glucose conditions across the cell lines (Figure 3.10D).
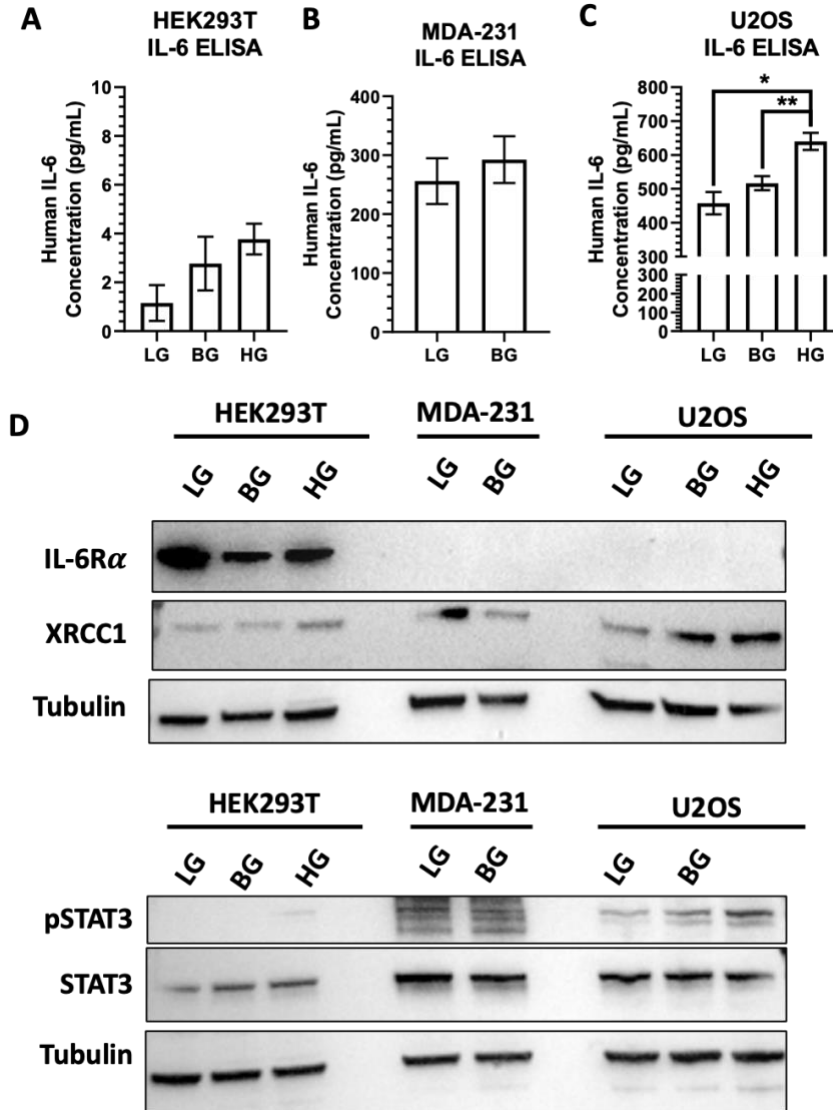


**Figure 3.10**. Expression of IL-6 and IL-6R$\alpha$ modulate the STAT3 activation and subsequent XRCC1 expression : A) Quantification of IL-6 concentration in the media of adapted HEK293T cell lines B) Quantification of IL-6 concentration in the media of adapted MDA-231 cell lines C) Quantification of IL-6 concentration in the media of adapted U2OS cell lines D) Representative western blot of pSTAT3, STAT3, IL-6R$\alpha$ and XRCC1 in HEK293T, MDA-231, and U2OS adapted cell line * $p < 0.05$ ** $p < 0.01$,*** $p < 0.001$, **** $p < 0.0001$.
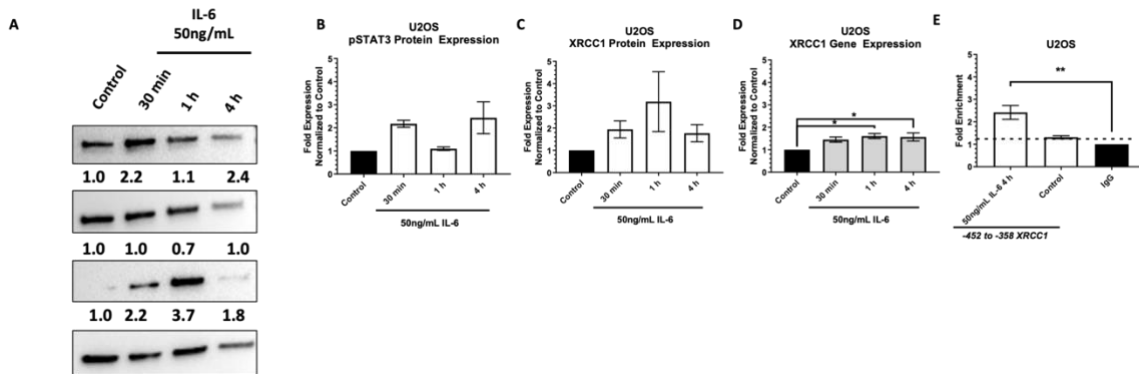
**Figure 3.11**. Acute IL-6 exposure in BG U2OS A) Representative western blot for pSTAT3, STAT3, and XRCC1 following 50ng/mL IL-6 exposure for 30 min, 1 h, and 4 h, tubulin as the loading control with mean values for three repeats B) Quantification of pSTAT3 protein following 50ng/mL of IL-6 exposure for 30 min, 1 h, and 4 h C) Quantification of XRCC1 protein expression following 50ng/mL of IL-6 exposure for 30 min, 1 h, and 4 h D) Quantification of *XRCC1* gene expression following 50ng/mL of IL-6 exposure for 30 min, 1 h, and 4 h E) ChIP analysis of STAT3 occupancy of the *XRCC1* promoter following 50ng/mL of IL-6 exposure for 4 h $*p<0.5$, $**p<0.01$

IL-6 binding to IL-6R$\alpha$ activates STAT3 through several signaling mechanisms, including interactions with EGFR and JAK [91,97]. We observed high levels of IL-6R$\alpha$ in the HEK293T, and the receptor levels fluctuated with glucose concentrations. The high levels of IL-6R$\alpha$ in the HEK293T made the immunoblot detection of the MDA-231 and U2OS more difficult.To investigate the links between glucose and IL-6 stimulation of STAT3, we then examined the activation of STAT3 relative to IL-6 protein and gene expression in HEK293T (Figure 3.10A, B and C) and U2OS (Figure 3.10D, E, and F). We verified that IL-6 stimulated pSTAT3 and subsequently increased XRCC1 expression

in BG U2OS (Figure 3.11A, B, C), which we previously reported in HEK293T and

MDA-231 [65]. Following 50ng/mL IL-6 exposure, increased STAT3 activation and

XRCC1 protein and gene expression occurred at 1 h in the U2OS ($3.5\pm0.42$ and

$1.7\pm0.091$, respectively) (Figure 3.12A, B, C, and D).

Using ChIP, an increase in STAT3 occupancy at the *XRCC1* promoter verified

STAT3 regulation of XRCC1 following IL-6 exposure in U2OS ($2.4\pm0.27$ enrichment

following IL-6 exposure compared to $1.3\pm0.03$ enrichment for control U2OS) (Figure

3.10E). These results are consistent with the previous findings in HEK293T with

increased inducibility following IL-6 exposure in the U2OS but differ from the

constitutively active MDA-231, which lack inducibility following IL-6 exposure (Figure

2.8 and 2.12). To investigate the links between glucose and IL-6 stimulation of STAT3,

we then examined activation of STAT3 relative to IL-6 protein and gene expression in

HEK293T (Figure 3.11A, B and C) and U2OS (Figure 3.11D, E, and F)
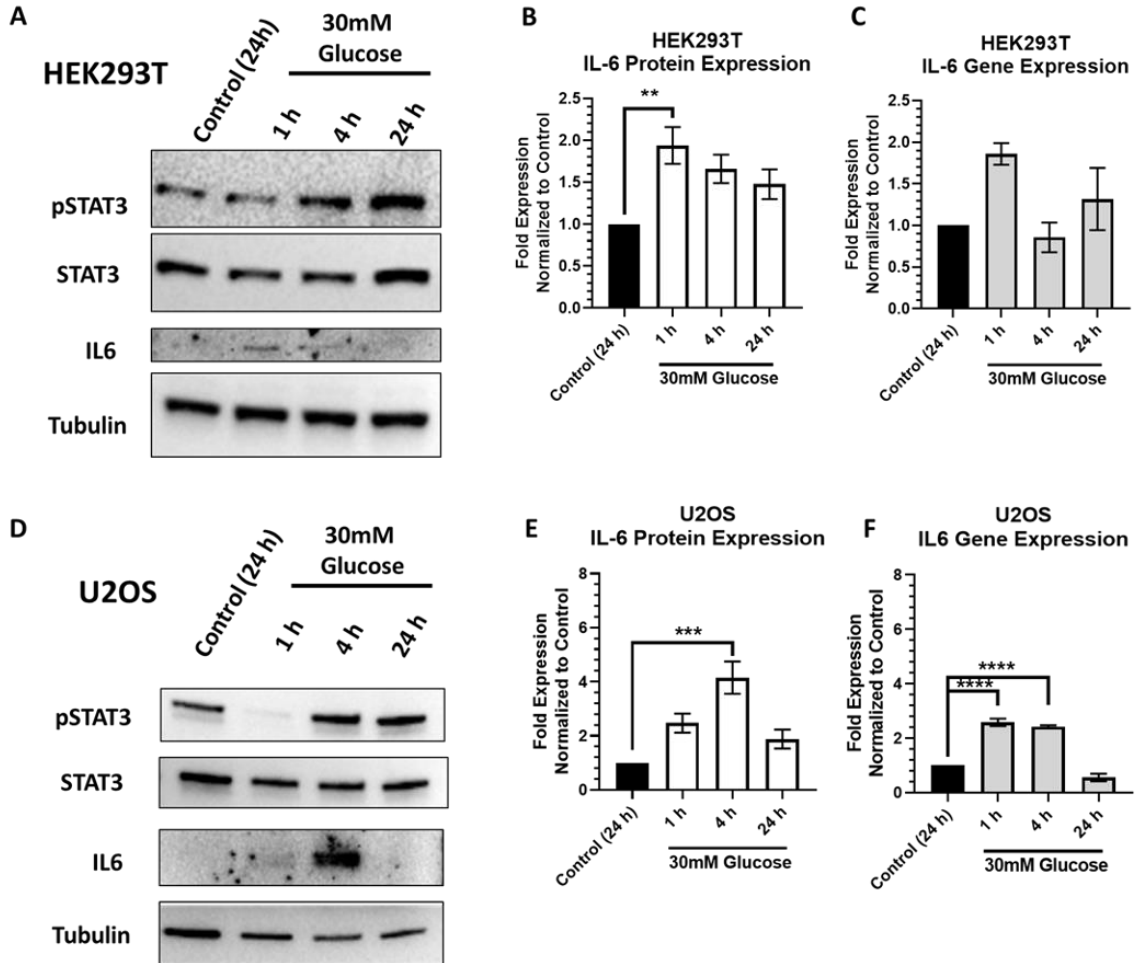


**Figure 3.12**. Acute hyperglycemia stimulates IL-6 protein and gene expression: A) Representative western blot showing increased pSTAT3 and IL-6 following acute hyperglycemia 30mM for 1 h, 4 h, and 24 h in HEK293T B) Quantification of IL-6 protein expression in HEK293T normalized to control C) Quantification of IL-6 gene expression in HEK293T normalized to control D) Representative western blot showing increased pSTAT3 and IL-6 following acute hyperglycemia 30mM for 1 h, 4 h, and 24 h in U2OS E) Quantification of IL-6 protein expression in U2OS normalized to control F) Quantification of IL-6 gene expression in U2OS normalized to control; Blots from this figure were used in Figure 3.1 as well to allow comparison * $p < 0.05$ ** $p < 0.01$,*** $p < 0.001$, **** $p < 0.0001$.
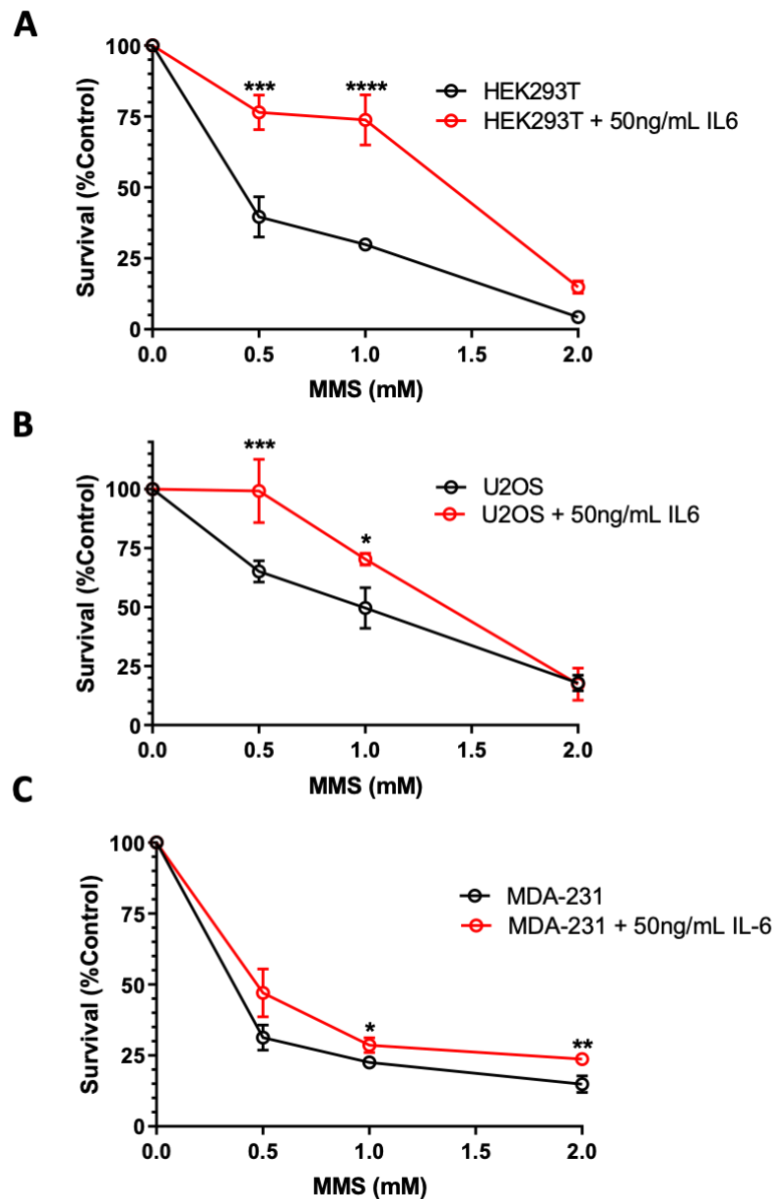
**Figure 3.13.** XRCC1 inducibility determines response to MMS: A) Cell counting survival curve following dosing of MMS in MDA-231, MDA-231 were dosed with 50ng/mL IL-6 for 30 min followed by continuous IL-6 exposure, mean survival (%) and SEM (%) normalized to control MDA-231 C) Cell counting survival curve following dosing of MMS in HEK293T, HEK293T were dosed with 50ng/mL IL-6 for 30 min followed by continuous IL-6 exposure, mean survival (%) and SEM (%) normalized to control HEK293T D) Cell counting survival curve following dosing of MMS in U2OS, U2OS were pre-treated with 50ng/mL IL-6 for 30 min followed by continuous IL-6 exposure, mean survival (%) and SEM (%) normalized to control U2OS.

Next, we examined the sensitivity of the cell lines to MMS following 30 min 50ng/mL IL-6 exposure before applying challenge with MMS followed by continuous exposure to IL-6. Increased resistance to MMS occurred following acute IL-6 exposure with the largest increase in resistance occurring in the HEK293T ($40\pm7.1\%$ survival for control compared to $76\pm6.1\%$ IL-6, respectively, following 0.5mM MMS), a moderate response in U2OS ($65\pm4.5\%$ survival for control compared to and $99\pm10\%$ for IL-6, following 0.5mM MMS), and a limited response in MDA-231 ($31\pm7.7\%$ survival for control compared to $47\pm8.4\%$ for IL-6, following 0.5mM MMS) (Figure 3.12).

**High EGFR expression in MDA-231 mitigates glucose-driven changes in pSTAT3**
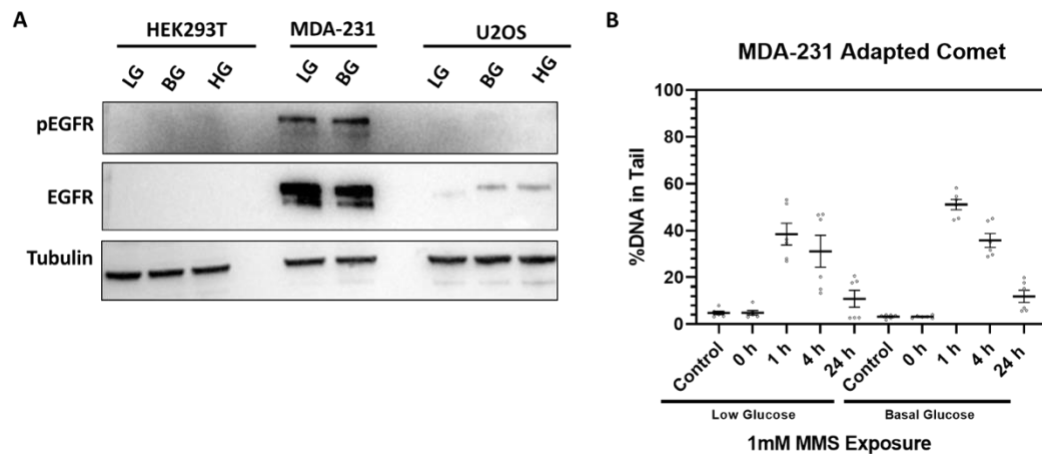


**Figure 3.14**. High expression of EGFR measures response in MDA-231: A) Representative western blot of pEGFR (Y1068) and EGFR in HEK293T, MDA-231, and U2OS adapted cell lines B) Comet assay in LG and BG MDA-231 following 1mM MMS exposure * $p < 0.05$ ** $p < 0.01$,*** $p < 0.001$, **** $p < 0.0001$.

The differences observed between MDA-231 and the HEK293T and U2OS cells suggest that another upstream regulator of STAT3 is involved. We previously reported

increases in STAT3 activation and XRCC1 expression in MDA-231 cells exposed to EGF [65]. With minimal IL-6 responses in MDA-231, we examined EGFR expression and activation across the cell line panel (Figure 3.14A). Immunoblotting revealed increased EGFR expression in MDA-231, moderate EGFR expression in U2OS, and non-detectable EGFR expression in HEK293T (Figure 3.14A). High activation and expression of EGFR MDA-231 may be responsible for the observed constitutive activation of STAT3. Even under low glucose, the MDA-231 lack a significant reduction in STAT3 activation (0.71 $\pm$ 0.08) and occupancy at the *XRCC1* promoter (1.8 $\pm$ 0.07, compared to IgG controls) compared to HEK293T and U2OS (0.98 $\pm$ 0.30 and 0.93 $\pm$ 0.19, compared to IgG controls, respectively) (Figure 3.7 and 3.8). We confirmed this lack of change in DNA repair through a comet assay with LG and BG MDA-231 adapted cell lines following 1mM exposure to MMS. The comet assay revealed no significant change in DNA repair following LG adaptation (Figure 3.14B), consistent with the maintenance of STAT3 driven expression of XRCC1 (Figure 3.9).

## Discussion

We have previously reported that STAT3 drives the dysregulation of XRCC1 in TNBC while serving as an inducible transcription factor in the non-tumorigenic HEK293T [65]. Here, we show high glucose drives STAT3 activation, increasing the expression of XRCC1. Acute high glucose (30mM) exposures increased STAT3 activation and XRCC1 protein and gene expression in the non-tumorigenic HEK293T and osteosarcoma U2OS cell lines. The XRCC1 gene and protein increases are linked to

the increased occupancy of STAT3 at the *XRCC1* gene. Further, acute high glucose induced XRCC1 increased survival to DNA damage and improved repair dynamics in HEK293T and U2OS cells exposed to MMS.

If unrepaired, single-strand breaks can increase mutations and chromosomal aberrations, promoting carcinogenesis. Exogenous and endogenous agents can induce the expression of DNA repair proteins to respond to increased lesions and breaks to maintain genomic fidelity. The *XRCC1* regulator E2F1 behaves in this manner, increasing the expression of XRCC1 after exogenous insult with MMS to increase repair and maintain genomic fidelity [14]. Therefore, high DNA repair protein expression serves as a safeguard to carcinogenesis. However, DNA repair is a double-edged sword. The DNA itself is damaged during repair, and too much repair can also be lethal to the cell. Therefore, DNA repair proteins are tightly regulated to prevent extraneous repair. Again, Sp1 and ATM are examples of how this process works for *XRCC1*. If the repair load becomes too high, ATM phosphorylates Sp1, halting Sp1 regulation of *XRCC1* expression in order to prepare the cell for apoptosis [13]. In cancers, the processes by which DNA repair proteins become dysregulated are largely unknown. Overexpression of BER proteins has been correlated with a hypermutability phenotype, which promotes cancer formation [98-100]. Overexpression of BER proteins is also correlated with chemotherapy and radiation therapy resistance, confirming that an imbalance of DNA repair proteins provides an advantage to cancer cells [30-32,63,78].

We first examined STAT3 regulation of XRCC1 in TNBC cell lines where STAT3 had become constitutively active, but the driving factors leading to dysregulation were not examined. Here, we confirmed that glucose challenge activated STAT3 and

drove XRCC1 expression in cells without constitutively active STAT3. These data

demonstrate that STAT3 induces XRCC1 expression in response to exogenous challenges

and that the effects are transient and reduce when cell equilibrium is reacquired. The

temporal increase and decrease in STAT3 activation and XRCC1 expression in the

HEK293T and U2OS cells demonstrate this inducible regulation (Figure 3.1). However,

when we adapted HEK293T and U2OS cells to high glucose continuously, we saw a

sustained activation of STAT3 and continued expression of XRCC1, which suggests that

continuous glucose exposure can lead to increased XRCC1 protein levels. Although

higher glucose concentrations were not tested, a leveling-off of glucose transport would

be expected at concentrations higher than 30mM. Previous reports have shown a plateau

of cytosolic glucose concentrations following exposure to 25mM and 30mM glucose

concentrations in HEK293T co-expressing GLUT1 and GLUT2 glucose transporters [101].

Additionally, at higher glucose concentrations, a reduction of high-affinity glucose

transporter, GLUT1 protein expression and increased low-affinity glucose transporter,

GLUT2,  protein expression has been observed [102]. Thus, at high glucose concentrations

above 30mM, minimal changes in transport would be expected. When studying changes

in glucose concentrations, osmolarity changes are sometimes observed, resulting in cell

swelling and potentially death to the cell. Mannitol is often used to control for potential

differences in osmolarity between different glucose concentrations. However, mannitol

was not used here due to its role in ROS scavenging [103-105]. It has been previously

reported that ROS production following high glucose exposure promotes the production

of IL-6 through activation of NF$\kappa$B [106]. Thus, introduction of a ROS scavenger could

attenuate STAT3 activation following high glucose exposure. Previous reports

investigating changes in UV-associated DNA repair in low and high glucose conditions used mannitol as an osmolarity control and did not observe any changes in repair [87]. Future work focusing on the adaptive transcriptional gene regulatory mechanism following continous glucose alterations is needed. These studies could provide a greater understanding of how glucose adaption alters gene regulation of XRCC1, which has been previously reported in nucleotide excision repair proteins following continous genotoxic exposure [17].

Here, we studied the DNA repair changes associated with increased XRCC1 expression following acute high glucose exposure. There is an advantage to increased XRCC1 expression shown through the improved cell survival and DNA repair after MMS challenge (Figures 3.5 and 3.6). DNA damaging agents are commonly used in cancer therapy, and altered expression of XRCC1 has been found to modulate responses in numerous cancers [28,31,32,34,63,78,107]. STAT3 was not previously identified as a regulator of XRCC1, but the data here demonstrate that STAT3 activation promotes resilience to DNA damage, which likely contributes to chemoresistance or even radiotherapy resistance in cancer cells.

Critically, these effects could be reversed when activated STAT3 is lowered through glucose restriction. Low glucose media (5mM) reduced STAT3 activation in HEK293T and U2OS, reducing the STAT3 enrichment at the *XRCC1* promoter as well as XRCC1 gene and protein expression compared to higher glucose media compositions. However, in MDA-231, which have constitutively activated STAT3, low glucose adaptation resulted in a less significant reduction of STAT3 activation (Figure 3.8), STAT3 enrichment at the *XRCC1* promoter, and XRCC1 protein expression. When we

examined the upstream regulators of STAT3 activation in these cell lines, the MDA-231 cells, unlike the U2OS and HEK293T cells, also had highly activated EGFR, which likely maintains the STAT3 activation and elevated XRCC1 expression.

In looking at other upstream regulators of STAT3 activation, we noted clear differences in the expression of IL-6R$\alpha$ and the stimulation of IL-6 release in these cells that correspond to increasing glucose concentration. It appears the increased expression of IL-6R$\alpha$ has a major role in the inducibility of the non-tumorigenic HEK293T, which we reported previously with IL-6 and here with high glucose (Figure 3.9) [65]. Together these findings suggest that multiple mechanisms drive the activation of STAT3 within cancer cells, but once STAT3 is activated, XRCC1 gene and protein levels will be elevated and impact the cells' responses to DNA damage.

Chronic inflammation, increased inflammatory cytokine signaling, and increased mitogenic signaling are all common in cancer. Here, we show that STAT3 activation induces XRCC1 expression, and continued activation of STAT3 drives BER dysregulation in non-tumorigenic HEK293T and tumorigenic U2OS. Additionally, the induction of this response following exogenous exposures alters the response to the DNA damaging agent MMS, with the most inducible HEK293T having the highest increase in resistance to MMS following STAT3 activation induced by exposure to high glucose and IL-6 (30 $\pm$ 1.8% survival for HEK293T compared to 65 $\pm$ 6.7% survival for HG and 74 $\pm$ 8.8% survival for IL-6 following 1mM MMS exposure) (Figure 3.12). We have also determined that these effects can be mitigated with glucose restriction if other drivers of dysregulated STAT3 activation are absent. These findings suggest that the degree to which these effects can be reversed through therapeutic intervention upstream of STAT3

would depend highly on the signaling nodes used to activate STAT3. Additionally, these findings indicate an inverse relationship between IL-6 concentrations and IL-6R$\alpha$ in HEK293T (low and high, respectively), MDA-231 (moderate and low, respectively) and U2OS (high and moderate, respectively), and a direct relationship between IL-6R$\alpha$ expression, inducibility of the cell lines, and resistance to DNA damaging agents in HEK293T (high), MDA-231 (low), and U2OS (moderate). A better therapeutic strategy for reversing the dysregulation of BER observed here would be targeting STAT3, which we previously demonstrated with alanolactone and shRNA in TNBC cell lines and here with alantolactone in HEK293T following acute high glucose exposure (Figure 3.2) [65].

In sum, this study identified a new transcriptional regulation mechanism for XRCC1, providing a novel link between exogenous exposures, activation of STAT3, and DNA repair. This regulatory mechanism could have major implications in promoting genomic instability and modulating therapeutic response, both critical in the formation and progression of cancer. This work also suggests that transcriptional regulation of BER proteins is highly responsive to exogenous and endogenous changes. Much more work is needed to understand known regulators such as E2F1 and STAT3 and the stimulating conditions that induce transcription through currently unknown regulators. Expression of BER factors, including PARP1, POL β, and XRCC1, are dysregulated in various cancers and associated with poor survival outcomes, and we need a better understanding of the

regulation landscape driving these changes to identify therapeutic targets and improve

patient survival.

# CHAPTER IV: STAT3 ROLE IN THE REGULATION OF BER PROTEINS POLYMERASE BETA AND POLY(ADP)RIBOSE POLYMERASE

## Introduction

Along with XRCC1, POL $\beta$ and PARP1 serve as critical DNA repair proteins in the BER pathway (Figure 1.1). Following the formation of SSBs, PARP1 binds the site of damage and undergoes auto modification in the form of PARylation, the covalent linkage of ADP-ribose polymers to proteins. This PARylation is critical in the recruitment and binding of other BER proteins, including XRCC1. POL $\beta$ is the primary polymerase responsible for DNA synthesis during the BER process. Key interactions between the N-terminal domain of XRCC1 and the thumb and/or palm domain of POL $\beta$ help facilitate its enzymatic activity [9,108].

In cancers, POL $\beta$ protein variants occur in 30% of human tumors. The K289M variant has been shown to have reduced polymerase activity and is tightly associated with colon cancers [11]. Another POL $\beta$ variant, P242R, increases resistance to cisplatin through increased translesion synthesis [109]. Overexpression of POL $\beta$ has been observed in a number of cancer associated tissue samples including breast, colon, and prostate [35]. POL $\beta$ overexpression also occurs in breast, ovarian, and colon cancer cell lines [35,110]. Alterations in POL $\beta$ expression are linked to genomic instability, a hallmark of cancer, with overexpression of POL $\beta$ in CHO cells resulting in a 3-8-fold increase in mutational rates and increased frameshift mutations in Ha cells derived from B-Cell lymphoma [98,111]. Increased expression of POL $\beta$ increases resistance to DNA damaging agents, including MMS [107]. Disruption of POL $\beta$ function results in increased platinum-based

chemotherapeutic sensitivity [29]. Despite these links to BER dysfunction and chemoresistance, no transcription factors have been implicated in the dysregulation of POL $\beta$ that is seen in TNBC. Several transcription factors, Sp1, NF$k$B, TEIF, and CREB-1 (Figure 1.3), have been identified to regulate POL $\beta$, but there are still gaps in our understanding of its transcriptional regulation [12].

PARP1 overexpression results in higher tumor grade and poorer outcomes in breast cancer tumors and is more closely associated with TNBC [112]. Overexpression of PARP1 has been documented in tissues isolated from breast, uterine, ovarian, skin, and lung cancers [113]. Increased PARP1 expression resulted in resistance to the PARP inhibitor Olaparib in human breast cancer cell lines [114]. Inhibition of PARP1 increases sensitization of cancer cells to therapeutics, including cisplatin, carboplatin, camptothecin, temozolomide, and ionizing radiation [115-118]. Dysregulation of PARP1 plays a critical role in therapeutic responses in multiple cancers. Additionally, PARP1 overexpression has been shown to sensitize cells to DNA damaging agents, including alkylating agents and $\gamma$-radiation [119,120]. This suggests an optimal activity and expression of PARP1. A PARP1 SNP, V762A, which has reduced ADP-ribosylation activity, has been correlated within increased risk of prostate and gastrointestinal cancers [121,122]. Thus, dysregulation of PARP1 and PARP1 activity could play a role in both therapeutic resistance and genomic instability, promoting the growth and formation of cancer. However, regulation of PARP1 still remains understudied with only five transcription

factors regulating its expression - Sp1, Sp3, YY-1, NF1, and ETS, none of which have been associated with PARP1 dysregulation in TNBC (Figure 1.4) [12].

We have identified dysregulation of POL $\beta$ and PARP1 in TNBC cell lines, and this dysregulation contributes to altered response to DNA damaging chemotherapeutics. Further understanding of the transcriptional regulation of POL $\beta$ and PARP1 could provide insight into the dysregulation of these proteins in TNBC.

## Materials and Methods

### Chemicals

Alantolactone was acquired from Selleckchem (Selleckchem #S8318) and resuspended in anhydrous DMSO to a concentration of 15mM.

### Cell Culture

MDA-MB-231(MDA-231), MDA-MB-468 (MDA-468), and HEK293T were purchased from the American Type Culture Collection (ATCC HTB-26, HTB-132, and CRL-3216, respectively; Manassas, VA, USA) within the last 24 months and passaged < 15 times for all experiments. Cells were tested biweekly during experiments for mycoplasma contamination using the Lonza MycoAlert® (Lonza #LT07-318). MDA-231 and MDA-468 cells were grown in DMEM High Glucose + GlutaMAX™ (Life Technologies, Carlsbad, CA, USA, #10566016) and supplemented with 1% sodium pyruvate (Life Technologies, #11360070) and 10% FBS (Premium Select, R&D systems, Minneapolis, MN, USA). HEK293T cells were grown in DMEM High Glucose + L-Glutamine (HyClone, Logan, UT, USA, # SH30022.01) and supplemented with 1%

sodium pyruvate (Life Technologies #11360070) and 10% FBS. Cells were maintained in a humidified 37 °C incubator with 5% carbon dioxide.

<div align="center">

***In Silico* Transcription Factor Search**

</div>

Potential transcription factor targets for the *POLB* promoter were identified using multiple *in silico* softwares. First, an ENCODE database search was performed to identify transcription factors binding the promoters of interest. IgV browser was used to define potential transcription factor binding sites further.

<div align="center">

**Chromatin Immunoprecipitation**

</div>

MDA-231, MDA-468, and HEK293T cells were grown to confluency in a 150mm dish. The cells were crosslinked by the addition of 1% formaldehyde in DMEM with gentle rocking at room temperature (RT ~23 °C) for 8–10 min. Then, 0.1 M glycine was added for 5 min at RT to quench the formaldehyde. The cells were washed with cold $1\times$ phosphate-buffered saline (PBS) and subsequently lysed with 1 mL of farnham lysis buffer (5 mM HEPES pH 8.0, 85 mM KCl. 0.5% NP-40) for 20 min on ice, then pelleted by centrifugation at 2000 rpm and resuspended in RIPA buffer (50mM Tris-HCl pH 8, 150mM NaCl, 1% sodium deoxycholate, 1mM EDTA, 0.1% SDS, 1% Triton X-100) for 20 min. Isolated chromatin was then sonicated on ice at an amplitude of 12 on a Misonix S-4000 with 15 s on/50 s off for a total process time of 2.5 min for MDA-231 and MDA-468 and an amplitude of 10 on a Misonix S-4000 with 15 s on/50 s off for a total process time of 3.5 min for HEK293T. Chromatin was incubated overnight at 4 °C on a rotator using an anti-STAT3 antibody diluted to manufacturers' recommendations for chromatin immunoprecipitation (Cell Signaling Technology, Danvers, MA, USA #9131S), an anti-Sp1 antibody (Abcam Cambridge, MA, USA #ab13370) diluted 1:100 as a positive

control, a mouse IgG isotype control (Cell Signaling Technology #5415S) and with

Protein A/G magnetic beads (Thermo Fisher Scientific #88802). Magnetic beads were

washed with cold LiCl wash buffer (100 mM Tris-HCl, 500 mM LiCl, 1% NP-40, 1%

Triton X-100) and TE Buffer (10mM Tris-HCl pH 7.5, 0.1mM EDTA). Proteinase K

(VWR Life Science Radnor, PA, USA # E195-5ML) was then added with ChIP Elution

Buffer (1% SDS, 0.1 M $NaHCO_3$) and incubated at 65 °C 950 rpm for 2 h. Proteinase K

was then inactivated at 90 °C for 10 min. DNA was purified using a PureLink PCR

Purification Kit (Life Technologies #K310002 kit). An IgV browser was used to design

primers examining the occupancy across the *POLB* and *PARP1* promoter (Appendix C).

### Western Blotting

Briefly, the cells were grown in 150mm dishes and cultured to 70–80%

confluence. Cells were rinsed with PBS, scraped, stored overnight at −80 °C, then lysed.

Protein content was quantified using a Bradford assay. Then, 20 µg of lysate was

separated on 7.5% or 4–15% SDS Page gel (Bio-Rad #s, 4561025 and 4561084) and

transferred to a nitrocellulose membrane. Membranes were blocked in 5% non-fat dry

milk in Tris-buffered saline (VWR #J640-4L) containing 0.1% Tween20 (Thermo Fisher

Scientific #BP337, TBS-T) and raised against the following primary antibodies: POL $\beta$

(1:1000 #ab175197) from Abcam (Boston, MA, USA); PARP1 (1:1000,556494 from BD

Pharmigen (San Diego, CA, USA); STAT3 (1:1000, #9139) and pSTAT3 Y705 (1:500,

#9131) from Cell Signaling Technology, Inc.; and α-tubulin (1:5000, #T9026) from

Millipore Sigma (St. Louis, MO, USA). The blots were incubated with either of the

horseradish peroxidase (HRP)-labeled secondary antibodies: goat anti-rabbit-HRP or goat

anti-mouse-HRP (#7074P2 and #7076S respectively) from Cell Signaling Technology,

Inc. HRP antibody target proteins were detected by incubating with WesternBright Sirius (Advansta San Jose, CA, USA #K-12043-D20). All immunoblotting was conducted with three biological replicates. Where indicated, protein quantification was conducted with Image Lab Software (Bio-Rad, Hercules, CA, USA). Band intensity was normalized to loading controls and averaged over the three biological replicates with SEM presented.

## Gene Expression and qPCR

Relative gene expression was performed through mRNA isolation from MDA-231, MDA-468, and HEK293T cell lines using Invitrogen Cell to $C_t$ kit (Life Technologies #4399002). Following the manufacturers' recommendations, the cells were plated in a 96-well plate, and the untreated cells were grown to 75% confluency. For transfection, 0.1 µg of plasmid DNA was added with Fugene 6 transfection reagent in a 1:6 ratio (plasmid DNA to Fugene). Cells were then allowed 48h to recover before being lysed for mRNA isolation using an Invitrogen Cell to $C_t$ kit (Life Technologies #4399002). The cells were then lysed, and RT-PCR was performed to produce cDNA using the reagents from the kit. After cDNA synthesis, qPCR was performed using TaqMan Gene expression primers *POLB* (Thermo Fisher #Hs01099715_m1) and *PARP1* (Thermo Fisher #Hs0024302_m1), and the TaqMan master mix provided with the kit (Applied Biosystems Foster City, CA, USA #4369016). The assay was performed in technical triplicate over three biological replicates. Results represent the average of the three biological replicates ± standard error of the mean (SEM).

## Modulation of STAT3

Plasmid constructs for stable depletion of human STAT3 mRNA, pSIH-puro-STAT3 shRNA (referred two as shRNA #1), and its control were gifts from Frank

Sinicrope (Addgene plasmid #26596 and #26597; Watertown, MA, USA). An additional

shRNA construct specific for STAT3 (shRNA Clone ID:NM_003150.3-458s21c1

referred to as shRNA #2 hereafter) and the pLKO.1 control were purchased from Sigma-

Aldrich (St. Louis, MO, USA). Both shRNA constructs and their controls were used to

validate the STAT3 binding site and expression changes. MDA-231 cells were plated at

200,000 cells/well in a 6-well culture plate. After 48h, cells were transfected with 5 μg

plasmid DNA (shRNA# 1 or 2 or appropriate vector control) and FuGene 6 (Promega) at

a 1:6 ratio (DNA to FuGene). Cells were allowed to recover for 48h following

transfection. STAT3 was overexpressed using a pcDNA3.1$^+$ STAT3 ORF clone from

Genscript (Piscataway, NJ, USA) with a C-terminal Flag-tag. MDA-231 cells were plated

at 200,000 cells/well in a 6-well culture plate, and HEK293T were plated in 10cm plates

at 500,000 cells/plate. After 48 h, MDA-231 cells were transfected with 5μg of plasmid

DNA (STAT3-FLAG and proper vector control) and Fugene 6 (Promega) in a 1:6 ratio

(DNA to Fugene). HEK239T cells were transfected with 10 μg of plasmid DNA

(STAT3-FLAG and proper vector control) and Jetprime transfection agent at a 1:2 ratio

(DNA to Jetprime). 48 h post-transfection, cells were rinsed with 1X PBS, plates were

scraped, and the pelleted cells were stored overnight at −80°C. Immunoblot was then

performed as described below.

**Cytokine Exposure**

Cytokine exposure was performed using recombinant Human IL-6 protein (R&D

Systems, Minneapolis, MN, USA, #206-IL-010/CF). IL-6 was aliquoted in PBS at 100

μg/mL concentration and stored at −80°C for no longer than three months before use, as

recommended by the manufacturers. Aliquoted IL-6 was added to the cell culture

medium to a final concentration of 50ng/mL. MDA-231 and HEK293T cells were plated

in 15 mm dishes and cultured to 70–80% confluency. Cells were then exposed to IL-6 at

a final concentration of 50ng/mL for 30 min, 1 h, and 4 h. Cells rinsed with 1X PBS

plates were scraped, and pelleted cells were stored overnight at −80°C. Immunoblot was

performed as described above.

## Statistical Analysis

Assays were performed as three biological replications. One-way ANOVA and

means were compared with Dunnett's post hoc analysis. Comparison groups are indicated

in graphs. All means are reported $\pm$ SEM. $*\ p < 0.05$, $**\ p < 0.01$, $***\ p < 0.001$,

$****\ p < 0.0001$.

## Results

### STAT3 shows significant enrichment at the *POLB* promoter
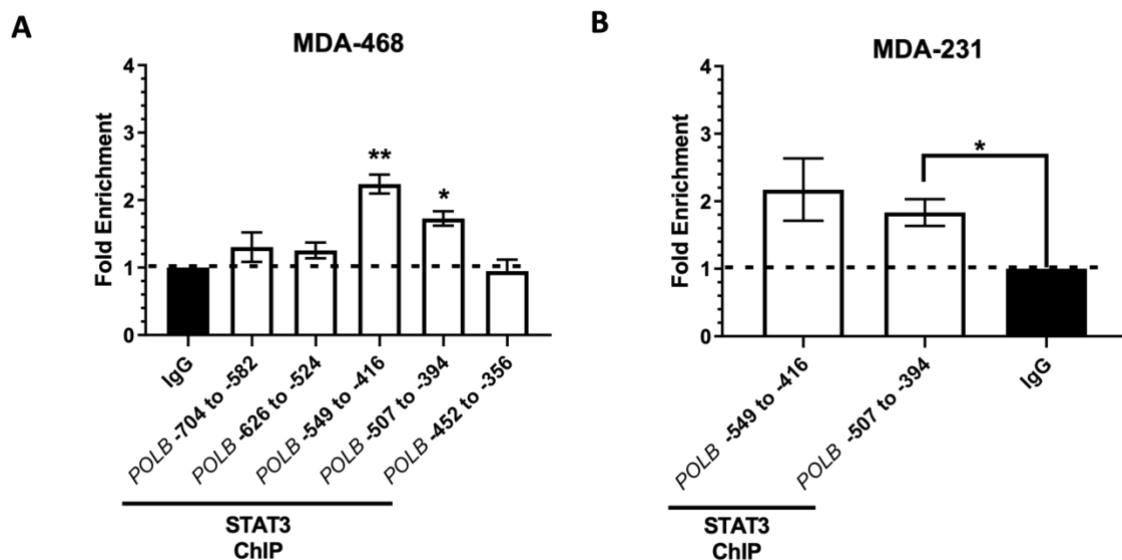


**Figure 4.1.** STAT3 shows significant enrichment at the *POLB* promoter in TNBC cell lines; A) MDA-468 STAT3 ChIP of the *POLB* promoter mapping of STAT3 binding compared IgG controls B) MDA-231 STAT3 ChIP of the *POLB* promoter compared IgG controls $*\ p < 0.05$ $**\ p < 0.01$,$***\ p < 0.001$, $****\ p < 0.0001$.

A potential STAT3 binding site in the *POLB* promoter was first identified via an

IgV browser *in silico* search. IgV browser, as previously described, was used to identify a

potential consensus binding sequence for STAT3 in the *POLB* promoter. ChIP analysis of

the *POLB* promoter showed increased STAT3 enrichment in MDA-468 ($2.2 \pm 0.14$) and

MDA-231 (2.2 ± 0.46) enrichment at a 133 base pair region ( -549 to -416) within the

*POLB* promoter and increased STAT3 enrichment in MDA-468 (1.7 ± 0.11) (Figure

4.1A) and MDA-231 (1.8 ± 0.20) at an overlapping 113 base pair region (-507 to -394)

compared to the respective IgG controls (Figure 4.1B).

## Modulation of STAT3 alters expression of POL $\beta$
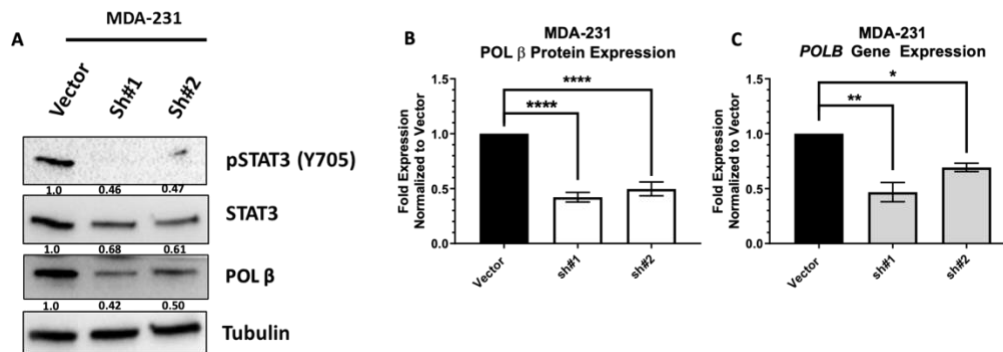


**Figure 4.2.** Attenuation of STAT3 alters expression of POL $\beta$ in MDA-231 ; A)
Representative western blot for pSTAT3, STAT3, and POL $\beta$ with tubulin used as
the loading control B) Quantification of POL $\beta$ protein expression from 3 westerns
blots, values displayed as mean ± SEM compared to vector controls C)
Quantification of *POLB* gene expression analysis, values displayed as mean ± SEM
compared to vector controls * $p < 0.05$ ** $p < 0.01$,*** $p < 0.001$, **** $p < 0.0001$.

We next wanted to further confirm a role for STAT3 in regulating POL $\beta$

expression. STAT3 expression was attenuated using two different shRNA constructs, and

subsequent alterations in POL $\beta$ protein and gene expression were monitored. Following

shRNA-mediated knockdown of STAT3, *POLB* gene expression was attenuated in

MDA-231 (sh#1 0.468 ± 0.088 and sh #2 0.69 ± 0.038) (Figure 4.2C). The reduction of

*POLB* gene expression translated to a reduction in POL $\beta$ protein expression compared to

respective vector controls (sh#1 0.42 $\pm$ 0.04 and sh #2 0.50 $\pm$ 0.04) (Figure 4.2A and B).

Reduced *POLB* gene expression for both shRNA constructs also occurred in MDA-468

(Figure 4.3C) (sh#1 0.67 $\pm$ 0.08 and sh #2 0.61 $\pm$ 0.02).
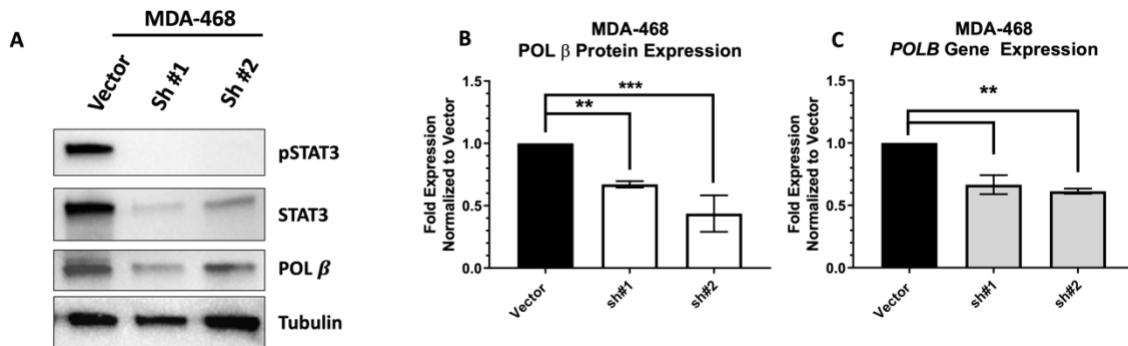


**Figure 4.3**. Attenuation of STAT3 alters expression of POL $\beta$ in MDA-468 ; A)
Representative western blot for pSTAT3, STAT3, and POL $\beta$ with tubulin used as the
loading control B) Quantification of POL $\beta$ protein expression from 3 westerns blots, values
displayed as mean $\pm$ SEM compared to vector controls C) Quantification of *POLB* gene
expression analysis, values displayed as mean $\pm$ SEM compared to vector controls * $p <$
0.05 ** $p < 0.01$,*** $p< 0.001$, **** $p < 0.0001$.

Reduced *POLB* gene expression resulted in attenuated POL $\beta$ protein expression

(sh#1 0.67 $\pm$ 0.03 and sh #2 0.44 $\pm$ 0.09) (Figure 4.3A and B). Ectopic expression of

STAT3 using STAT3-FLAG overexpression vector was used to test the effect of

increased STAT3 expression on POL $\beta$ expression. Following STAT3-FLAG

transfection, immunoblotting and gene expression analysis revealed an increase in POL $\beta$

protein and *POLB* gene expression in MDA-231 ($1.6 \pm 0.09$ and $1.8 \pm 0.14$,

respectively) (Figure 4.4A, B, and C).
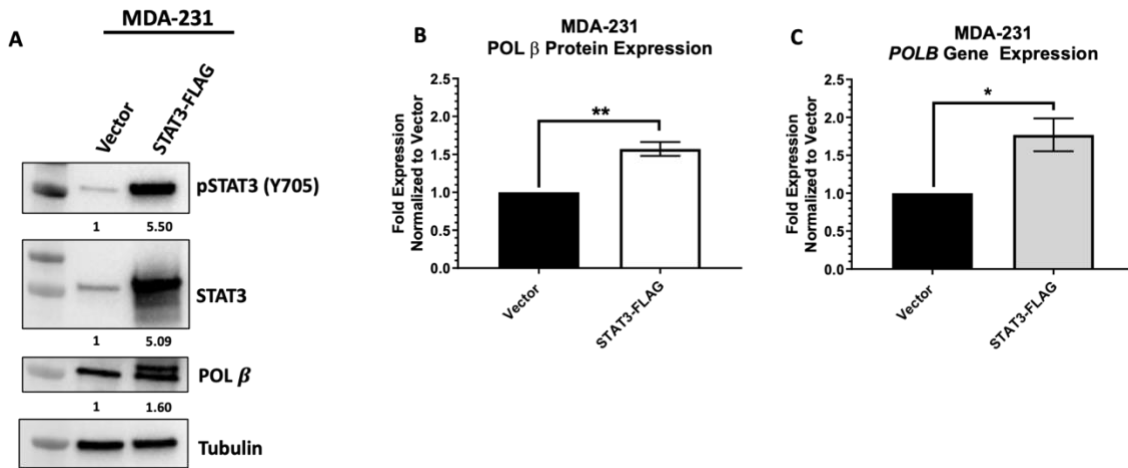


**Figure 4.4.** Ectopic expression of STAT3 increases expression of POL $\beta$ ; A)
Representative western blot for pSTAT3, STAT3, and POL $\beta$ with $\alpha$tubulin used as the
loading control B) Quantification of POL $\beta$ protein expression from 3 westerns blots,
values displayed as mean $\pm$ SEM compared to vector controls C) Quantification of *POLB*
gene expression analysis, values displayed as mean $\pm$ SEM compared to vector controls
* $p < 0.05$ ** $p < 0.01$,*** $p< 0.001$, **** $p < 0.0001$.

### Pharmacological inhibition of STAT3 attenuates POL $\beta$ expression

To further confirm a regulatory role for STAT3 in POL $\beta$ expression, we next

wanted to test the effect that inhibition of STAT3 activation had on POL $\beta$ expression.

STAT3 activation was attenuated by exposing cells with $15\mu$M alantolactone for 4 h.

Subsequent immunoblotting revealed a reduction of POL $\beta$ protein expression in both

MDA-231 and MDA-468 ($0.54 \pm 0.19$ and $0.72 \pm 0.01$, respectively) (Figure 4.5A, B,

D, and E). Gene expression analysis also revealed that reduced STAT3 activation resulted

in a significant reduction in *POLB* gene expression following alantolactone treatment in

both MDA-231 and MDA-468 ($0.77 \pm 0.04$ and $0.74 \pm 0.05$, respectively)(Figure 4.5C and F).
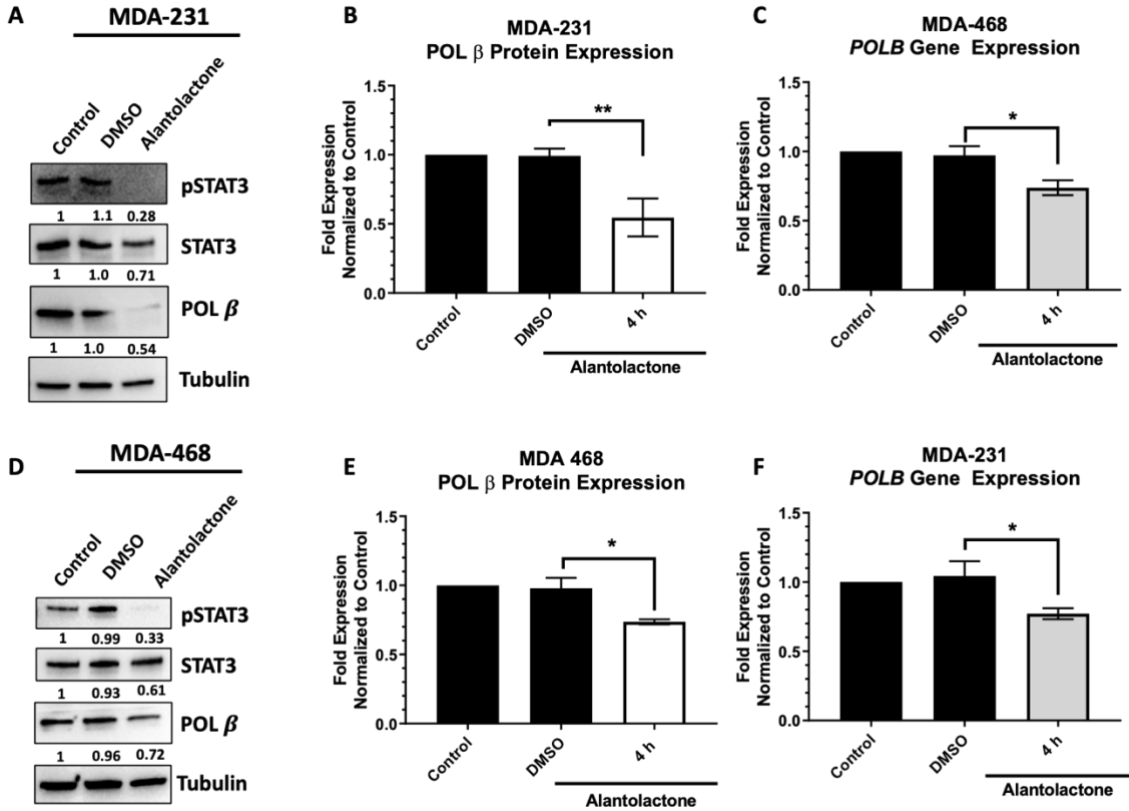


**Figure 4.5.** Pharmacological inhibition of STAT3 attenuates POL $\beta$ expression; A) MDA-231 representative western blot following $15\mu$M alantolactone for 4 h for pSTAT3, STAT3, and POL $\beta$ with tubulin used as the loading control B) Quantification of POL $\beta$ protein expression in MDA-231 from 3 westerns blots following $15\mu$M alantolactone for 4 h, values displayed as mean $\pm$ SEM compared to vector controls C) Quantification of *POLB* gene expression analysis of MDA-231 following $15\mu$M alantolactone for 4 h, values displayed as mean $\pm$ SEM compared to vector controls D) MDA-468 representative western blot following $15\mu$M alantolactone for 4 h for pSTAT3, STAT3, and POL $\beta$ with tubulin used as the loading control E) Quantification of POL $\beta$ protein expression in MDA-468 from 3 westerns blots following $15\mu$M alantolactone for 4 h, values displayed as mean $\pm$ SEM compared to vector controls F) Quantification of *POLB* gene expression analysis of MDA-468, values displayed as mean $\pm$ SEM compared following $15\mu$M alantolactone for 4 h to vector controls $* p < 0.05 ** p < 0.01, *** p < 0.001, **** p < 0.0001$.

**Binding of STAT3 to the *POLB* promoter in HEK293T requires STAT3 activation**

Next, the binding of STAT3 to the *POLB* promoter in the non-tumorigenic cell

line HEK293T was assessed using ChIP. Similar to *XRCC1*, the enrichment of STAT3 at

the *POLB* promoter was low under basal conditions in HEK293T in the overlapping

*POLB* regions ($1.3 \pm 0.06$ and $0.98 \pm 0.50$) (Figure 4.6) compared to the enrichment in

MDA-231 ($2.2 \pm 0.46$ and $1.8 \pm 0.20$). We next wanted to see if the binding of STAT3

to the *POLB* promoter could be stimulated through increases in STAT3 expression or

increased STAT3 activation. Using the STAT3-FLAG ectopic expression vector, STAT3

expression was increased in HEK293T cells, and ChIP analysis revealed increased

STAT3 enrichment at the *POLB* promoter at the overlapping regions ($3.5 \pm 0.68$ and $2.6$

$\pm 0.59$) comparable to the enrichment in the TNBC cell line, MDA-231 ($2.2 \pm 0.46$ and

$1.8 \pm 0.20$) (Figure 4.6A). STAT3 activation in the HEK293T was stimulated through the

exposure of 50 ng/mL IL-6 for 4 h, which was previously shown to stimulate XRCC1

protein and gene expression as well as STAT3 binding to the *XRCC1* promoter in

HEK293T (Figure 2.).
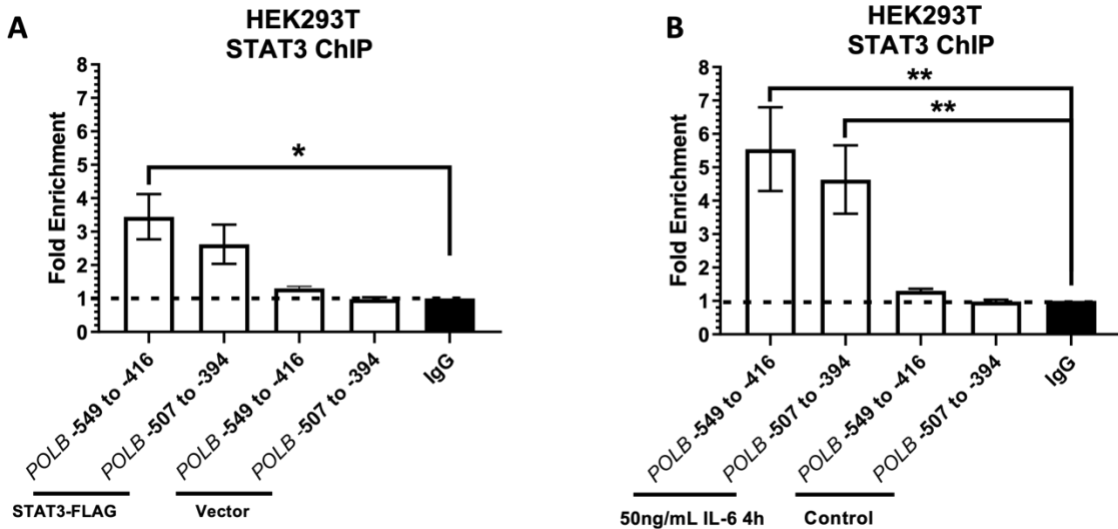


**Figure 4.6**. Binding of STAT3 to the *POLB* promoter in non-TNBC cell line requires STAT3 activation; A) HEK293T STAT3-FLAG STAT3 ChIP of the *POLB* promoter, values normalized to respective IgG controls B) HEK293T STAT3 ChIP of the *POLB* promoter following exposure of 50ng/mL IL-6 for 4 h, values normalized to respective IgG controls * $p < 0.05$ ** $p < 0.01$, *** $p < 0.001$, **** $p < 0.0001$.

Following IL-6 exposure, STAT3 enrichment increased at the overlapping

binding regions in the *POLB* promoter ($5.5 \pm 1.3$ and $4.6 \pm 1.0$) to a level similar to the

MDA-231 ($2.2 \pm 0.46$ and $1.8 \pm 0.20$), which has constitutively active STAT3 (Figure

4.6B). Additionally, *POLB* gene expression increased at 30 min ($1.6 \pm 0.22$) following

50ng/mL IL-6 exposure in HEK293T. A peak increase in POL $\beta$ protein expression

occurred at 1 h ($2.4 \pm 0.53$) following 50 ng/mL IL-6 exposure in HEK293T (Figure

4.7A, B). Similar increases in POL $\beta$ gene and protein expression were seen in MDA-231

with peaks in protein expression occurring at 30 min and 4 h (2.4 $\pm$ 0.12 and 2.7 $\pm$ 0.29)
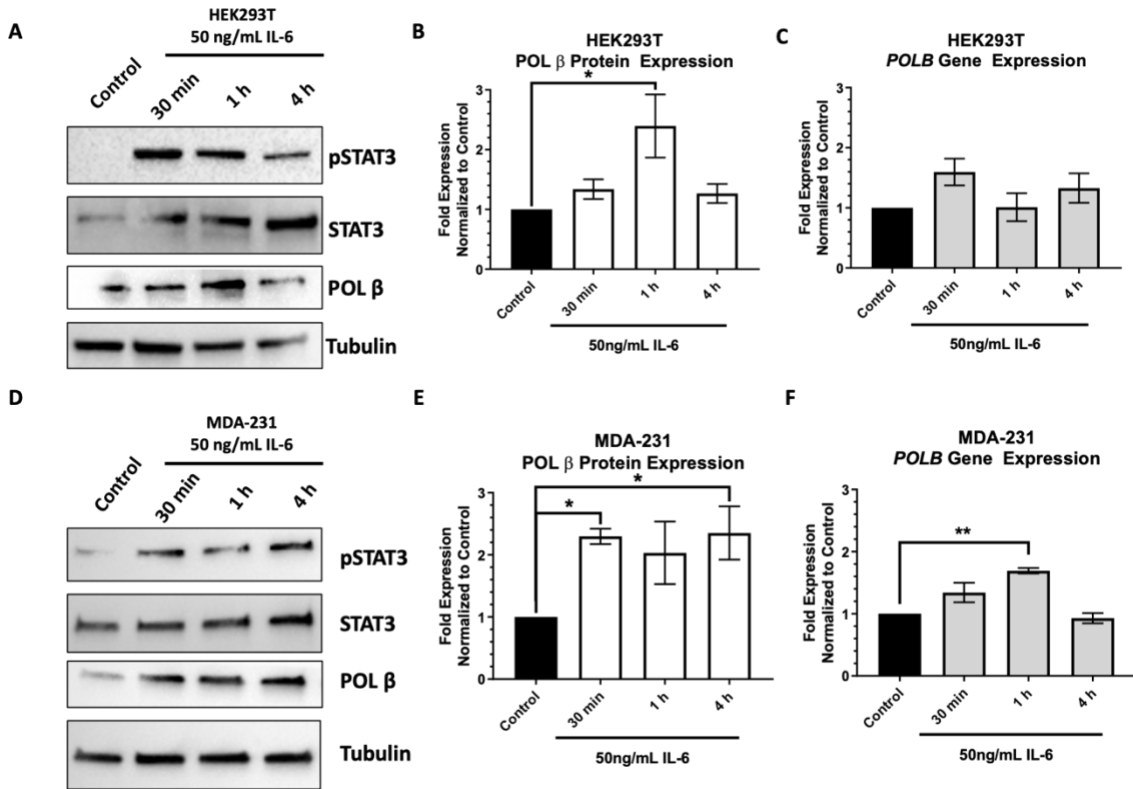


**Figure 4.7**. IL-6 increases phospho-STAT3 and increases the expression of POL $\beta$ in HEK293T and MDA-231. A) Representative immunoblot of phospho-STAT3 (Y705), STAT3 and POL $\beta$ protein expression after 30 min, 1 h, and 4 h exposure to 50 ng/mL IL-6 in HEK293T, α-tubulin is used as a loading control. B) Quantification of protein expression changes in POL $\beta$ resulting from 50 ng/mL IL-6 in HEK293T. C) Quantification of *POLB* mRNA expression following 50 ng/mL IL-6 in HEK293T. D) Representative immunoblot of phospho-STAT3 (Y705), STAT3 and POL $\beta$ protein expression after 30 min, 1 h, and 4 h exposure to 50 ng/mL IL-6 in MDA-231, α-tubulin is used as a loading control. E) Quantification of protein expression changes in POL $\beta$ resulting from 50 ng/mL IL-6 in MDA-231. F) Quantification of *POLB* mRNA expression following 50 ng/mL IL-6 in MDA-231. *p<0.05, **p< 0.01, ***p<0.001

following IL-6 and peaks in gene expression at 1 h ($1.69 \pm 0.0438$) (Figure 4.7D, E, and

F).

**The *PARP1* promoter does not contain a STAT3 binding site**
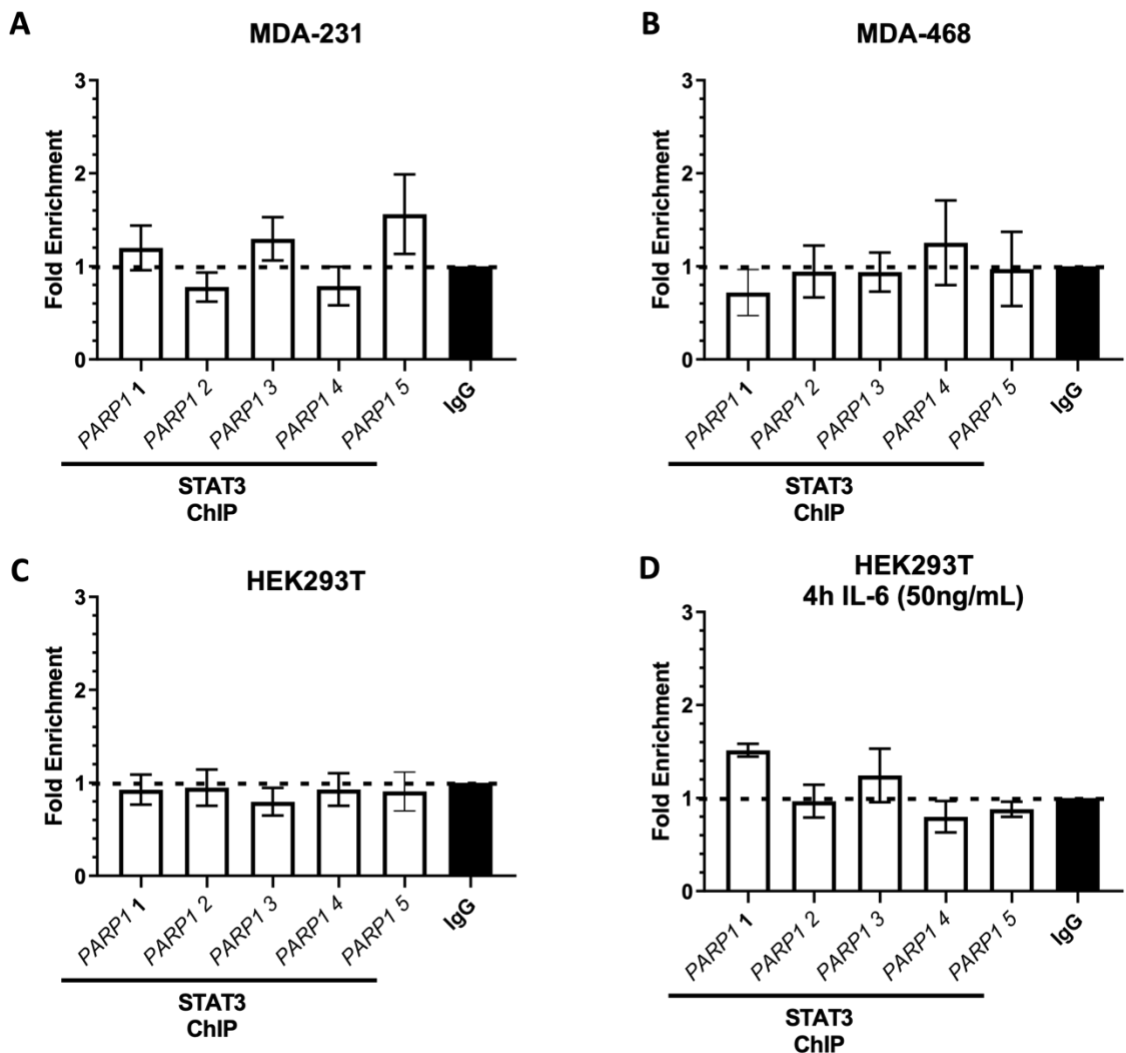


**Figure 4.8.** The *PARP1* promoter does not show significant STAT3 enrichment A) MDA-231 STAT3 ChIP of the *PARP1* promoter, normalized to respective IgG controls B) MDA-468 STAT3 ChIP of the *PARP1* promoter, normalized to respective IgG controls C) HEK293T STAT3 ChIP of the *PARP1* promoter, normalized to respective IgG controls D) HEK293T STAT3 ChIP of the *PARP1* promoter following exposure to 50ng/mL of IL-6 for 4 h, normalized to respective IgG controls * $p < 0.05$ ** $p < 0.01$,*** $p < 0.001$, **** $p < 0.0001$.

We first assessed the potential for a STAT3 binding site within the *PARP1* promoter using an *in silico* search with the IgV browser. A potential STAT3 binding site was predicted within the *PARP1* promoter. To further characterize the potential STAT3 binding site, STAT3 ChIP analysis was performed at the *PARP1* promoter. No STAT3 enrichment was seen at the *PARP1* promoter, indicating no strong STAT3 binding site within the region for MDA-231 and MDA-468 (Figure 4.8A and B). No binding site was



**Figure 4.9.** Attenuation of STAT3 does not alter expression of PARP1 in MDA-231 ; A) Representative western blot for pSTAT3, STAT3, and PARP1 with α-tubulin used as the loading control B) Quantification of PARP1 protein expression from 3 westerns blots, values displayed as mean ± SEM compared to vector controls C) Quantification of *PARP1* gene expression analysis, values displayed as mean ± SEM compared to vector controls * $p < 0.05$ ** $p < 0.01$,*** $p < 0.001$, **** $p < 0.0001$.

identified in the non-tumorigenic HEK293T (Figure 4.8C). Following stimulation with

IL-6, no STAT3 enrichment occurred at the *PARP1* promoter (Figure 4.8D).

**Differential expression of PARP1 following STAT3 modulation**

Because of the many roles of PARP1, including modulation of STAT3 activity

through PARylation, we wanted to test how STAT3 modulation would alter protein and

gene expression of PARP1.

Using two shRNA constructs targeting different regions of STAT3, a STAT3

knockdown was performed. Subsequent gene expression analysis revealed no significant

changes in *PARP1* gene expression following STAT3 knockdown in MDA-231 (sh#1

$0.83 \pm 0.12$ and sh #2 $1.3 \pm 0.19$) (Figure 4.9C) and MDA-468 (sh#1 $0.89 \pm 0.08$ and sh

#2 $0.88 \pm 0.13$) (Figure 4.10C). As expected STAT3 knockdown did not result in

reduced PARP1 in MDA-231 (sh#1 $0.84 \pm 0.01$ and sh #2 $1.1 \pm 0.28$) (Figure 4.9 A and

B) and MDA-468 (sh#1 $0.93 \pm 0.08$ and sh #2 $1.0 \pm 0.15$) (Figure 4.10A and B). To

further confirm that STAT3 does not have a strong regulatory role in the expression of

PARP1, we used the STAT3 inhibitor alantolactone. MDA-231 and MDA-468 cells were

dosed with $15\mu$M alantolactone for 4 h. Following alantolactone treatment, a non-

significant change in *PARP1* gene expression occurred in MDA-231 ($0.88 \pm 0.02$) and in

MDA-468 ($0.94 \pm 0.05$) compared to the respective DMSO control (Figure 4.11C and F).



**Figure 4.10.** Attenuation of STAT3 does not alter expression of PARP1 in MDA-468 ; A) Representative western blot for pSTAT3, STAT3, and PARP1 with tubulin used as the loading control B) Quantification of PARP1 protein expression from 3 westerns blots, values displayed as mean $\pm$ SEM compared to vector controls C) Quantification of *PARP1* gene expression analysis, values displayed as mean $\pm$ SEM compared to vector controls * $p < 0.05$ ** $p < 0.01$,*** $p < 0.001$, **** $p < 0.0001$.

Immunoblots revealed a slight reduction of PARP1 protein expression in MDA-468 ($0.79 \pm 0.07$) and a non-significant reduction in MDA-231 ($0.92 \pm 0.25$) (Figure 4.11 A, B, C, and D). These results were further confirmed by no changes in PARP1

protein or gene expression following overexpression of STAT3 through the STAT3-

FLAG in MDA-231 ($1.2 \pm 0.10$ and $1.2 \pm 0.14$, respectively) (Figure 4.12).
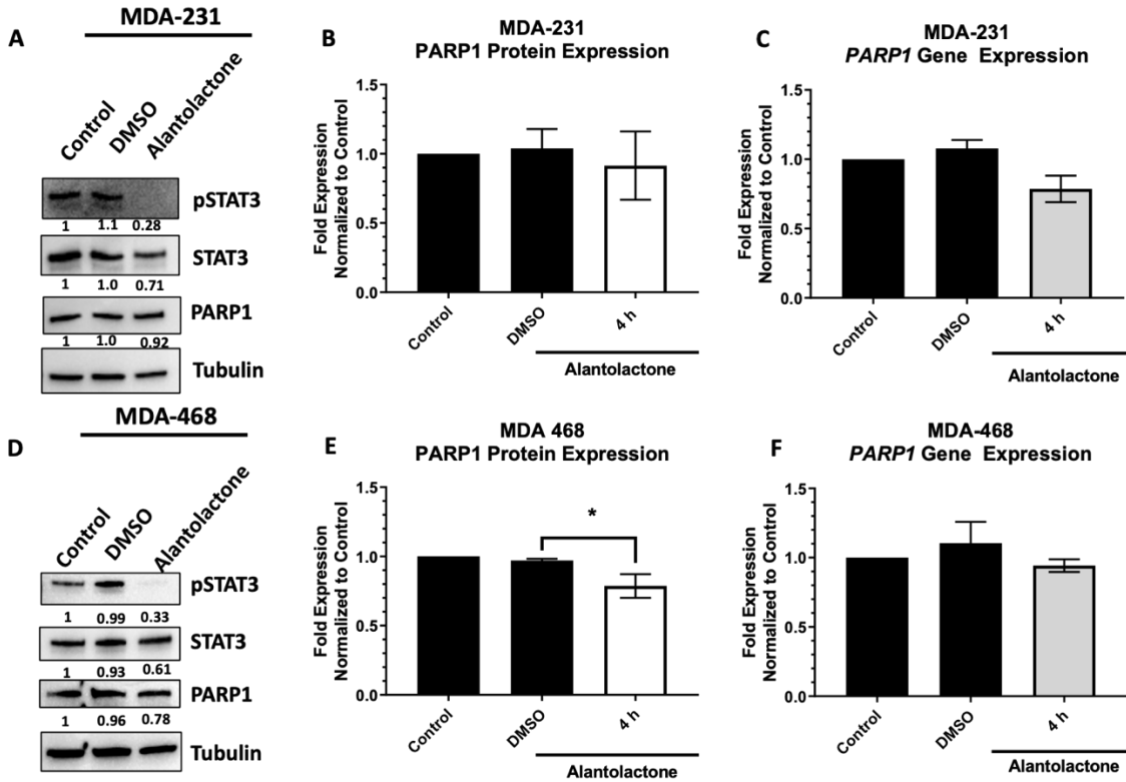


**Figure 4.11.** Pharmacological inhibition of STAT3 does not alter PARP1 expression A) MDA-231 representative western blot following $15 \mu$M alantolactone for 4 h for pSTAT3, STAT3, and PARP1 with tubulin used as the loading control B) Quantification of PARP1 protein expression in MDA-231 from 3 westerns blots following $15 \mu$M alantolactone for 4 h, values displayed as mean $\pm$ SEM compared to vector controls C) Quantification of *PARP1* gene expression analysis of MDA-231 following $15 \mu$M alantolactone for 4 h, values displayed as mean $\pm$ SEM compared to vector controls D) MDA-468 representative western blot following $15 \mu$M alantolactone for 4 h for pSTAT3, STAT3, and PARP with tubulin used as the loading control E) Quantification of PARP1protein expression in MDA-468 from 3 westerns blots following $15 \mu$M alantolactone for 4 h, values displayed as mean $\pm$ SEM compared to vector controls F) Quantification of *PARP1* gene expression analysis of MDA-468, values displayed as mean $\pm$ SEM compared following $15 \mu$M alantolactone for 4 h to vector controls * $p < 0.05$ ** $p < 0.01$,*** $p< 0.001$, **** $p < 0.0001$.
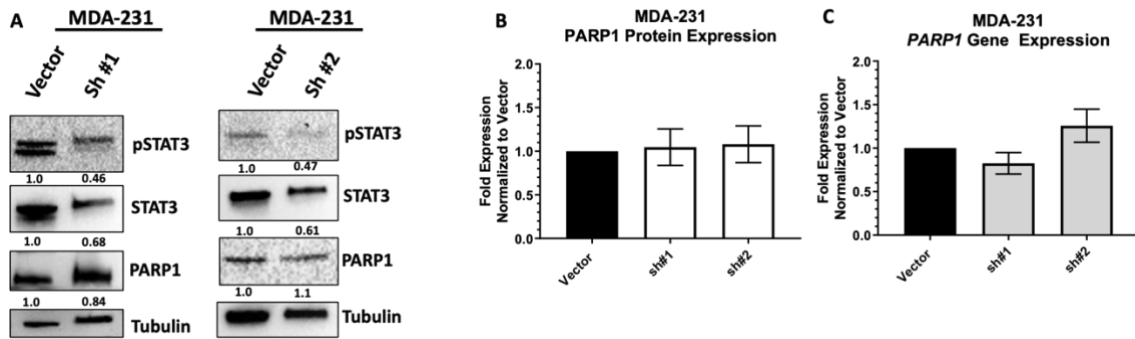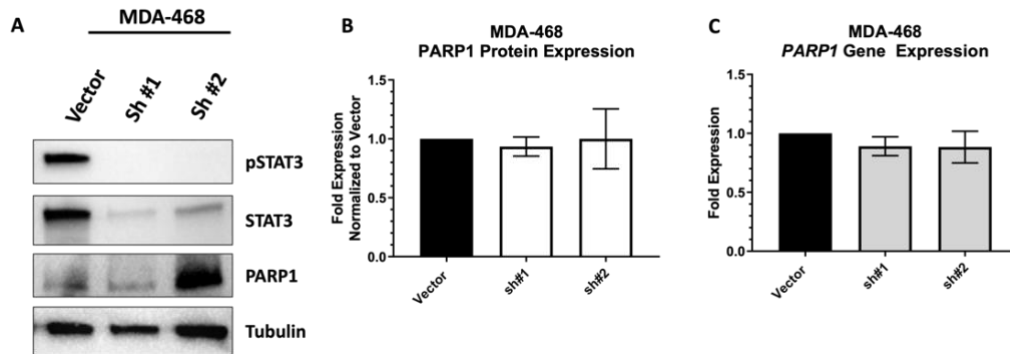
**Figure 4.12.** Ectopic expression of STAT3 does not alter the expression of PARP1 A) Representative western blot for pSTAT3, STAT3, and PARP1 with tubulin used as the loading control B) Quantification of POL $\beta$ protein expression from 3 westerns blots, values displayed as mean $\pm$ SEM compared to vector controls C) Quantification of *PARP1* gene expression analysis, values displayed as mean $\pm$ SEM compared to vector controls * $p < 0.05$ ** $p < 0.01$,*** $p < 0.001$, **** $p < 0.0001$.

## Discussion

Here we report that STAT3 is a novel regulator of POL $\beta$ in TNBC cell lines MDA-231 and MDA-468. STAT3 regulation of POL $\beta$ occurs constitutively in MDA-231 and MDA-468 through constitutive activation of STAT3. Attenuation of STAT3 through STAT3 knockdown and inhibition of STAT3 activation through alantolactone treatment resulted in reduced POL $\beta$ expression at the protein and gene expression level. In the non-tumorigenic cell line HEK293T, a low amount of STAT3 enrichment at the *POLB* promoter was seen ($1.3 \pm 0.06$ and $0.98 \pm 0.50$, for overlapping *POLB* promoter regions) compared to the TNBC cell lines MDA-231 ($2.2 \pm 0.14$ and $1.73 \pm 0.11$) and MDA-468 ($2.2 \pm 0.46$ and $1.8 \pm 0.20$). Given the regulatory mechanism identified for

XRCC1, we wanted to test physiologically relevant exogenous exposures known to stimulate STAT3. Interestingly, the binding of STAT3 to the *POLB* promoter was stimulated by both the ectopic expression of STAT3 and STAT3 activation through IL-6 exposure. Expression of POL $\beta$ was also stimulated by exogenous exposure to IL-6 in HEK293T similar to STAT3 occupancy of the *XRCC1* promoter.

The regulation of BER proteins XRCC1 and POL $\beta$ by STAT3 suggested other BER proteins may be altered by STAT3, including PARP1, which is also dysregulated in TNBC cell lines. Although *in silico* searches revealed a potential STAT3 binding site within the *PARP1* promoter, ChIP revealed no STAT3 enrichment within the *PARP1* promoter. Following shRNA-mediated knockdown of STAT3, no change in PARP1 gene or protein expression occurred in TNBC cell lines MDA-231 and MDA-468. Pharmacological inhibition of STAT3 using the STAT3 inhibitor alantolactone also resulted in no PARP1 gene or protein expression changes. Finally, overexpression of STAT3 using the STAT3-FLAG ectopic expression vector did not result in increased PARP1 expression in MDA-231. Stimulation of STAT3 expression and activation through ectopic expression and IL-6 exposure, respectively, did not stimulate binding in

non-tumorigenic HEK293T. These data indicate STAT3 does not have a significant role in the regulation *PARP1* transcription.
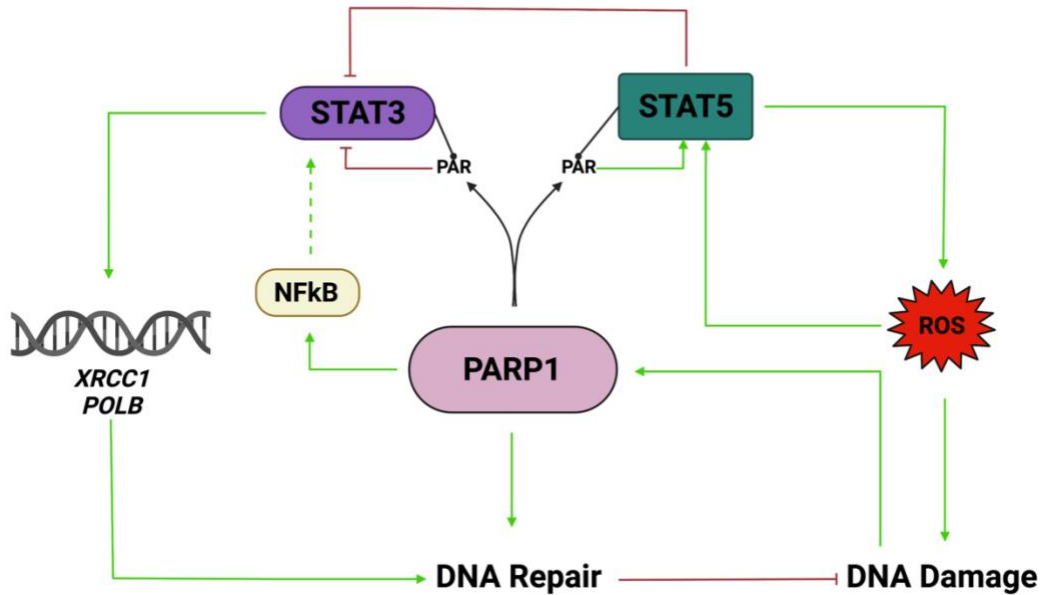


**Figure 4.13.** Role of PARP1 in the regulation of STAT3 and STAT5 activity. PARP1 PARylates STAT3 and STAT5, reducing the activity of STAT3 and promoting the activity of STAT5, which have been shown to have reciprocal functions. This Figure was generated using Biorender.com with citation provided in Appendix B.

Interestingly, STAT3 is PARylated by PARP1, reducing the activity of STAT3, while for STAT5, another STAT family member previously mentioned, PARylation increases the activity of STAT5. An interesting explanation for the lack of STAT3 regulation of PARP1 arises when comparing the reciprocal functions of STAT3 and STAT5 and the role PARP1 has in regulating their activity (Figure 4.13). STAT5 is known to suppress the function of STAT3 and is activated following PARylation by PARP1 [46,48,123,124]. STAT5 increases ROS production, increasing oxidative DNA damage

and further stimulating PARP1 activation [123]. On the other hand, STAT3 activity is suppressed following PARylation [24]. Thus, increased expression of PARP1 would ultimately shut off regulation by STAT3 through both PARylation of STAT3 and PARylation STAT5, which shuts off STAT3 regulation. Because STAT3 has been shown to drive the regulation of XRCC1 and POL $\beta$, PARP1 regulation of STAT3 and STAT5 activity provide an additional mechanism for cells to prevent overexpression of BER proteins. Yet these regulatory schemes are subverted in TNBC, contributing to its aggressive nature.

Dysregulation of DNA repair proteins is a hallmark of cancer. Here we identified that POL $\beta$ is regulated by STAT3, an oncogene constitutively activated in 70% of human cancers, including TNBC [45,50]. Because of the molecular status of TNBC, molecularly targeted therapies are ineffective in the treatment of TNBC. Thus, DNA damaging chemotherapeutics serve as first-line treatment options for patients with TNBC. This work provides a novel link between STAT3 and POL $\beta$ and suggests that constitutive activation may potentially serve as a novel biomarker for therapeutic sensitivity and resistance through BER dysregulation. In addition to the role in therapeutic response, POL $\beta$ overexpression has been documented to promote 'mutator phenotypes' through genomic instability [29,98]. This also provides a novel link to inflammation and other conditions promoting STAT3 activation and increased genomic instability through POL $\beta$, potentially promoting cancer formation and progression. Both increased POL $\beta$ and increased STAT3 activation play a critical role in carcinogenesis [35,125]. Thus, sustained STAT3 activation, which commonly occurs in cancer, drives POL $\beta$ and XRCC1 expression. In concert, these could drive genomic instability and promote

carcinogenesis. Future studies should work to futher delinate the role of STAT3 driven overexpression of POL $\beta$ and XRCC1 on these processes.

This chapter describes work uncovering STAT3 as a novel constitutive regulator of POL $\beta$ in TNBC cell lines MDA-231 and MDA-468 and a conditional regulator in the non-tumorigenic HEK293T. This work could provide a novel biomarker that could be used to determine the therapeutic response to some DNA damaging chemotherapeutics. This work also provides a novel link between inflammation and POL $\beta$, potentially promoting cancer through genomic instability. Although STAT3 was not shown to regulate the expression of PARP1, PARP1 could serve as a barrier to BER protein overexpression, promoting carcinogenic events through PARylation of STAT3 and STAT5, effectively shutting of STAT3 regulation of BER proteins. The subversion of this mechanism in TNBC requires further investigation and could provide new insight for therapeutic intervention.

# CHAPTER V: CONCLUSIONS

Through this work, I have validated the hypothesis that STAT3 regulates the BER proteins XRCC1, and POL $\beta$, though surprisingly does not regulate PARP1. Further, I have uncovered this regulation scheme is highly relevant to TNBC, where constitutive activation of STAT3 induced overexpression of these proteins and increased DNA repair. For the first time, this work links the overexpression of BER proteins to STAT3 and offers a potential explanation for the observed chemoresistance observed in TNBC. Additionally, I have identified this STAT3-BER regulation axis occurs as a stress response mechanism in other cell line models without constitutive activation of STAT3. Using non-tumorigenic HEK293T, I have demonstrated exogenous stress and mitogenic signal induce the overexpression of XRCC1 and POL $\beta$. This work highlights the beneficial role the STAT3-BER regulation axis may play in normal cell growth and development. More work is needed to understand the conditions under which this healthy DNA damage response loop can be repurposed or reprogrammed in cancer development

and progression. This work is a critical first step in understanding BER regulation in cancer, which has been underappreciated to date.
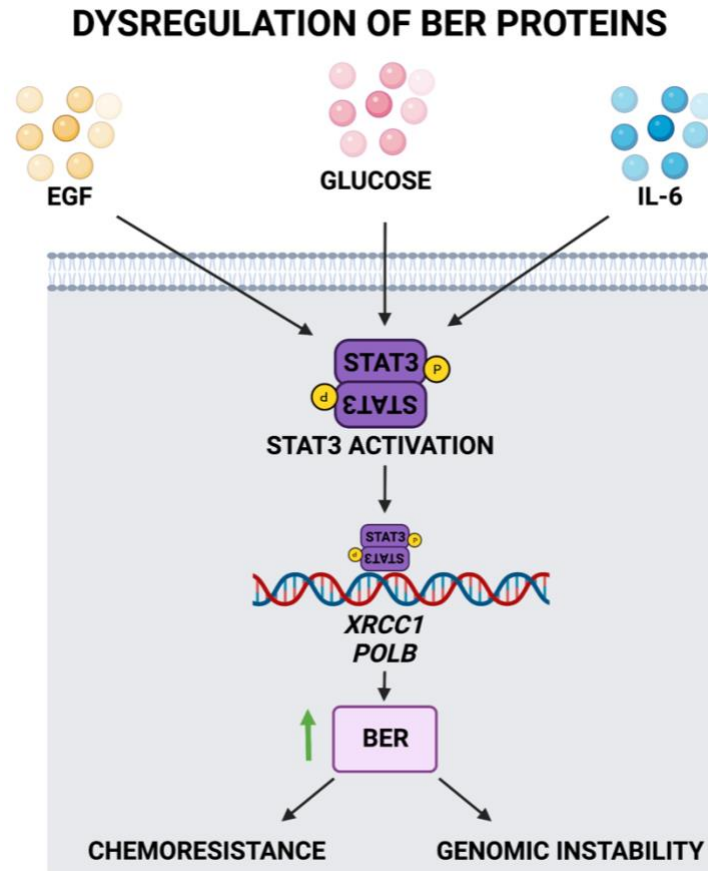


**Figure 5.1.** STAT3 dysregulation of BER proteins: Exogenous exposures, including EGF, IL-6, and Glucose, increase the activation of STAT3, subsequently increasing the occupancy of STAT3 at the promoters of BER genes *XRCC1* and *POLB* and driving the expression of BER proteins, increasing DNA repair and promoting chemoresistance and genomic instability. This Figure was generated using Biorender.com with citation provided in Appendix B.

We also describe a novel link between high glucose exposure and increased XRCC1 expression. Acute high glucose increased STAT3 occupancy of the *XRCC1* promoter and subsequently increased XRCC1 expression. Increased XRCC1 expression

following acute glucose exposure resulted in increased DNA repair and increased

resistance to the alkylating agent MMS. Low glucose adaptation (5mM) in HEK293T and

U2OS reduced the activation of STAT3 and expression of *XRCC1*. Adapting these cell

lines to high glucose (30mM) resulted in dysregulation of XRCC1 gene and protein

expression through sustained STAT3 activation. These data indicate a novel role for

inflammatory signaling and exogenous exposures, including dietary choices, on

regulating BER proteins and modulating DNA repair.
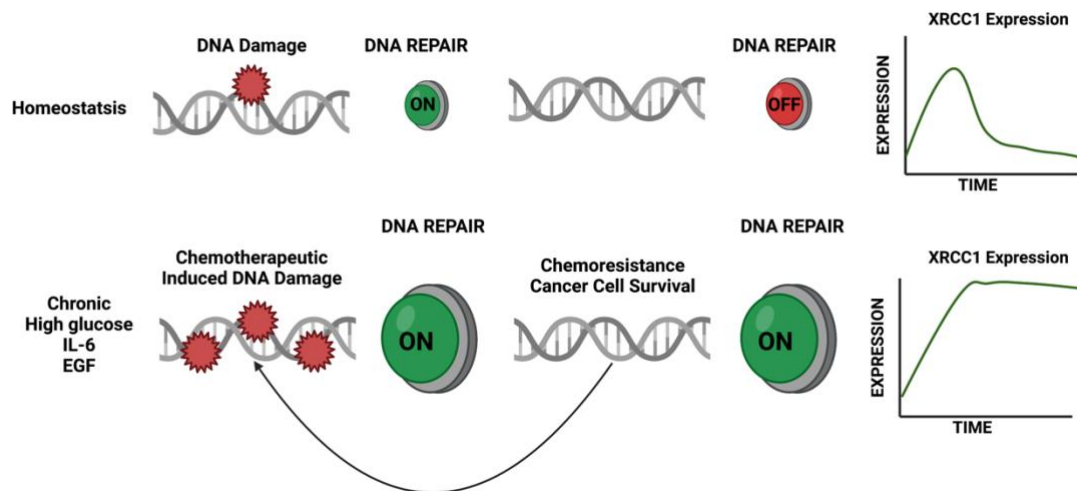


**Figure 5.2.** Dysregulation of XRCC1 promotes increased therapeutic resistance: At homeostasis, acute exposures promote the rapid repair of DNA damage. Chronic exogenous exposures promote sustained STAT3 activation, promoting dysregulation of XRCC1 and therapeutic resistance. This Figure was generated using Biorender.com with citation provided in Appendix B.

Differential XRCC1 expression changes in HEK293T, MDA-231, and U2OS

following exogenous exposures suggest changes in activating cytokines or mitogens and

their receptors that activate STAT3 are responsible for BER protein expression changes.

We found that low release of IL-6, low EGFR activation and expression, and high IL-6R$\alpha$ expression in HEK293T resulted in a highly inducible XRCC1 response upon STAT3 activation. For U2OS, we identified moderate expression of EGFR, high basal STAT3 activation, and high IL-6 release compared to MDA-231 and HEK293T, resulting in an inducible but sustained high XRCC1 expression. Constitutive activation of STAT3 in MDA-231 is likely a result of the high activation and expression of EGFR and low IL-6R$\alpha$ expression compared to HEK293T, resulting in high basal XRCC1 expression with limited inducibility.

Chronic inflammation, hyperglycemia, and inflammatory signaling are common in cancer. Here we identify that continuous exposure to glucose results in the dysregulation of XRCC1 through sustained STAT3 activation in the non-tumorigenic cell lines with limited modulation in the constitutively activated MDA-231. These data indicated that upstream regulators of STAT3 activation play a critical role in the modulation of DNA repair and the potential therapeutic responses following DNA damaging agents (Figure 5.2).

DNA damaging chemotherapeutics have become a mainstay in the treatment of most cancers. STAT3 plays a critical role in the formation and maintenance of many cancers and is constitutively activated in 70% of human cancers. Additionally, BER proteins XRCC1 and POL $\beta$ are overexpressed in a myriad of human cancers, including breast, colorectal, and ovarian. Overexpression of BER proteins promotes genomic instability, a hallmark of cancer, and resistance to DNA damaging chemotherapeutics, including cisplatin. Here we identified a novel regulatory mechanism in which STAT3 promotes the dysregulation of BER proteins XRCC1 and POL $\beta$ (Figure 5.1). This

114

regulation could serve as a novel avenue for cancer cells to gain resistance to DNA

damaging chemotherapeutics by increasing DNA repair. We have also shown that

sustained STAT3 activation promotes the dysregulation of XRCC1 in tumorigenic and

non-tumorigenic cell lines. These data indicate a role for sustained STAT3 activation in

promoting genomic instability and potentially promoting tumorigenesis.

# REFERENCES

1.	Tubbs A, Nussenzweig A. Endogenous DNA damage as a source of genomic instability in cancer. *Cell*. Feb 9 2017;168(4):644-656. doi:10.1016/j.cell.2017.01.002

2.	Wallace SS. Base excision repair: a critical player in many games. *DNA Repair (Amst)*. Jul 2014;19:14-26. doi:10.1016/j.dnarep.2014.03.030

3.	Caldecott KW. Mammalian DNA base excision repair: dancing in the moonlight. *DNA Repair (Amst)*. Sep 2020;93:102921. doi:10.1016/j.dnarep.2020.102921

4.	Lee KJ, Piett CG, Andrews JF, Mann E, Nagel ZD, Gassman NR. Defective base excision repair in the response to DNA damaging agents in triple negative breast cancer. *PLoS One*. Oct 9 2019;14(10):e0223725. doi:10.1371/journal.pone.0223725

5.	Wallace SS, Murphy DL, Sweasy JB. Base excision repair and cancer. *Cancer Lett*. Dec 31 2012;327(1-2):73-89. doi:10.1016/j.canlet.2011.12.038

6.	Krokan HE, Standal R, Slupphaug G. DNA glycosylases in the base excision repair of DNA. *Biochem J*. Jul 1 1997;325(Pt 1)(Pt 1):1-16. doi:10.1042/bj3250001

7.	Spiegel JO, Van Houten B, Durrant JD. PARP1: structural insights and pharmacological targets for inhibition. *DNA Repair (Amst)*. Jul 2021;103:103125. doi:10.1016/j.dnarep.2021.103125

8.	de Murcia G, Ménissier de Murcia J. Poly(ADP-ribose) polymerase: a molecular nick-sensor. *Trends Biochem Sci*. Apr 1994;19(4):172-176. doi:10.1016/0968-0004(94)90280-1

9.      London RE. The structural basis of XRCC1-mediated DNA repair. *DNA Repair (Amst)*. Jun 2015;30:90-103. doi:10.1016/j.dnarep.2015.02.005

10.     Dantzer F, Schreiber V, Niedergang C, Trucco C, Flatter E, De La Rubia G, Oliver J, Rolli V, Ménissier-de Murcia J, de Murcia G. Involvement of poly(ADP-ribose) polymerase in base excision repair. *Biochimie*. Jan-Feb 1999;81(1-2):69-75. doi:10.1016/s0300-9084(99)80040-6

11.     Starcevic D, Dalal S, Sweasy JB. Is there a link between DNA polymerase beta and cancer? *Cell Cycle*. Aug 2004;3(8):998-1001. doi:10.4161/cc.3.8.1062

12.     Wright G, Gassman NR. Transcriptional dysregulation of base excision repair proteins in breast cancer. *DNA Repair (Amst)*. Sep 2020;93:102922. doi:10.1016/j.dnarep.2020.102922

13.     Fletcher SC, Grou CP, Legrand AJ, Chen X, Soderstrom K, Poletto M, Dianov GL. Sp1 phosphorylation by ATM downregulates BER and promotes cell elimination in response to persistent DNA damage. *Nucleic Acids Res*. Feb 28 2018;46(4):1834-1846. doi:10.1093/nar/gkx1291

14.     Chen, Yu Z, Zhu Z, Lopez CD. E2F1 regulates the base excision repair gene XRCC1 and promotes DNA repair. *J Biol Chem*. May 30 2008;283(22):15381-15389. doi:10.1074/jbc.M710296200

15.     Narayan S, Wilson SH. Kinetic analysis of Sp1-mediated transcriptional activation of the human DNA polymerase beta promoter. *Oncogene*. Sep 28 2000;19(41):4729-4735. doi:10.1038/sj.onc.1203823

16.     Kedar PS, Widen SG, Englander EW, Fornace AJ, Jr., Wilson SH. The ATF/CREB transcription factor-binding site in the polymerase beta promoter mediates

the positive effect of N-methyl-N'-nitro-N-nitrosoguanidine on transcription. *Proc Natl Acad Sci U S A*. May 1 1991;88(9):3729-3733. doi:10.1073/pnas.88.9.3729

17.     Christmann M, Kaina B. Transcriptional regulation of human DNA repair genes following genotoxic stress: trigger mechanisms, inducible responses and genotoxic adaptation. *Nucleic Acids Res*. Oct 2013;41(18):8403-8420. doi:10.1093/nar/gkt635

18.     He F, Yang XP, Srivastava DK, Wilson SH. DNA polymerase beta gene expression: the promoter activator CREB-1 is upregulated in Chinese hamster ovary cells by DNA alkylating agent-induced stress. *Biol Chem*. Jan 2003;384(1):19-23. doi:10.1515/bc.2003.003

19.     Faumont N, Le Clorennec C, Teira P, Goormachtigh G, Coll J, Canitrot Y, Cazaux C, Hoffmann JS, Brousset P, Delsol G, Feuillard J, Meggetto F. Regulation of DNA polymerase beta by the LMP1 oncoprotein of EBV through the nuclear factor-kappaB pathway. *Cancer Res*. Jun 15 2009;69(12):5177-5185. doi:10.1158/0008-5472.can-08-2866

20.     Zhao Y, Zheng J, Ling Y, Hou L, Zhang B. Transcriptional upregulation of DNA polymerase beta by TEIF. *Biochem Biophys Res Commun*. Aug 5 2005;333(3):908-916. doi:10.1016/j.bbrc.2005.05.172

21.     Li M, Naidu P, Yu Y, Berger NA, Kannan P. Dual regulation of AP-2alpha transcriptional activation by poly(ADP-ribose) polymerase-1. *Biochem J*. Aug 15 2004;382(Pt 1):323-329. doi:10.1042/bj20040593

22.     Oei SL, Shi Y. Transcription factor Yin Yang 1 stimulates poly(ADP-ribosyl)ation and DNA repair. *Biochem Biophys Res Commun*. Jun 8 2001;284(2):450-454. doi:10.1006/bbrc.2001.4985

23.     Zaniolo K, Desnoyers S, Leclerc S, Guérin SL. Regulation of poly(ADP-ribose) polymerase-1 (PARP-1) gene expression through the post-translational modification of Sp1: a nuclear target protein of PARP-1. *BMC Mol Biol*. Oct 25 2007;8:96. doi:10.1186/1471-2199-8-96

24.     Ding L, Chen X, Xu X, Qian Y, Liang G, Yao F, Yao Z, Wu H, Zhang J, He Q, Yang B. PARP1 suppresses the transcription of PD-L1 by poly(ADP-ribosyl)ating STAT3. *Cancer Immunol Res*. Jan 2019;7(1):136-149. doi:10.1158/2326-6066.cir-18-0071

25.     Laniel MA, Poirier GG, Guerin SL. Nuclear factor 1 interferes with Sp1 binding through a composite element on the rat poly(ADP-ribose) polymerase promoter to modulate its activity in vitro. *J Biol Chem*. Jun 8 2001;276(23):20766-20773. doi:10.1074/jbc.M010360200

26.     Roberts MR, Shields PG, Ambrosone CB, Nie J, Marian C, Krishnan SS, Goerlitz DS, Modali R, Seddon M, Lehman T, Amend KL, Trevisan M, Edge SB, Freudenheim JL. Single-nucleotide polymorphisms in DNA repair genes and association with breast cancer risk in the web study. *Carcinogenesis*. Aug 2011;32(8):1223-1230. doi:10.1093/carcin/bgr096

27.     Wei B, Zhou Y, Xu Z, Ruan J, Zhu M, Jin K, Zhou D, Hu Q, Wang Q, Wang Z, Yan Z. XRCC1 Arg399Gln and Arg194Trp polymorphisms in prostate cancer risk: a meta-analysis. *Prostate Cancer Prostatic Dis*. Sep 2011;14(3):225-231. doi:10.1038/pcan.2011.26

28.     De Summa S, Pinto R, Pilato B, Sambiasi D, Porcelli L, Guida G, Mattioli E, Paradiso A, Merla G, Micale L, De Nittis P, Tommasi S. Expression of base excision

119

repair key factors and miR17 in familial and sporadic breast cancer. *Cell Death Dis*. Feb 20 2014;5(2):e1076. doi:10.1038/cddis.2014.30

29.     Ali R, Alblihy A, Miligy IM, Alabdullah ML, Alsaleem M, Toss MS, Algethami M, Abdel-Fatah T, Moseley P, Chan S, Mongan NP, Narayan S, Rakha EA, Madhusudan S. Molecular disruption of DNA polymerase β for platinum sensitisation and synthetic lethality in epithelial ovarian cancers. *Oncogene*. Apr 2021;40(14):2496-2508. doi:10.1038/s41388-021-01710-y

30.     Abdel-Fatah T, Sultana R, Abbotts R, Hawkes C, Seedhouse C, Chan S, Madhusudan S. Clinicopathological and functional significance of XRCC1 expression in ovarian cancer. *Int J Cancer*. Jun 15 2013;132(12):2778-2786. doi:10.1002/ijc.27980

31.     Wu Z, Miao X, Zhang Y, Li D, Zou Q, Yuan Y, Liu R, Yang Z. XRCC1 is a promising predictive biomarker and facilitates chemo-resistance in gallbladder cancer. *Front Mol Biosci*. Apr 24 2020;7:70. doi:10.3389/fmolb.2020.00070

32.     Xu W, Wang S, Chen Q, Zhang Y, Ni P, Wu X, Zhang J, Qiang F, Li A, Røe OD, Xu S, Wang M, Zhang R, Zhou J. TXNL1-XRCC1 pathway regulates cisplatin-induced cell death and contributes to resistance in human gastric cancer. *Cell Death Dis*. Feb 13 2014;5(2):e1055. doi:10.1038/cddis.2014.27

33.     Ali R, Al-Kawaz A, Toss MS, Green AR, Miligy IM, Mesquita KA, Seedhouse C, Mirza S, Band V, Rakha EA, Madhusudan S. Targeting PARP1 in XRCC1-deficient sporadic invasive breast cancer or preinvasive ductal carcinoma *in situ* induces synthetic lethality and chemoprevention. *Cancer Res*. Dec 15 2018;78(24):6818-6827. doi:10.1158/0008-5472.can-18-0633

34.     Sultana R, Abdel-Fatah T, Abbotts R, Hawkes C, Albarakati N, Seedhouse C, Ball G, Chan S, Rakha EA, Ellis IO, Madhusudan S. Targeting XRCC1 deficiency in breast cancer for personalized therapy. *Cancer Res*. Mar 1 2013;73(5):1621-1634. doi:10.1158/0008-5472.can-12-2929

35.     Srivastava DK, Husain I, Arteaga CL, Wilson SH. DNA polymerase beta expression differences in selected human tumors and cell lines. *Carcinogenesis*. Jun 1999;20(6):1049-1054. doi:10.1093/carcin/20.6.1049

36.     Bianchini G, Balko JM, Mayer IA, Sanders ME, Gianni L. Triple-negative breast cancer: challenges and opportunities of a heterogeneous disease. *Nat Rev Clin Oncol*. Nov 2016;13(11):674-690. doi:10.1038/nrclinonc.2016.66

37.     Lee KJ, Mann E, Wright G, Piett CG, Nagel ZD, Gassman NR. Exploiting DNA repair defects in triple negative breast cancer to improve cell killing. *Ther Adv Med Oncol*. Sept 18 2020;12:1758835920958354. doi:10.1177/1758835920958354

38.     Siddharth S, Sharma D. Racial disparity and triple-negative breast cancer in African-American women: a multifaceted affair between obesity, biology, and socioeconomic determinants. *Cancers (Basel)*. Dec 14 2018;10(12):514. doi:10.3390/cancers10120514

39.     Maughan KL, Lutterbie MA, Ham PS. Treatment of breast cancer. *Am Fam Physician*. Jun 1 2010;81(11):1339-1346.

40.     Yin L, Duan JJ, Bian XW, Yu SC. Triple-negative breast cancer molecular subtyping and treatment progress. *Breast Cancer Res*. Jun 9 2020;22(1):61. doi:10.1186/s13058-020-01296-5

41.	Cavalieri E, Frenkel K, Liehr JG, Rogan E, Roy D. Estrogens as endogenous genotoxic agents--DNA adducts and mutations. *J Natl Cancer Inst Monogr*. 2000;(27):75-93. doi:10.1093/oxfordjournals.jncimonographs.a024247

42.	Missmer SA, Eliassen AH, Barbieri RL, Hankinson SE. Endogenous estrogen, androgen, and progesterone concentrations and breast cancer risk among postmenopausal women. *J Natl Cancer Inst*. Dec 15 2004;96(24):1856-1865. doi:10.1093/jnci/djh336

43.	Tian JM, Ran B, Zhang CL, Yan DM, Li XH. Estrogen and progesterone promote breast cancer cell proliferation by inducing cyclin G1 expression. *Braz J Med Biol Res*. Jan 23 2018;51(3):1-7. doi:10.1590/1414-431x20175612

44.	Rowe LA, Degtyareva N, Doetsch PW. DNA damage-induced reactive oxygen species (ROS) stress response in *Saccharomyces cerevisiae*. *Free Radic Biol Med*. Oct 15 2008;45(8):1167-1177. doi:10.1016/j.freeradbiomed.2008.07.018

45.	Yu H, Pardoll D, Jove R. STATs in cancer inflammation and immunity: a leading role for STAT3. *Nat Rev Cancer*. Nov 2009;9(11):798-809. doi:10.1038/nrc2734

46.	Verhoeven Y, Tilborghs S, Jacobs J, De Waele J, Quatannens D, Deben C, Prenen H, Pauwels P, Trinh XB, Wouters A, Smits ELJ, Lardon F, van Dam PA. The potential and controversy of targeting STAT family members in cancer. *Semin Cancer Biol*. Feb 2020;60:41-56. doi:10.1016/j.semcancer.2019.10.002

47.	Yue C, Xu J, Tan Estioko MD, Kotredes KP, Lopez-Otalora Y, Hilliard BA, Baker DP, Gallucci S, Gamero AM. Host STAT2/type I interferon axis controls tumor growth. *Int J Cancer*. Jan 1 2015;136(1):117-126. doi:10.1002/ijc.29004

48.    Walker SR, Nelson EA, Zou L, Chaudhury M, Signoretti S, Richardson A, Frank DA. Reciprocal effects of STAT5 and STAT3 in breast cancer. *Mol Cancer Res*. Jun 2009;7(6):966-976. doi:10.1158/1541-7786.mcr-08-0238

49.    Carpenter RL, Lo HW. STAT3 target genes relevant to human cancers. *Cancers (Basel)*. Apr 16 2014;6(2):897-925. doi:10.3390/cancers6020897

50.    Banerjee K, Resat H. Constitutive activation of STAT3 in breast cancer cells: a review. *Int J Cancer*. Jun 1 2016;138(11):2570-2578. doi:10.1002/ijc.29923

51.    Guanizo AC, Fernando CD, Garama DJ, Gough DJ. STAT3: a multifaceted oncoprotein. *Growth Factors*. Apr 2018;36(1-2):1-14. doi:10.1080/08977194.2018.1473393

52.    Huynh J, Chand A, Gough D, Ernst M. Therapeutically exploiting STAT3 activity in cancer - using tissue repair as a road map. *Nat Rev Cancer*. Feb 2019;19(2):82-96. doi:10.1038/s41568-018-0090-8

53.    Owen KL, Brockwell NK, Parker BS. JAK-STAT signaling: a double-edged sword of immune regulation and cancer progression. *Cancers (Basel)*. Dec 12 2019;11(12):2002. doi:10.3390/cancers11122002

54.    Johnson DE, O'Keefe RA, Grandis JR. Targeting the IL-6/JAK/STAT3 signalling axis in cancer. *Nat Rev Clin Oncol*. Apr 2018;15(4):234-248. doi:10.1038/nrclinonc.2018.8

55.    Audebert M, Salles B, Calsou P. Involvement of poly(ADP-ribose) polymerase-1 and XRCC1/DNA ligase III in an alternative route for DNA double-strand breaks rejoining. *J Biol Chem*. Dec 31 2004;279(53):55117-55126. doi:10.1074/jbc.M404524200

56.     Frit P, Barboule N, Yuan Y, Gomez D, Calsou P. Alternative end-joining pathway(s): bricolage at DNA breaks. *DNA Repair (Amst)*. May 2014;17:81-97. doi:10.1016/j.dnarep.2014.02.007

57.     Mladenov E, Iliakis G. Induction and repair of DNA double strand breaks: the increasing spectrum of non-homologous end joining pathways. *Mutat Res*. Jun 3 2011;711(1-2):61-72. doi:10.1016/j.mrfmmm.2011.02.005

58.     Moser J, Kool H, Giakzidis I, Caldecott K, Mullenders LHF, Fousteri MI. Sealing of chromosomal DNA nicks during nucleotide excision repair requires XRCC1 and DNA ligase III alpha in a cell-cycle-specific manner. *Mol Cell*. Jul 20 2007;27(2):311-323. doi:10.1016/j.molcel.2007.06.014

59.     Sykora P, Yang JL, Ferrarelli LK, Tian J, Tadokoro T, Kulkarni A, Weissman L, Keijzers G, Wilson DM, Mattson MP, Bohr VA. Modulation of DNA base excision repair during neuronal differentiation. *Neurobiol of Aging*. Jul 2013;34(7):1717-1727. doi:10.1016/j.neurobiolaging.2021.12.016

60.     Narciso L, Fortini P, Pajalunga D, Franchitto A, Liu P, Degan P, Frechet M, Demple B, Crescenzi M, Dogliotti E. Terminally differentiated muscle cells are defective in base excision DNA repair and hypersensitive to oxygen injury. *Proc Natl Aca Sci U S A*. Oct 23 2007;104(43):17010-17015. doi:10.1006/dbio.1999.9232

61.     Tebbs R, Flannery ML, Meneses JJ, Hartmann A, Tucker JD, Thompson LH, Cleaver JE, Pedersen RA. Requirement for the Xrcc1 DNA base excision repair gene during early mouse development. *Dev Biol*. Apr 15 1999;208(2):513-529. doi:10.1006/dbio.1999.9232

62.     Chandrashekar DS, Bashel B, Balasubramanya SAH, Creighton CJ, Ponce-Rodriguez I, Chakravarthi BVSK, Varambally S. UALCAN: a portal for facilitating tumor subgroup gene expression and survival analyses. *Neoplasia*. Aug 2017;19(8):649-658. doi:10.1016/j.neo.2017.05.002

63.     Sak SC, Harnden P, Johnston CF, Paul AB, Kiltie AE. APE1 and XRCC1 protein expression levels predict cancer-specific survival following radical radiotherapy in bladder cancer. *Clin Cancer Res*. Sep 1 2005;11(17):6205-6211. doi:10.1158/1078-0432.ccr-05-0045

64.     Hartman ZC, Poage GM, den Hollander P, Tsimelzon A, Hill J, Panupinthu N, Zhang Y, Mazumdar A, Hilsenbeck SG, Mills GB, Brown PH. Growth of triple-negative breast cancer cells relies upon coordinate autocrine expression of the proinflammatory cytokines IL-6 and IL-8. *Cancer Res*. Jun 1 2013;73(11):3470-3480. doi:10.1158/0008-5472.can-12-4524-t

65.     Wright G, Sonavane M, Gassman NR. Activated STAT3 is a novel regulator of the XRCC1 promoter and selectively increases XRCC1 protein levels in triple negative breast cancer. *Int J Mol Sci*. May 22 2021;22(11):5475. doi:10.3390/ijms22115475

66.     Huang W, Dong Z, Chen Y, Wang F, Wang CJ, Peng H, He Y, Hangoc G, Pollok K, Sandusky G, Fu XY, Broxmeyer HE, Zhang ZY, Liu JY, Zhang JT. Small-molecule inhibitors targeting the DNA-binding domain of STAT3 suppress tumor growth, metastasis and STAT3 target gene expression in vivo. *Oncogene*. Feb 11 2016;35(6):783-792. doi:10.1038/onc.2015.215

67.     Heo TH, Wahler J, Suh N. Potential therapeutic implications of IL-6/IL-6R/gp130-targeting agents in breast cancer. *Oncotarget*. Mar 29 2016;7(13):15460-15473. doi:10.18632/oncotarget.7102

68.     Knüpfer H, Preiss R. Significance of interleukin-6 (IL-6) in breast cancer (review). *Breast Cancer Res Treat*. Apr 1 2007;102(2):129-135. doi:10.1007/s10549-006-9328-3

69.     Weng YS, Tseng HY, Chen YA, Shen PC, Al Haq AT, Chen LM, Tung YC, Hsu HL. MCT-1/miR-34a/IL-6/IL-6R signaling axis promotes EMT progression, cancer stemness and M2 macrophage polarization in triple-negative breast cancer. *Mol Cancer*. Mar 18 2019;18(1):42. doi:10.1186/s12943-019-0988-0

70.     Conway ME, McDaniel JM, Graham JM, Guillen KP, Oliver PG, Parker SL, Yue P, Turkson J, Buchsbaum DJ, Welm BE, Myers RM, Varley KE. STAT3 and GR cooperate to drive gene expression and growth of basal-like triple-negative breast cancer. *Cancer Res*. Oct 15 2020;80(20):4355-4370. doi:10.1158/0008-5472.CAN-20-1379

71.     McDaniel JM, Varley KE, Gertz J, Savic DS, Roberts BS, Bailey SK, Shevde LA, Ramaker RC, Lasseigne BN, Kirby MK, Newberry KM, Partridge EC, Jones AL, Boone B, Levy SE, Oliver PG, Sexton KC, Grizzle WE, Forero A, Buchsbaum DJ, Cooper SJ, Myers RM. Genomic regulation of invasion by STAT3 in triple negative breast cancer. *Oncotarget*. Jan 31 2017;8(5):8226-8238. doi:10.18632/oncotarget.14153

72.     Huang L, Hu B, Ni J, Wu J, Jiang W, Chen C, Yang L, Zeng Y, Wan R, Hu G, Wang X. Transcriptional repression of SOCS3 mediated by IL-6/STAT3 signaling via DNMT1 promotes pancreatic cancer growth and metastasis. *J Exp Clin Cancer Res*. Feb 4 2016;35(1):27. doi:10.1186/s13046-016-0301-7

73.     Centurione L, Aiello FB. DNA repair and cytokines: TGF-beta, IL-6, and thrombopoietin as different biomarkers of radioresistance. *Front Oncol*. Jul 22 2016;6:175. doi:10.3389/fonc.2016.00175

74.     Deshmukh SK, Srivastava SK, Bhardwaj A, Singh AP, Tyagi N, Marimuthu S, Dyess DL, Dal Zotto V, Carter JE, Singh S. Resistin and interleukin-6 exhibit racially-disparate expression in breast cancer patients, display molecular association and promote growth and aggressiveness of tumor cells through STAT3 activation. *Oncotarget*. May 10 2015;6(13):11231-11241. doi:10.18632/oncotarget.3591

75.     Qin JJ, Yan L, Zhang J, Zhang WD. STAT3 as a potential therapeutic target in triple negative breast cancer: a systematic review. *J Exp Clin Cancer Res*. May 14 2019;38(1):195. doi:10.1186/s13046-019-1206-z

76.     Marsden CG, Dragon JA, Wallace SS, Sweasy JB. Base excision repair variants in cancer. *Methods Enzymol*. 2017;591:119-157. doi:10.1016/bs.mie.2017.03.003

77.     Wolf DM, Yau C, Sanil A, Glas A, Petricoin E, Wulfkuhle J, Severson TM, Linn S, Brown-Swigart L, Hirst G, Buxton M, DeMichele A, Hylton N, Symmans F, Yee D, Paoloni M, Esserman L, Berry D, Rugo H, Olopade O, van 't Veer L. DNA repair deficiency biomarkers and the 70-gene ultra-high risk signature as predictors of veliparib/carboplatin response in the I-SPY 2 breast cancer trial. *NPJ Breast Cancer*. Aug 25 2017;3:31. doi:10.1038/s41523-017-0025-7

78.     Xu W, Chen Q, Wang Q, Sun Y, Wang S, Li A, Xu S, Røe OD, Wang M, Zhang R, Yang L, Zhou J. JWA reverses cisplatin resistance via the CK2-XRCC1 pathway in human gastric cancer cells. *Cell Death Dis*. Dec 4 2014;5(12):e1551. doi:10.1038/cddis.2014.517

79.     Pang J, Xi C, Dai Y, Gong H, Zhang TM. Altered expression of base excision repair genes in response to high glucose-induced oxidative stress in HepG2 hepatocytes. *Med Sci Monit*. Jul 2012;18(7):BR281-BR285. doi:10.12659/msm.883206

80.     Mármol I, Sánchez-de-Diego C, Pradilla Dieste A, Cerrada E, Rodriguez Yoldi MJ. Colorectal carcinoma: a general overview and future perspectives in colorectal cancer. *Int J Mol Sci*. Jan 19 2017;18(1):197. doi:10.3390/ijms18010197

81.     Kang C, LeRoith D, Gallagher EJ. Diabetes, obesity, and breast cancer. *Endocrinology*. Nov 1 2018;159(11):3801-3812. doi:10.1210/en.2018-00574

82.     Kolb R, Sutterwala FS, Zhang W. Obesity and cancer: inflammation bridges the two. *Curr Opin Pharmacol*. Aug 2016;29:77-89. doi:10.1016/j.coph.2016.07.005

83.     Reuter S, Gupta SC, Chaturvedi MM, Aggarwal BB. Oxidative stress, inflammation, and cancer: how are they linked? *Free Radic Biol Med*. Dec 1 2010;49(11):1603-1616. doi:10.1016/j.freeradbiomed.2010.09.006

84.     Ishihara M. Acute hyperglycemia in patients with acute myocardial infarction. *Circ J*. 2012;76(3):563-571. doi:10.1253/circj.cj-11-1376

85.     Ramteke P, Deb A, Shepal V, Bhat MK. Hyperglycemia associated metabolic and molecular alterations in cancer risk, progression, treatment, and mortality. *Cancers (Basel)*. Sep 19 2019;11(9):1402. doi:10.3390/cancers11091402

86.     Qiu J, Zheng Q, Meng X. Hyperglycemia and chemoresistance in breast cancer: from cellular mechanisms to treatment response. *Front Oncol*. Feb 25 2021;11:628359. doi:10.3389/fonc.2021.628359

87.    Zhong A, Chang M, Yu T, Gau R, Riley DJ, Chen Y, Chen PL. Aberrant DNA damage response and DNA repair pathway in high glucose conditions. *J Can Res Updates*. 2018;7(3):64-74.

88.    Ye C, Li X, Wang Y, Zhang Y, Cai M, Zhu B, Mu P, Xia X, Zhao Y, Weng J, Gao X, Wen X. Diabetes causes multiple genetic alterations and downregulates expression of DNA repair genes in the prostate. *Lab Invest*. Sep 2011;91(9):1363-1374. doi:10.1038/labinvest.2011.87

89.    Manoel-Caetano FS, Xavier DJ, Evangelista AF, Takahashi P, Collares CV, Puthier D, Foss-Freitas MC, Foss MC, Donadi EA, Passos GA, Sakamoto-Hojo ET. Gene expression profiles displayed by peripheral blood mononuclear cells from patients with type 2 diabetes mellitus focusing on biological processes implicated on the pathogenesis of the disease. *Gene*. Dec 15 2012;511(2):151-160. doi:10.1016/j.gene.2012.09.090

90.    Das S, Bailey SK, Metge BJ, Hanna A, Hinshaw DC, Mota M, Forero-Torres A, Chatham JC, Samant RS, Shevde LA. O-GlcNAcylation of GLI transcription factors in hyperglycemic conditions augments Hedgehog activity. *Lab Invest*. Feb 2019;99(2):260-270. doi:10.1038/s41374-018-0122-8

91.    Wegenka UM, Buschmann J, Lütticken C, Heinrich PC, Horn F. Acute-phase response factor, a nuclear factor binding to acute-phase response elements, is rapidly activated by interleukin-6 at the posttranslational level. *Mol Cell Biol*. Jan 1993;13(1):276-288. doi:10.1128/mcb.13.1.276-288.1993

92.    Saengboonmee C, Seubwai W, Pairojkul C, Wongkham S. High glucose enhances progression of cholangiocarcinoma cells via STAT3 activation. *Sci Rep*. Jan 8 2016;6:18995. doi:10.1038/srep18995

93.     Du W, Wang N, Li F, Jia K, An J, Liu Y, Wang Y, Zhu L, Zhao S, Hao J. STAT3 phosphorylation mediates high glucose-impaired cell autophagy in an HDAC1-dependent and -independent manner in Schwann cells of diabetic peripheral neuropathy. *FASEB J*. Jul 2019;33(7):8008-8021. doi:10.1096/fj.201900127R

94.     Esposito K, Nappo F, Marfella R, Giugliano G, Giugliano F, Ciotola M, Quagliaro L, Ceriello A, Giugliano D. Inflammatory cytokine concentrations are acutely increased by hyperglycemia in humans: role of oxidative stress. *Circulation*. Oct 15 2002;106(16):2067-2072. doi:10.1161/01.CIR.0000034509.14906.AE

95.     Saengboonmee C, Phoomak C, Supabphol S, Covington KR, Hampton O, Wongkham C, Gibbs RA, Umezawa K, Seubwai W, Gingras MC, Wongkham S. NF-κB and STAT3 co-operation enhances high glucose induced aggressiveness of cholangiocarcinoma cells. *Life Sci*. Dec 1 2020;262:118548. doi:10.1016/j.lfs.2020.118548

96.     Zhang P, Dai H, Peng L. Involvement of STAT3 signaling in high glucose-induced epithelial mesenchymal transition in human peritoneal mesothelial cell line HMrSV5. *Kidney Blood Press Res*. 2019;44(2):179-187. doi:10.1159/000498965

97.     Zhong Z, Wen Z, Darnell JE, Jr. Stat3: a STAT family member activated by tyrosine phosphorylation in response to epidermal growth factor and interleukin-6. *Science*. Apr 1 1994;264(5155):95-98. doi:10.1126/science.8140422

98.     Chan K, Houlbrook S, Zhang QM, Harrison M, Hickson ID, Dianov GL. Overexpression of DNA polymerase beta results in an increased rate of frameshift mutations during base excision repair. *Mutagenesis*. May 2007;22(3):183-188. doi:10.1093/mutage/gel070

99.     Frosina G. Overexpression of enzymes that repair endogenous damage to DNA. *Eur J Biochem*. Apr 2000;267(8):2135-2149. doi:10.1046/j.1432-1327.2000.01266.x

100.    Yoshizawa K, Jelezcova E, Brown AR, Foley JF, Nyska A, Cui X, Hofseth LJ, Maronpot RM, Wilson SH, Sepulveda AR, Sobol RW. Gastrointestinal hyperplasia with altered expression of DNA polymerase beta. *PLoS One*. Aug 5 2009;4(8):e6493. doi:10.1371/journal.pone.0006493

101.    Hou BH, Takanaga H, Griesbeck O, Frommer WB. Osmotic induction of calcium accumulation in human embryonic kidney cells detected with a high sensitivity FRET calcium sensor. *Cell Calcium*. Aug 2009;46(2):130-135. doi:10.1016/j.ceca.2009.06.003

102.    Jóźwiak P, Krześlak A, Bryś M, Lipińska A. Glucose-dependent glucose transporter 1 expression and its impact on viability of thyroid cancer cells. *Oncol Rep*. Feb 2015;33(2):913-920. doi:10.3892/or.2014.3673

103.    Conrozier T, Mathieu P, Rinaudo M. Mannitol preserves the viscoelastic properties of hyaluronic acid in an in vitro model of oxidative stress. *Rheumatol Ther*. Dec 2014;1(1):45-54. doi:10.1007/s40744-014-0001-8

104.    Yang JL, Chao JI, Lin JG. Reactive oxygen species may participate in the mutagenicity and mutational spectrum of cadmium in Chinese hamster ovary-K1 cells. *Chem Res Toxicol*. Dec 1996;9(8):1360-1367. doi:10.1021/tx960122y

105.    Lehka LV, Panchuk RR, Berger W, Rohr J, Stoika RS. The role of reactive oxygen species in tumor cells apoptosis induced by landomycin A. *Ukr Biochem J*. Sep-Oct 2015;87(5):72-82. doi:10.15407/ubj87.05.072

106.    Panahi G, Pasalar P, Zare M, Rizzuto R, Meshkani R. High glucose induces inflammatory responses in HepG2 cells via the oxidative stress-mediated activation of

NF-κB, and MAPK pathways in HepG2 cells. *Arch Physiol Biochem*. Dec

2018;124(5):468-474. doi:10.1080/13813455.2018.1427764

107.    Horton JK, Watson M, Stefanick DF, Shaughnessy DT, Taylor JA, Wilson SH.

XRCC1 and DNA polymerase beta in cellular protection against cytotoxic DNA single-

strand breaks. *Cell Res*. Jan 2008;18(1):48-63. doi:10.1038/cr.2008.7

108.    Marintchev A, Robertson A, Dimitriadis EK, Prasad R, Wilson SH, Mullen GP.

Domain specific interaction in the XRCC1-DNA polymerase beta complex. *Nucleic*

*Acids Res*. May 15 2000;28(10):2049-2059. doi:10.1093/nar/28.10.2049

109.    Nemec AA, Abriola L, Merkel JS, de Stanchina E, DeVeaux M, Zelterman D,

Glazer PM, Sweasy JB. DNA polymerase beta germline variant confers cellular response

to cisplatin therapy. *Mol Cancer Res*. Mar 2017;15(3):269-280. doi:10.1158/1541-

7786.mcr-16-0227-t

110.    Canitrot Y, Hoffmann JS, Calsou P, Hayakawa H, Salles B, Cazaux C. Nucleotide

excision repair DNA synthesis by excess DNA polymerase beta: a potential source of

genetic instability in cancer cells. *FASEB J*. Sep 2000;14(12):1765-1774.

doi:10.1096/fj.99-1063com

111.    Bergoglio V, Pillaire MJ, Lacroix-Triki M, Raynaud-Messina B, Canitrot Y,

Bieth A, Garès M, Wright M, Delsol G, Loeb LA, Cazaux C, Hoffmann JS. Deregulated

DNA polymerase beta induces chromosome instability and tumorigenesis. *Cancer Res*.

Jun 15 2002;62(12):3511-3514.

112.    Rojo F, García-Parra J, Zazo S, Tusquets I, Ferrer-Lozano J, Menendez S, Eroles

P, Chamizo C, Servitja S, Ramírez-Merino N, Lobo F, Bellosillo B, Corominas JM,

Yelamos J, Serrano S, Lluch A, Rovira A, Albanell J. Nuclear PARP-1 protein

overexpression is associated with poor overall survival in early breast cancer. *Ann Oncol*. May 2012;23(5):1156-1164. doi:10.1093/annonc/mdr361

113.    Ossovskaya V, Koo IC, Kaldjian EP, Alvares C, Sherman BM. Upregulation of poly (ADP-ribose) polymerase-1 (PARP1) in triple-negative breast cancer and other primary human tumor types. *Genes Cancer*. Aug 2010;1(8):812-821. doi:10.1177/1947601910383418

114.    Gilabert M, Launay S, Ginestier C, Bertucci F, Audebert S, Pophillat M, Toiron Y, Baudelet E, Finetti P, Noguchi T, Sobol H, Birnbaum D, Borg JP, Charafe-Jauffret E, Gonçalves A. Poly(ADP-ribose) polymerase 1 (PARP1) overexpression in human breast cancer stem cells and resistance to olaparib. *PLoS One*. Aug 21 2014;9(8):e104302. doi:10.1371/journal.pone.0104302

115.    Clark CC, Weitzel JN, O'Connor TR. Enhancement of synthetic lethality via combinations of ABT-888, a PARP inhibitor, and carboplatin in vitro and in vivo using BRCA1 and BRCA2 isogenic models. *Mol Cancer Ther*. Sep 2012;11(9):1948-1958. doi:10.1158/1535-7163.mct-11-0597

116.    Daniel RA, Rozanska AL, Thomas HD, Mulligan EA, Drew Y, Castelbuono DJ, Hostomsky Z, Plummer ER, Boddy AV, Tweddle DA, Curtin NJ, Clifford SC. Inhibition of poly(ADP-ribose) polymerase-1 enhances temozolomide and topotecan activity against childhood neuroblastoma. *Clin Cancer Res*. Feb 15 2009;15(4):1241-1249. doi:10.1158/1078-0432.ccr-08-1095

117.    Delaney CA, Wang LZ, Kyle S, White AW, Calvert AH, Curtin NJ, Durkacz BW, Hostomsky Z, Newell DR. Potentiation of temozolomide and topotecan growth inhibition

and cytotoxicity by novel poly(adenosine diphosphoribose) polymerase inhibitors in a panel of human tumor cell lines. *Clin Cancer Res*. Jul 2000;6(7):2860-2867.

118. Plummer R, Jones C, Middleton M, Wilson R, Evans J, Olsen A, Curtin N, Boddy A, McHugh P, Newell D, Harris A, Johnson P, Steinfeldt H, Dewji R, Wang D, Robson L, Calvert H. Phase I study of the poly(ADP-ribose) polymerase inhibitor, AG014699, in combination with temozolomide in patients with advanced solid tumors. *Clin Cancer Res*. Dec 1 2008;14(23):7917-7923. doi:10.1158/1078-0432.ccr-08-1223

119. Bernges F, Bürkle A, Küpper JH, Zeller WJ. Functional overexpression of human poly(ADP-ribose) polymerase in transfected rat tumor cells. *Carcinogenesis*. Apr 1997;18(4):663-668. doi:10.1093/carcin/18.4.663

120. Van Gool L, Meyer R, Tobiasch E, Cziepluch C, Jauniaux JC, Mincheva A, Lichter P, Poirier GG, Bürkle A, Küpper JH. Overexpression of human poly(ADP-ribose) polymerase in transfected hamster cells leads to increased poly(ADP-ribosyl)ation and cellular sensitization to gamma irradiation. *Eur J Biochem*. Feb 15 1997;244(1):15-20. doi:10.1111/j.1432-1033.1997.00015.x

121. Ko HL, Ng HJ, Goh EH, Ren EC. Reduced ADP-ribosylation by PARP1 natural polymorphism V762A and by PARP1 inhibitors enhance Hepatitis B virus replication. *J Viral Hepat*. Sep 2013;20(9):658-665. doi:10.1111/jvh.12100

122. Hu Y, Zhou M, Li K, Zhang K, Kong X, Zheng Y, Li J, Liu L. Two DNA repair gene polymorphisms on the risk of gastrointestinal cancers: a meta-analysis. *Tumour Biol*. Mar 2014;35(3):1715-1725. doi:10.1007/s13277-013-1320-z

123.    Mi T, Wang Z, Bunting KD. The cooperative relationship between STAT5 and reactive oxygen species in leukemia: mechanism and rherapeutic potential. *Cancers (Basel)*. Sep 27 2018;10(10):359. doi:10.3390/cancers10100359

124.    Walker SR, Xiang M, Frank DA. Distinct roles of STAT3 and STAT5 in the pathogenesis and targeted therapy of breast cancer. *Mol Cell Endocrinol*. Jan 25 2014;382(1):616-621. doi:10.1016/j.mce.2013.03.010

125.    Kim DJ, Chan KS, Sano S, Digiovanni J. Signal transducer and activator of transcription 3 (Stat3) in epithelial carcinogenesis. *Mol Carcinog*. Aug 2007;46(8):725-731. doi:10.1002/mc.20342

**APPENDICES**

## Appendix A: Authorship Rights

Chapter 1 figures and text from "Transcription dysregulation of base excision repair proteins in breast cancer" published in DNA Repair were used with permission from the publisher Elsevier per the author rights in Elsevier's proprietary journals.

Chapter 2 figures and text from "Activated STAT3 Is a Novel Regulator of the *XRCC1* Promoter and Selectively Increases XRCC1 Protein Levels in Triple Negative Breast Cancer" published in International Journal of Molecular Sciences was used in accordance with the open access article distributed under the Creative Commons Attribution License (CY BY 4.0)

## Appendix B: Biorender Figure Citation

Figures 1.1 was adapted from "Base Exicision Repair" (1996) using

Biorender.com, 1.5, 4.13, 5.1, and 5.2 were created with BioRender.com.

## Appendix C: ChIP Primers

| Primer | Sequence |
|---|---|
| *XRCC1* -564 to -457 Forward | TGGGCAACATGGCAAGA |
| *XRCC1* -564 to -457 Reverse | CTCCTAAGTAGCTGGGATTACAC |
| *XRCC1* -452 to -358 Forward | AGTGGGAGGATCCCTTGG |
| *XRCC1* -452 to -358 Reverse | ACAGGGTCTTGCTCTCTCA |
| *XRCC1* -312 to -236 Forward | AAAGATTTGCTTTCTCGGCTTC |
| *XRCC1* -312 to -236 Reverse | CAGTCGCGCCTCTCTTC |
| *XRCC1* -251 to -110 Forward | TTTCTTCCAGACACCAATCCC |
| *XRCC1* -251 to -110 Reverse | TAGCAACGAGCGTTTCCTC |
| *XRCC1* -127 to -16 Forward | AGGAAACGCTCGTTGCTAA |
| *XRCC1* -127 to -16 Reverse | TCGGGCCTTTCAAACCC |
| *XRCC1* SP1 Site Forward | ATTGGGAGGCGAGGCTA |
| *XRCC1* SP1 Site Reverse | TCTCCAGAGCGGGAAGAG |
| *POLB* -704 to -582 Forward | CAGACTGTAAATTTCTCAGATGTAGG |
| *POLB* -704 to -582 Reverse | TTGCGGTAGGGACCAAATTA |

| | |
|---|---|
| *POLB* -626 to -524 Forward | CTCCCTTTCTTGTGGTCTCTTC |
| *POLB* -626 to -524 Reverse | TGTTAGTACACCTGCCAACC |
| *POLB* -549 to -416 Forward | TGGTTGGCAGGTGTACTAAC |
| *POLB* -549 to -416 Reverse | TCTAAGGATACCGGGCAGT |
| *POLB* -507 to -394 Forward | CTGTTCTCGGCATGGTTCA |
| *POLB* -507 to -394 Reverse | TGGCGTCACACTGTCAAA |
| *POLB* -452 to -356 Forward | GCACTGGAGTGTGACTG |
| *POLB* -452 to -356 Reverse | CAATGCATGGCGCGTTT |
| *PARP1* 1 Forward | GTAACTGTGTCCGGGAAGG |
| *PARP1* 1 Reverse | CGCCAACTGCACCATGA |
| *PARP1* 2 Forward | GGCCATCATGGTGCAGTT |
| *PARP1* 2 Reverse | CGTACTCGACTCGATAGAGCTT |
| *PARP1* 3 Forward | ATGGCGGAGTCTTCGGATAA |
| *PARP1* 3 Reverse | CCGCCGTTCCCTGATAGATA |
| *PARP1* 4 Forward | GGGTCCTCCAAAGAGCTACTA |

| | |
|---|---|
| *PARP1* 4 Reverse | ACCCAGGAAGTCTTACTTGATTTC |
| *PARP1* 5 Forward | GTTCCGTGGGCGTTCC |
| *PARP1* 5 Reverse | CCCTTTGATTGTTCTGTCCCT |

## Appendix D: Funding

# BIOGRAPHICAL SKETCH

Name of Author: Griffin M. Wright

Degrees Awarded:

B.S., Auburn University, 2017

Awards and Honors

| | |
|---|---|
| 2021 - 2022 | CCTS TL1 Pre-doctoral Fellow, University of Alabama at Birmingham CCTS |
| 2020 - 2021 | Dean's Predoctoral Fellowship Award, University of South Alabama College of Medicine |
| 2018 - 2019 | Edwin R Hughes Memorial Award, University of South Alabama College of Medicine |
| 2016 - 2017 | Undergraduate Research Fellowship, Auburn University |
| 2016 - 2017 | Dean Simmons Alumni Scholarship, Auburn University |
| 2015 - 2017 | Dr. Hilmer Jones Endowed Scholarship, Auburn University |
| 2013 - 2014 | AU Board of Trustees Scholarship, Auburn University |

Publications:

Lee KJ, Wright G, Bryant H, Wiggins LA, Dal Zotto VL, Schuler M, Malozzi C, Cohen MV, Gassman NR. Cytoprotective Effect of Vitamin D on Doxorubicin-Induced Cardiac Toxicity in Triple Negative Breast Cancer. Int J Mol Sci. 2021 Jul 12;22(14) PubMed Central PMCID: PMC8305038.

Wright G, Sonavane M, Gassman NR. Activated STAT3 Is a Novel Regulator of the *XRCC1* Promoter and Selectively Increases XRCC1 Protein Levels in Triple Negative Breast Cancer. Int J Mol Sci. 2021 May 22;22(11) PubMed Central PMCID: PMC8196947.

Wright G, Gassman NR. Transcriptional dysregulation of base excision repair proteins in breast cancer. DNA Repair (Amst). 2020 Sep;93:102922. PubMed PMID: 33087263.

Lee KJ, Wright G, Bryant H, Wiggins L, Schuler M, Gassman NR. EGFR signaling promotes resistance to CHK1 inhibitor prexasertib in triple negative breast cancer. Cancer drug resistance. 2020. Available from: http://dx.doi.org/10.20517/cdr.2020.73

Beno SM, Riegler AN, Gilley RP, Brissac T, Wang Y, Kruckow KL, Jadapalli JK, Wright GM, Shenoy AT, Stoner SN, Restrepo MI, Deshane JS, Halade GV, González-Juarbe N, Orihuela CJ. Inhibition of Necroptosis to Prevent Long-term Cardiac Damage During Pneumococcal Pneumonia and Invasive Disease. J Infect Dis. 2020 Nov 9;222(11):1882-1893. PubMed Central PMCID: PMC7896277.

Lee KJ, Wright G, Bryant H, Wiggins L, Schuler M, Gassman NR. EGFR signaling promotes resistance to CHK1 inhibitor prexasertib in triple negative breast cancer. Cancer drug resistance. 2020. Available from: http://dx.doi.org/10.20517/cdr.2020.73

Halade GV, Kain V, Wright GM, Jadapalli JK. Subacute treatment of carprofen facilitate splenocardiac resolution deficit in cardiac injury. J Leukoc Biol. 2018 Dec;104(6):1173-1186. PubMed Central PMCID: PMC7837411.

Jadapalli JK, Wright GW, Kain V, Sherwani MA, Sonkar R, Yusuf N, Halade GV. Doxorubicin triggers splenic contraction and irreversible dysregulation of COX and LOX that alters the inflammation-resolution program in the myocardium. Am J Physiol Heart Circ Physiol. 2018 Nov 1;315(5):H1091-H1100. PubMed Central PMCID: PMC6734064.